Study of neutron-rich β-delayed emitters relevant for understanding the formation of the r -process rare earth-peak around mass A∼160

Max Pallàs Solís

TU Darmstadt / GSI
Former UPC-INTE

Stellar nucleosynthesis

In the core of stars, **nuclear fusion** takes place.

1. H burning (PP-Chain / CNO-cycle)
2. He burning (Triple-α)
3. …..

+Z

Stops at Fe (Z=26)!

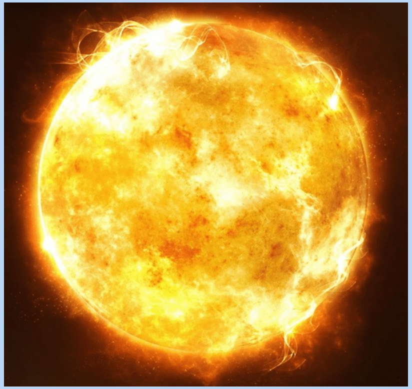

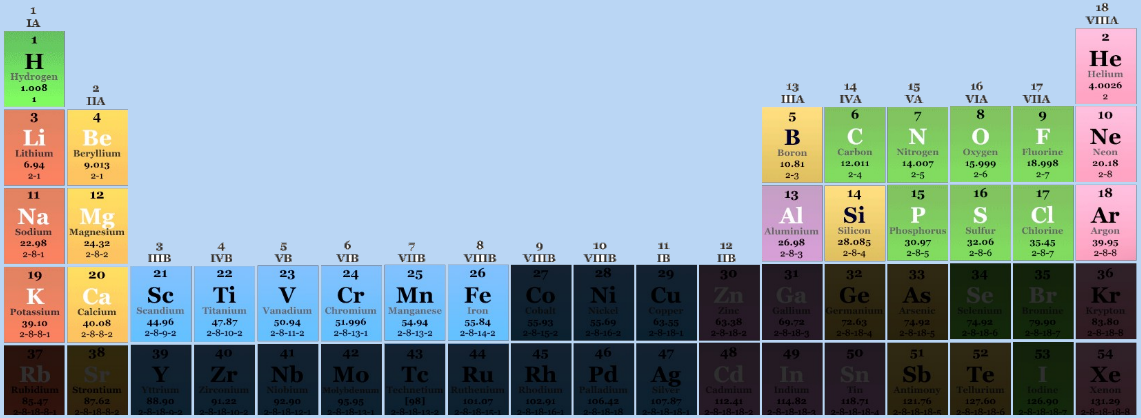

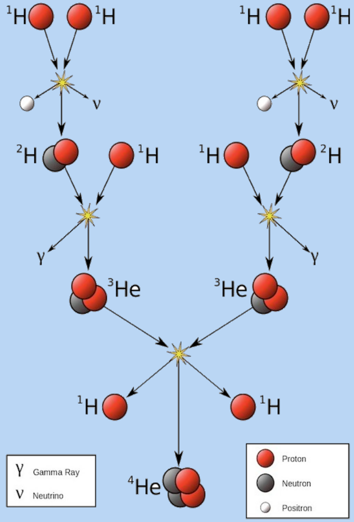

Science Learning Hub (Adapted)

And heavy nuclei?

In 1957, the B²FH paper was published, proposing a solution for the formation of heavy elements: The neutron capture reaction (n,γ).

Neutron capture (n,γ)

↓ Tends to unstability

β^--decay

↓ Tends to stability

Z increase

Neutron capture

$$\overbrace{{}^{A}_{Z}X + n \rightarrow {}^{A+1}_{Z}X} \rightarrow {}^{A+1}_{Z+1}Y + e^- + \bar{\nu}$$

β^-- decay

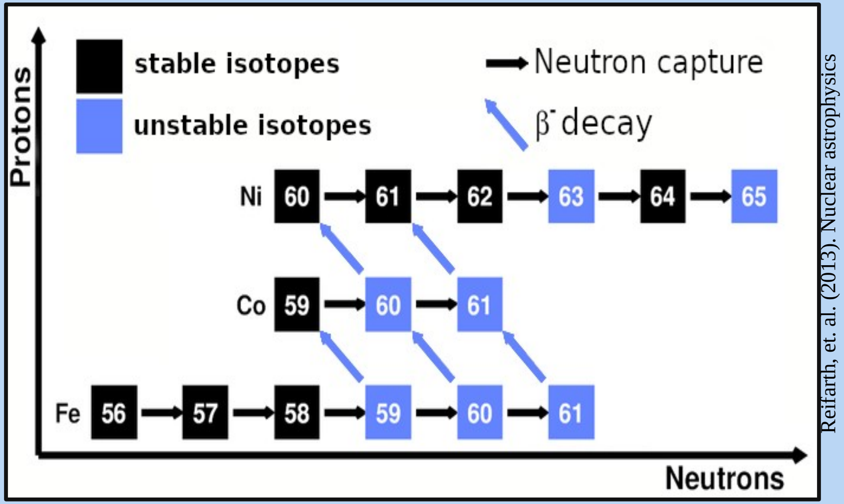

Reifarth, et. al. (2013). Nuclear astrophysics with radioactive ions at FAIR. (Adapted)

Neutron capture

Two processes can be distinguished based on the **relative timescales of neutron capture (T_{neu}) and β-decay ($T_β$).**

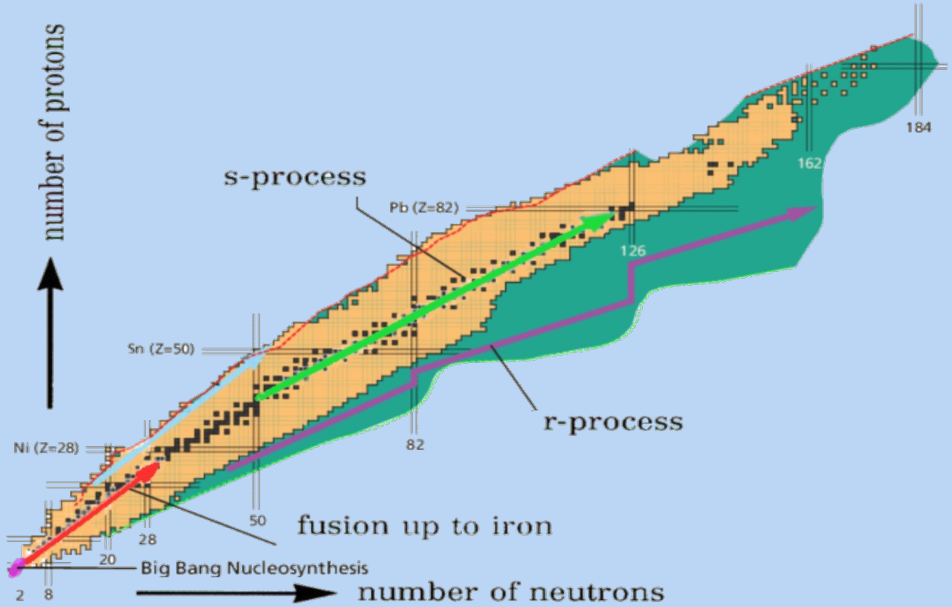

Rodríguez+ JPCS 503 (2014)

Slow neutron-capture process:

- Low neutron density: $T_{Neu} > T_β$
- Around the stability line.
- Timescale: stellar burning.

Rapid neutron-capture process:

- High neutron density: $T_{Neu} << T_β$
- Far from stability line.
- Timescale: μs to ms.

β-delayed neutron emission

- The **β^--decay** is characteristic of neutron-rich nuclei.
- The energy available is called **Q_β**.
- If $Q_\beta > S_{xn}$ --> **β-delayed neutron emission**.

$$ {}^{A}_{Z}X \rightarrow {}^{A-1}_{Z+1}Y + e^{-} + \bar{\nu} + n $$

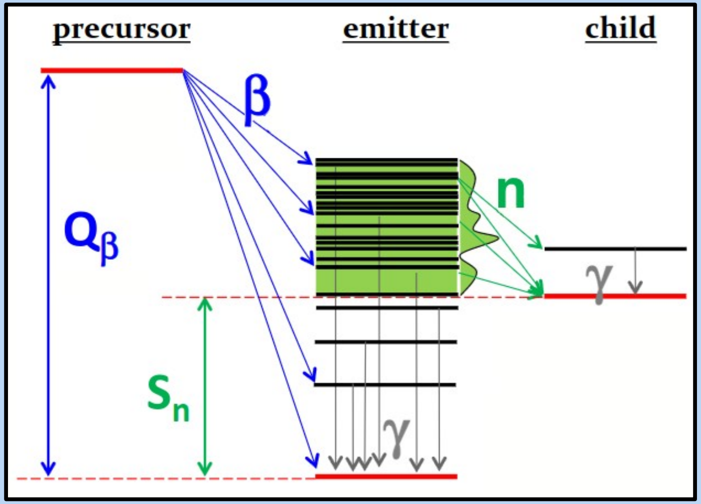

Strauss+ (2016) (adapted)

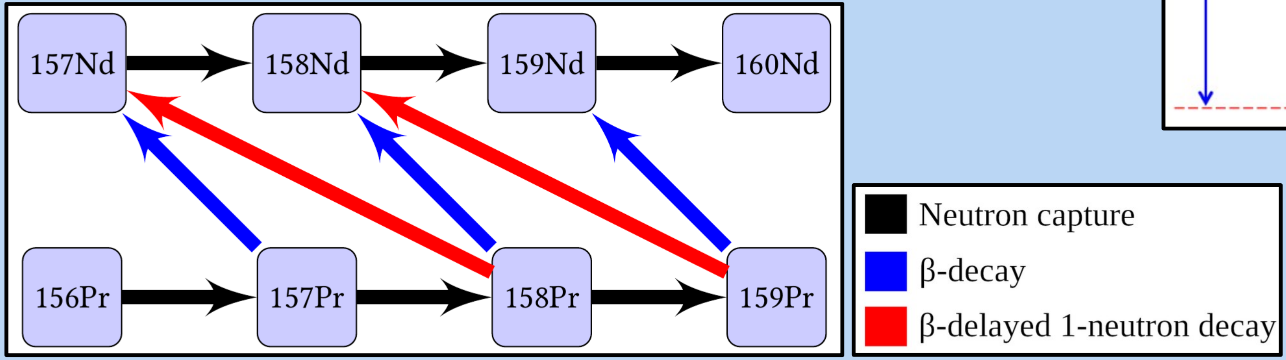

BRIKEN project

- Built the **largest β-delayed neutron detector** in the world to conduct experiments at the RIKEN Nishina Center (Japan).
- Study the **most exotic** experimentally accessible neutron-rich nuclei.
  - **Half-life ($T_{1/2}$)**
  - **Beta-delayed neutron emission probabilities (P_{xn})**
- **International collaboration:** Over 50 participants from 18 international institutions.

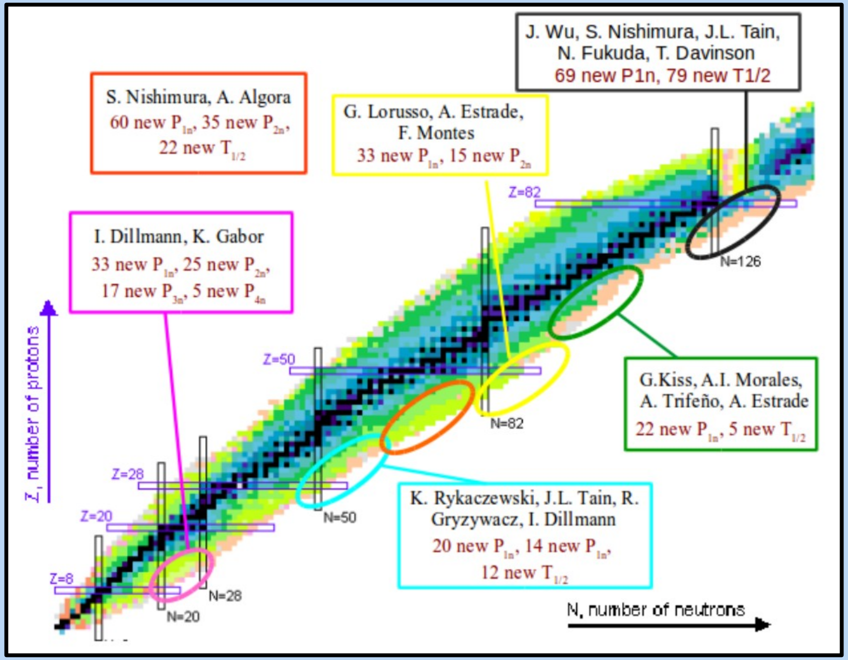

REP relevance

- The **only** r-process peak formed after the **freeze-out**.

- **Unique probe** for the study of the **late-time conditions** on the r-process site (e. g. Temperature)

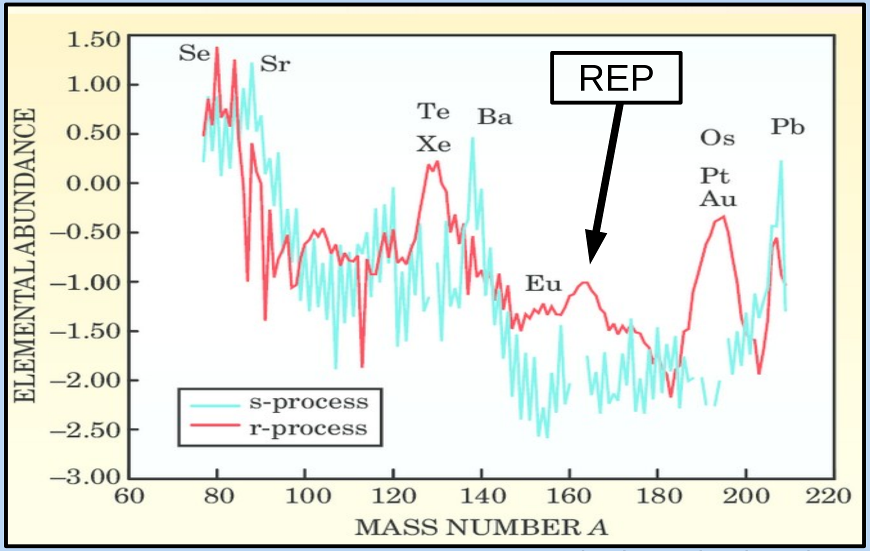

Cowan+ Physics Today (2004)

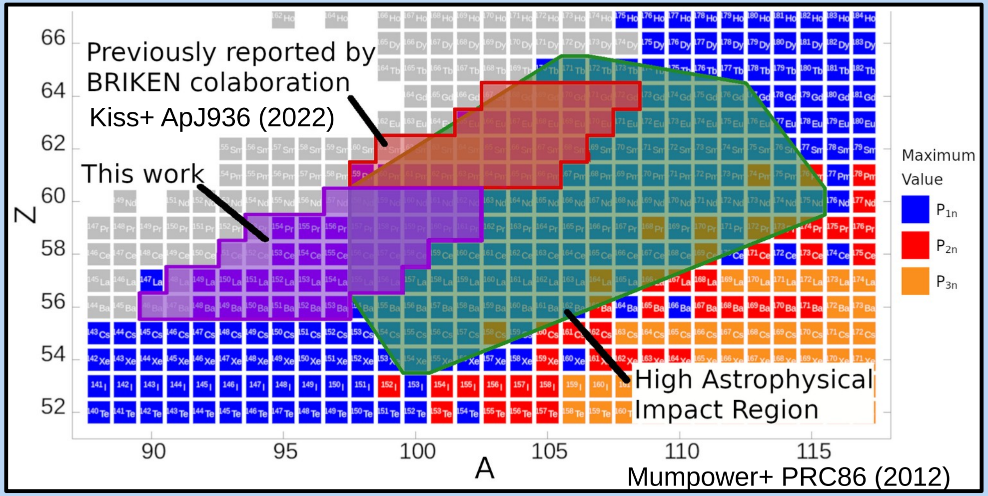

Mumpower+ PRC86 (2012)

- **$T_{1/2}$ and P_{xn}** of very neutron-rich nuclei for $55 \leq Z \leq 64$ are **key for the REP formation**.

Experimental setup

1. **BigRIPS:** Production, separation and identification
2. **AIDA:** Implantation and β-decay detection.
3. **BRIKEN:** β-delayed neutron (+gamma) detection

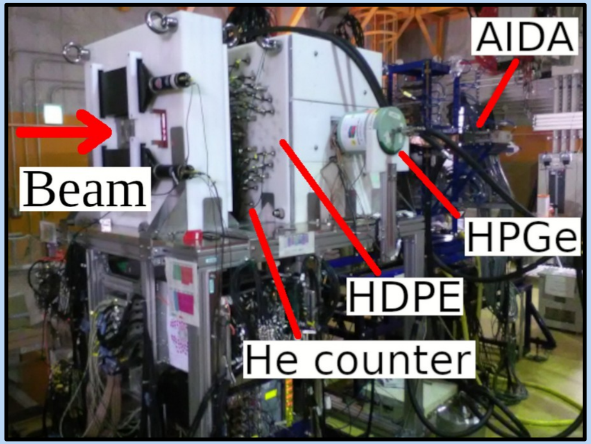

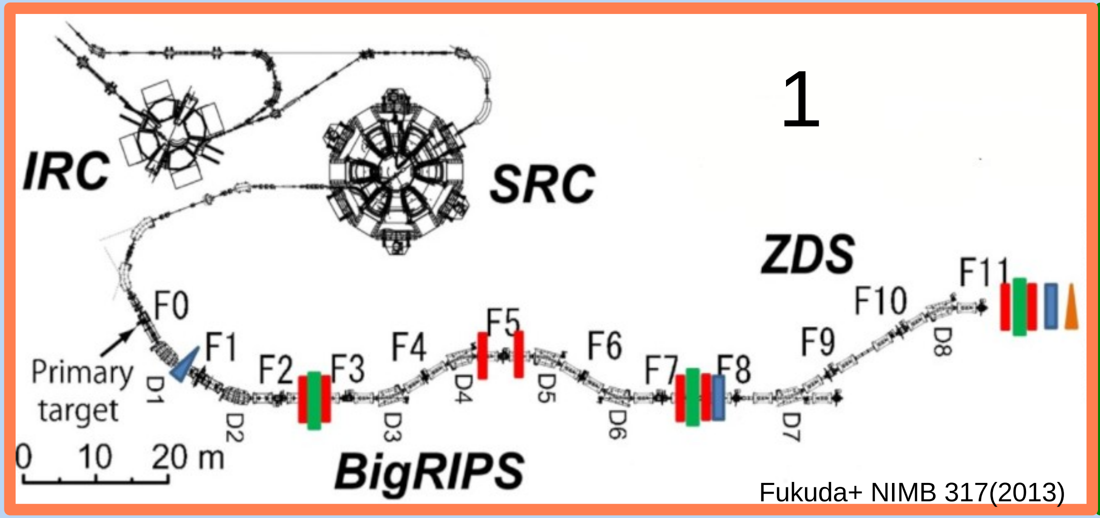

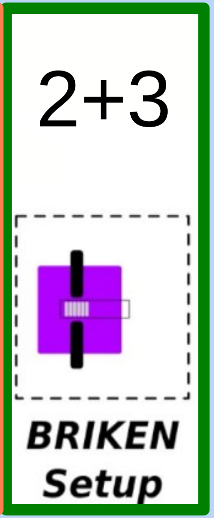

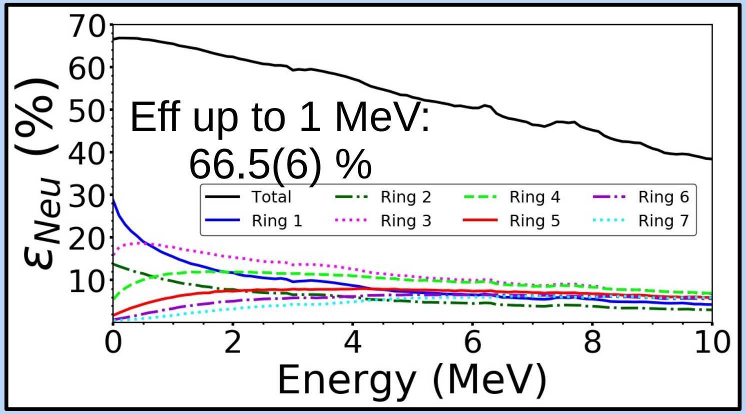

Data analysis

- **Simultaneous fit** of the coincidence curves using binned maximum likelihood.

- **Fitted parameters:** parent isotope decays (N_1 (t=0)), its $T_{1/2}$, and its P_{1n}.

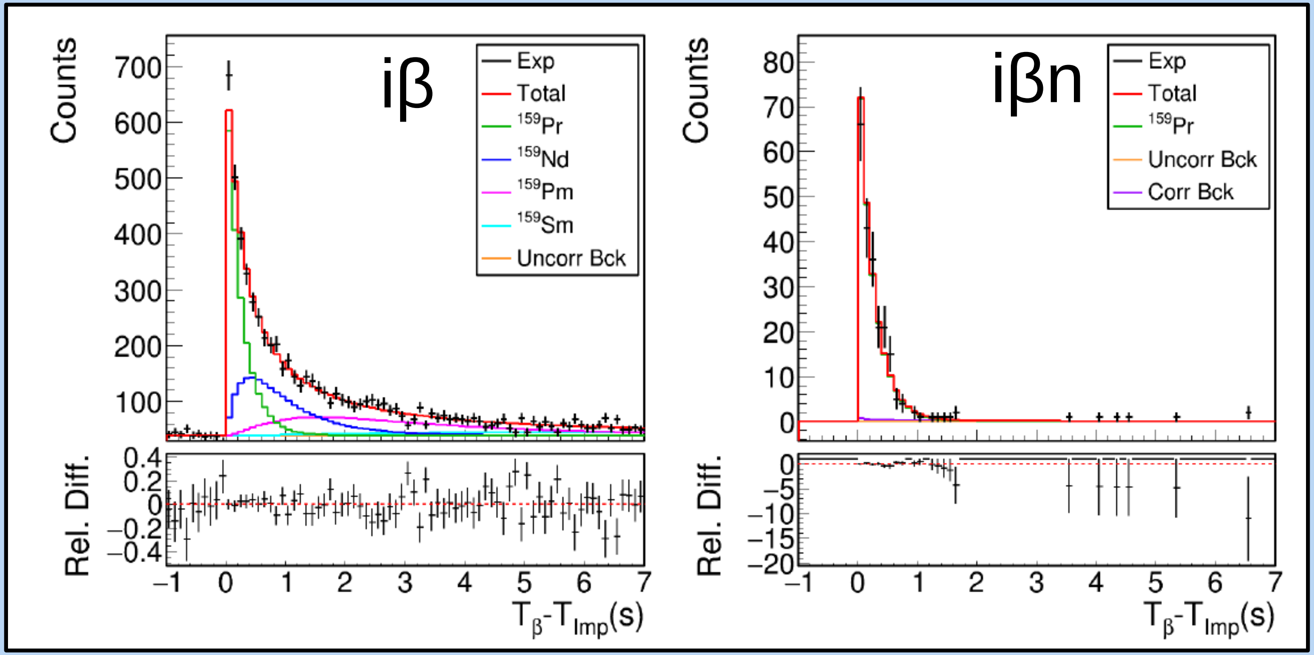

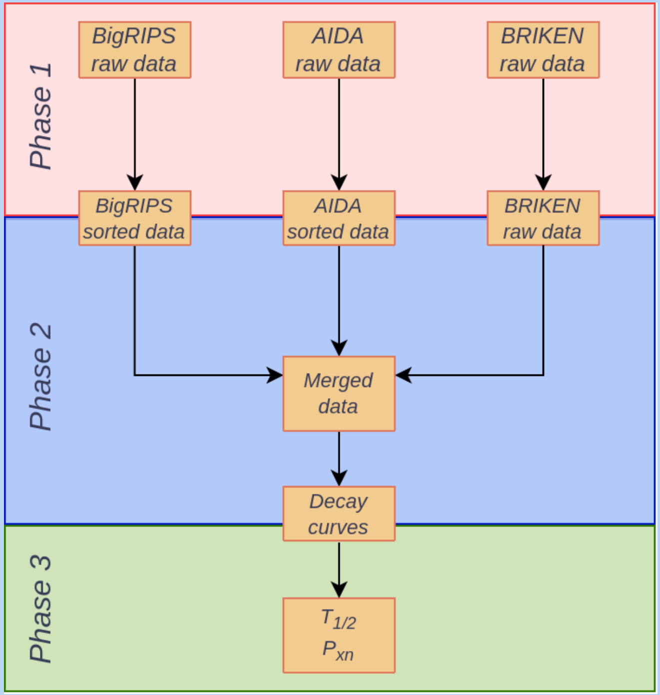

Global results

- **36 $T_{1/2}$**, including a **first-time** measurement (^{161}Pr).
- The $T_{1/2}$ reported **overall consistent** results with previous measurements, reducing the uncertainties of 13 nuclei.

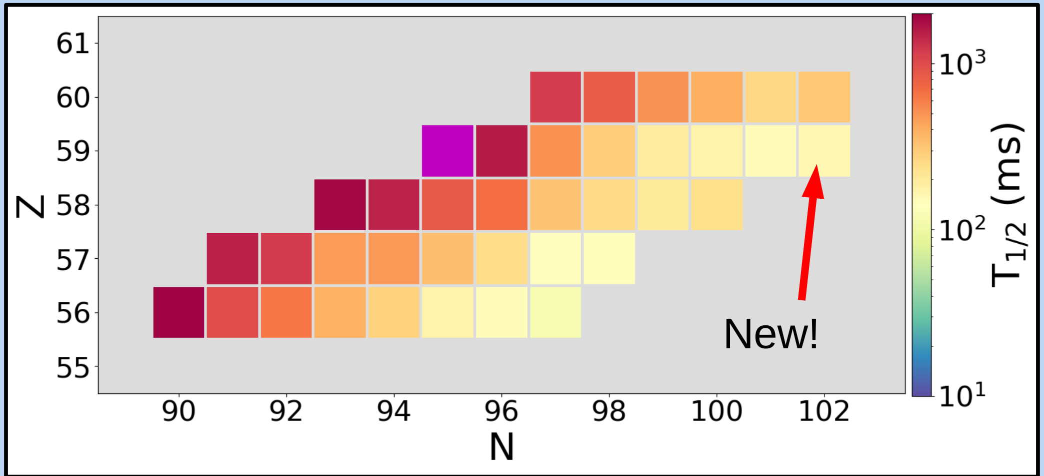

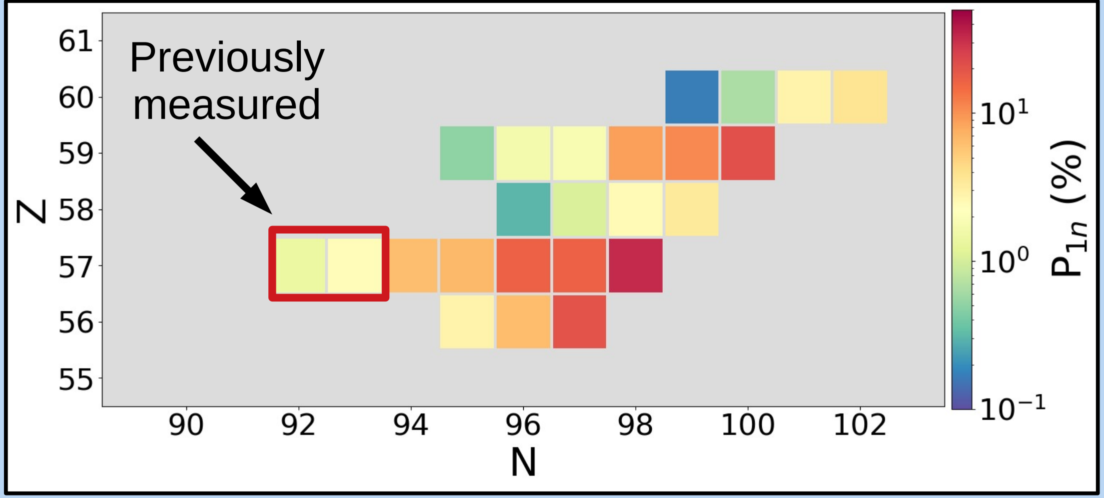

- **24 P_{1n}** values have been measured, **22** of them for the **first-time**.

R-process calculation

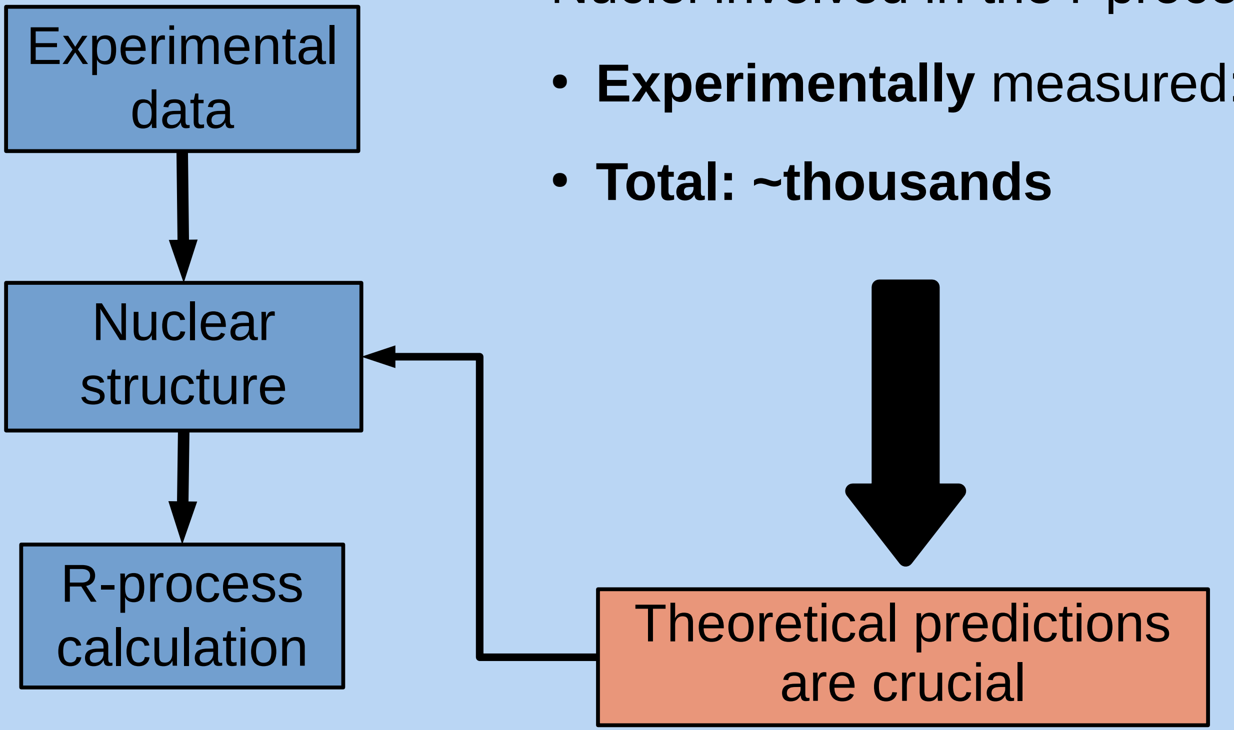

Nuclei involved in the r-process:

- **Experimentally** measured: **~hundreds**
- **Total: ~thousands**

Nuclear structure calculations

In collaboration with GSI Theoretical Nuclear Astrophysics Group.

1. Compute the **β-Strength** (Diana's PhD).
2. Calculate **$T_{1/2}$ and P_{xn}.**
3. **Compared** with the experimental data from REP-BRIKEN.
4. **Refine** the model parameters.

Diana Alvear Terrero

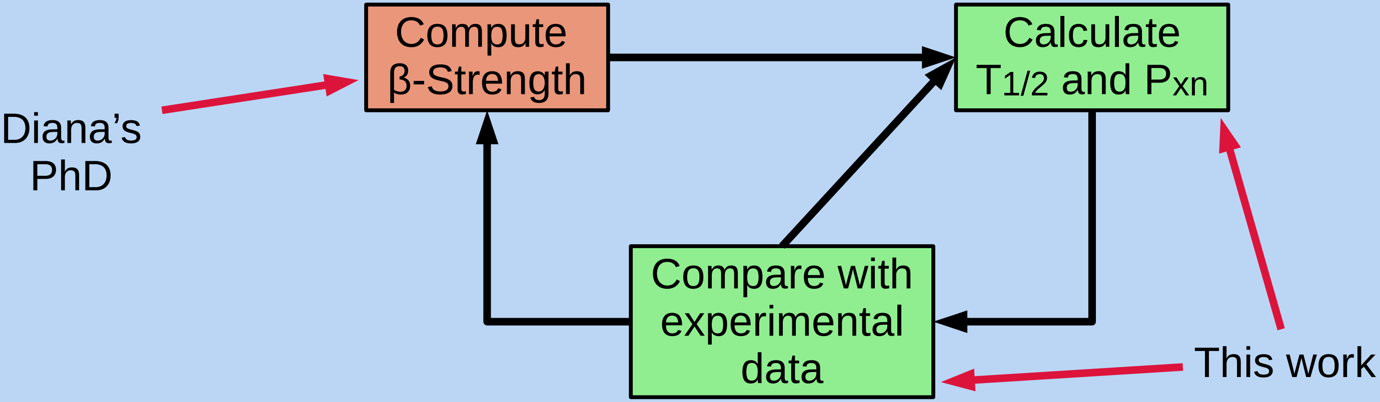

Nuclear structure calculations

- **Revision** of the Marketin et al. Model (QRPA).
- The calculation includes **GT and FF** transitions.
- The states are computed as **discrete energy** levels.
- P_{xn} calculated using **HF** model through TALYS.
- **FRDM** mass model to compute Q_β and S_{xn}.

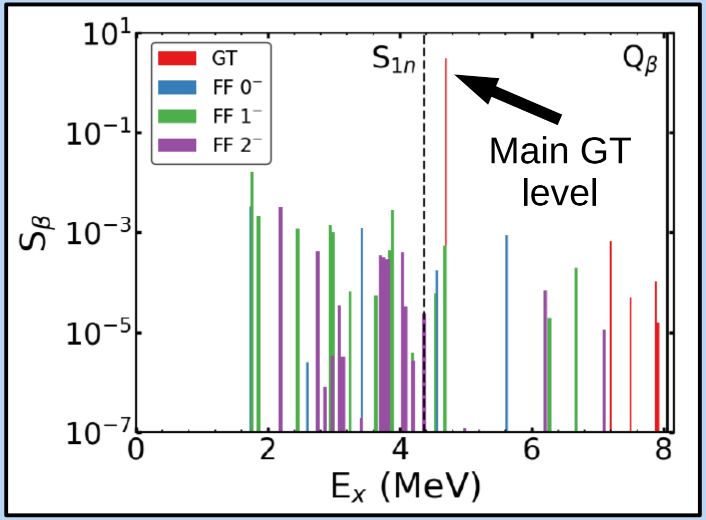

$$\lambda^{(m)} = \frac{\ln 2}{K} \int_1^{W_0^{(m)}} F(Z,W)\, W\, p\, (W - W_0^{(m)})^2\, C^{(m)}(W, W_0^{(m)})\, dW$$

Decay rate

Fermi function

Shape factor

$$\lambda(E_x) = \sum_m^{E_m^* < Q_\beta} \lambda^{(m)}\, \delta(E_x - E_m^*)$$

$$\lambda = \frac{\ln 2}{T_{1/2}} = \int_0^{Q_\beta} \lambda(E_x)\, dE_x$$

$$P_{xn} = \int_0^{Q_\beta} \lambda(E_x) \cdot p_{xn}(E_x)\, dE_x$$

TALYS

Some results T1/2

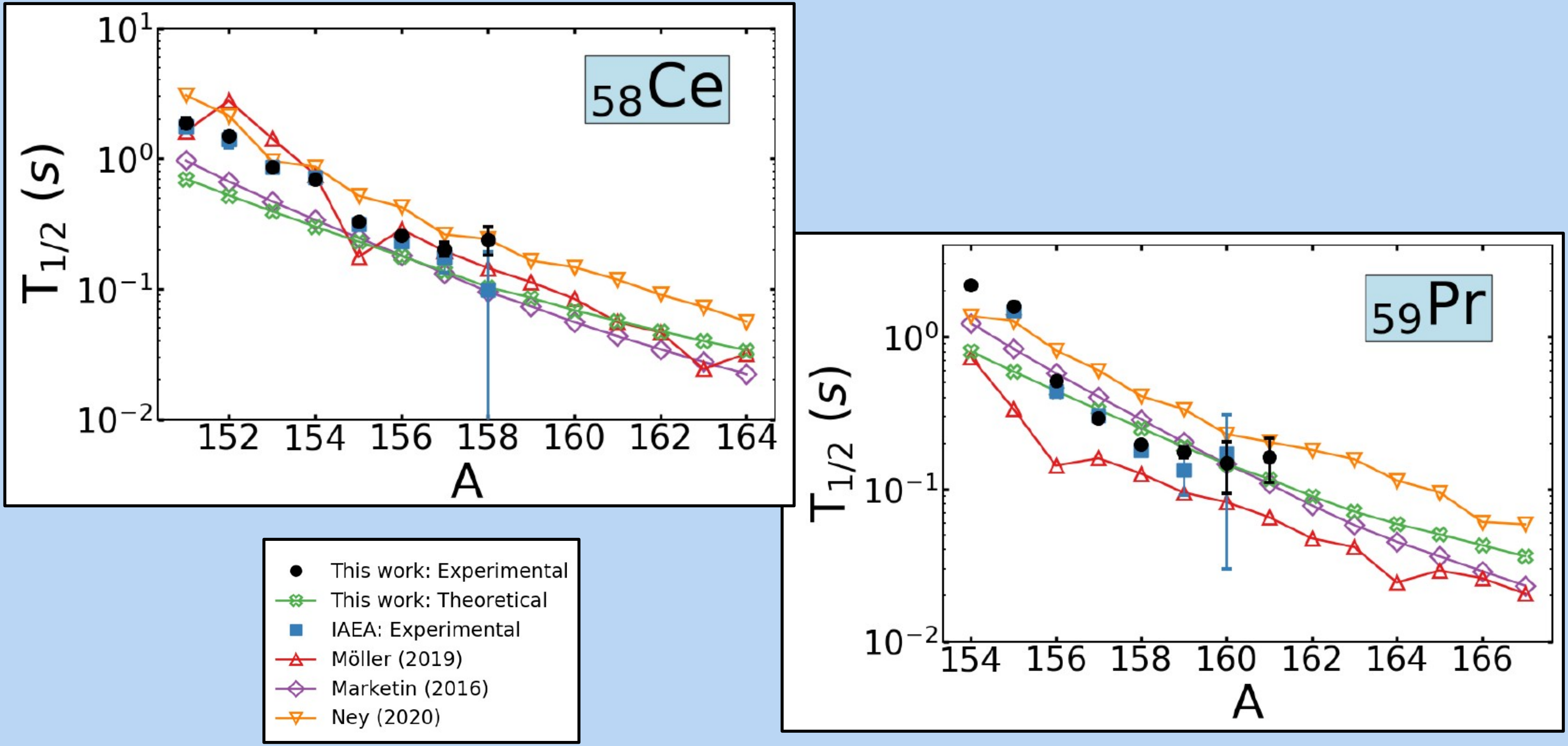

Some results P_{1n}

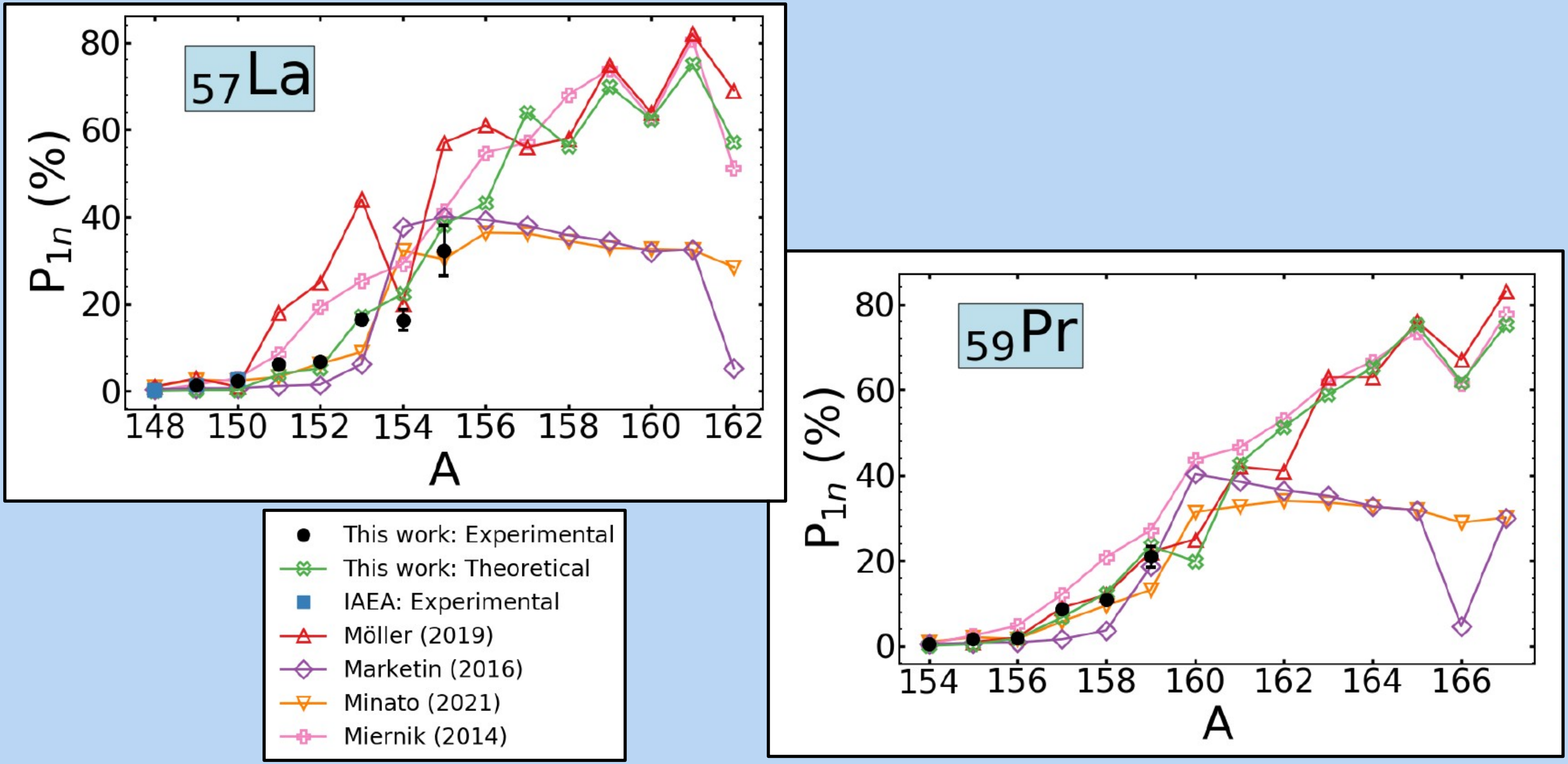

Preliminary astrophysical impact

- Input: Our new **experimental** data + refined nuclear **model** from Ba to Nd.
- Trajectories of the **dynamical ejecta** from a neutron star merger.
- The **impact depends** hugely on the **trajectories** selected.

Single trajectory

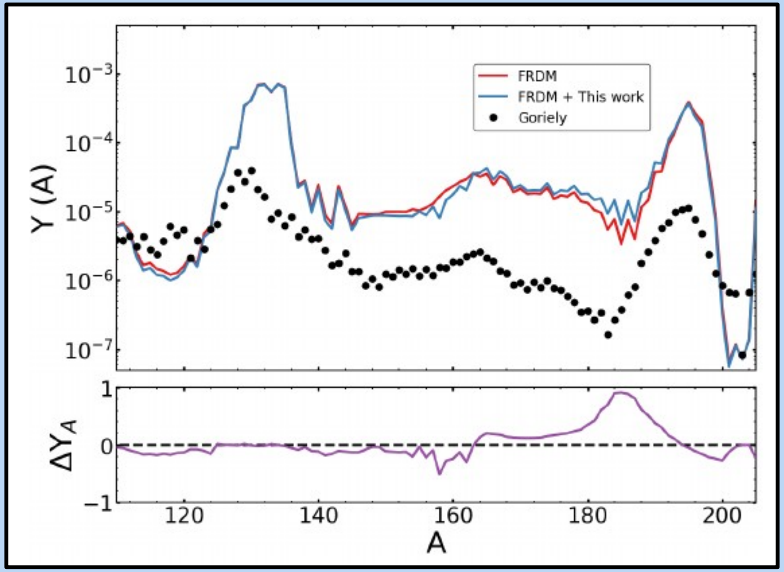

Average of multiple trajectories

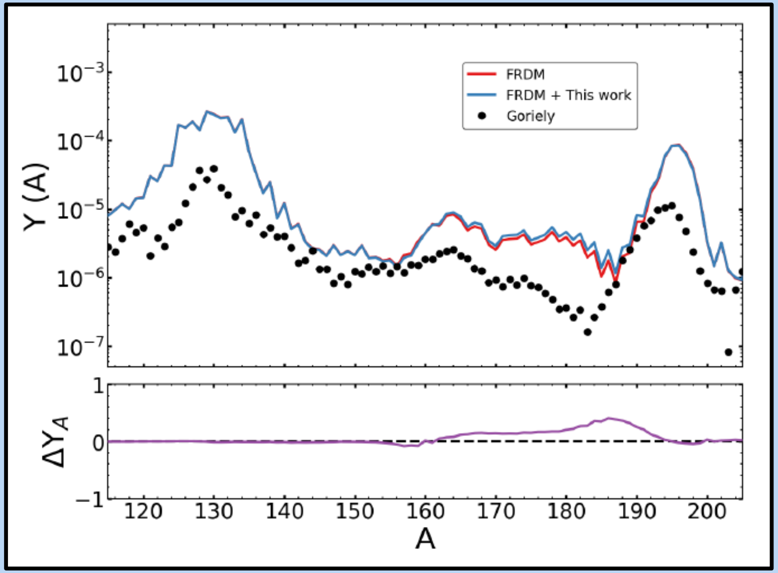

Conclusions

- First comprehensive **characterization** of the BRIKEN neutron counter.
- The analysis of the **REP-BRIKEN experiment** was successful, yielding:
  - **36 $T_{1/2}$,** of which 13 with improved precision and **1 first-time** measure.
  - **24 P_{1n},** of which **22 are first-time** measurements.
- We updated and benchmarked a **QRPA nuclear structure model** using our new experimental data. This new model predicted with **good accuracy the P_{1n}** of the odd-Z nuclei studied in this thesis.
- We presented a first overview of the **astrophysical impact** of both the experimental and theoretical new data on the r-process final abundances.

Acknoowledgments

Collaborators

A. Tarifeño-Saldivia[1], A. Tolosa-Delgado[2,1], D. Alvear-Terrero[3,4], G. Martínez-Pinedo[3,4,5], Z. Xiong[5], G. G. Kiss[6], J. L. Tain[2], A. Vitéz-Sveiczer[6], BRIKEN collaboration[9]

[1] Instituto de Física Corpuscular (CSIC-UV), Spain. [2] European Organization for Nuclear Research (CERN), Switizerland. [3] Institut für Kernphysik (TU Darmstadt), Germany. [4] Helmholtz Forschungsakademie Hessen für FAIR (GSI), Germany. [5] GSI Helmholtzzentrum fúur Schwerionenforschung, Germany. [6] Institute for Nuclear Research (Atomki), Hungary. [7] www.wiki.edu.ac.uk/display/BRIKEN/Home.

This work has been supported by the Spanish Ministerio de Economía y Competitividad under Grants nos. FPA2014-52823-C2-1-P, FPA2014-52823-C2-2-P, FPA2017-83946-C2-1-P, FPA2017-83946-C2-2-P and grants from Ministerio de Ciencia e Innovacion nos PID2019-104714GB-C21, PID2019-104714GB-C22 and PID2022-138297NB-C22. Also supported by SANDA project funded under H2020-EURATOM-1.1 Grant No. 847552. Grant PID2022-138297NB-C22 funded by MCIN/AEI/10.13039/501100011033 and by "ERDF A way of making Europe"

MINISTERIO DE CIENCIA E INNOVACIÓN

UNIÓN EUROPEA

FONDO EUROPEO DE DESARROLLO REGIONAL

"Una manera de hacer Europa"

AGENCIA ESTATAL DE INVESTIGACIÓN

UNIVERSITAT POLITÈCNICA DE CATALUNYA BARCELONATECH

Institut de Tècniques Energètiques

RIKEN NiSHiNA CENTER

atomki DEBRECEN

GSI

β-delayed neutrons at RIKEN

IFIC INSTITUT DE FÍSICA CORPUSCULAR

CSIC CONSEJO SUPERIOR DE INVESTIGACIONES CIENTÍFICAS

Neutron spectrometry

Smearing function

- The QRPA calculation only computes **some** of the excited levels.

- To account for **higher-order terms**, we add a **smearing function** to obtain a smoother distribution.

$$G_\sigma(W, W_0) = \frac{1}{\sigma\sqrt{2\pi}} \exp\left(-\frac{(W - W_0)^2\, m_e^2}{2\sigma^2}\right)$$

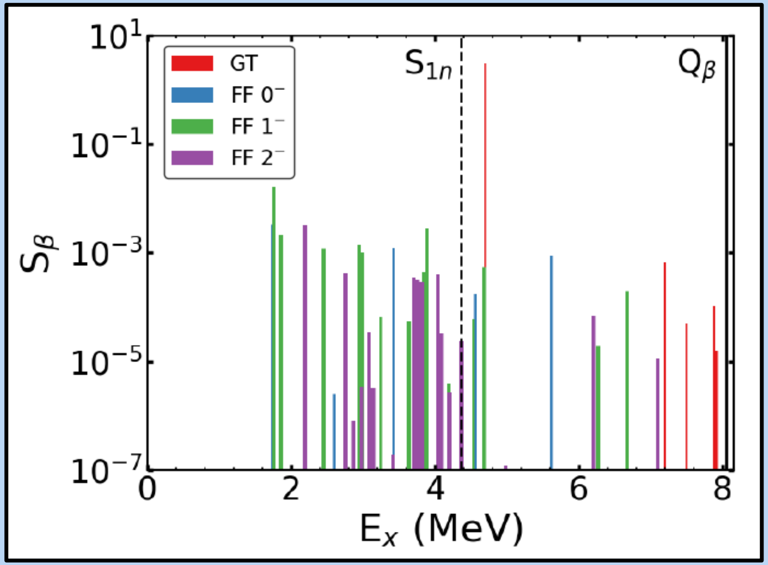

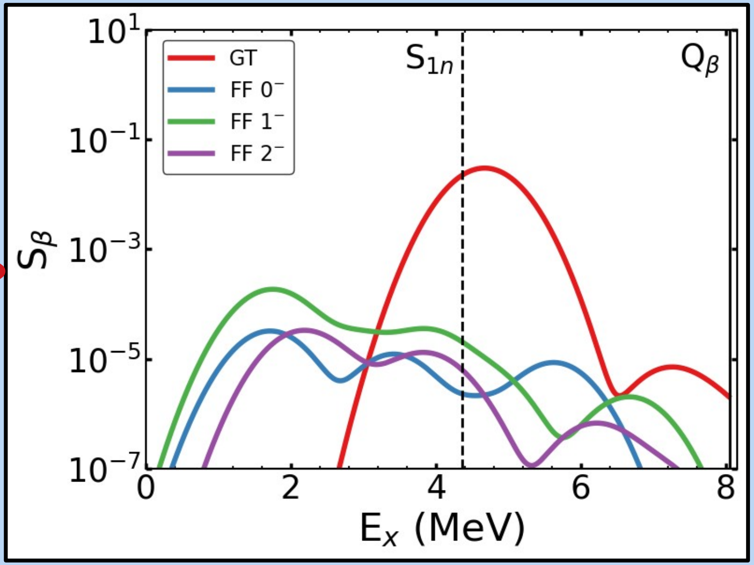

Neutron spectrometry

- Using different moderator designs, one can detect neutrons of different energies.
- The detection mechanism is based on neutron thermalization (bonner spheres).
- Energy sensitivity from meV to MeV (even GeV).

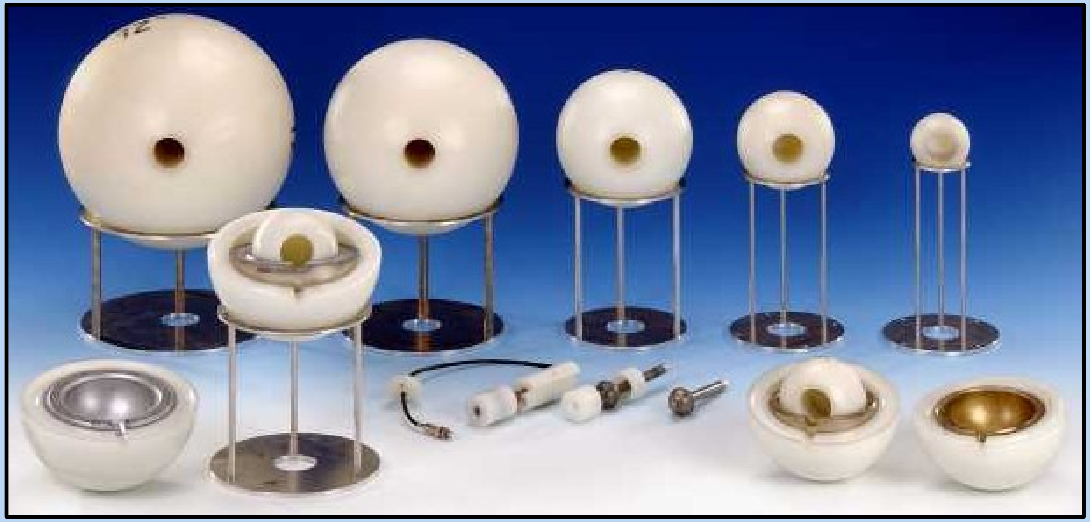

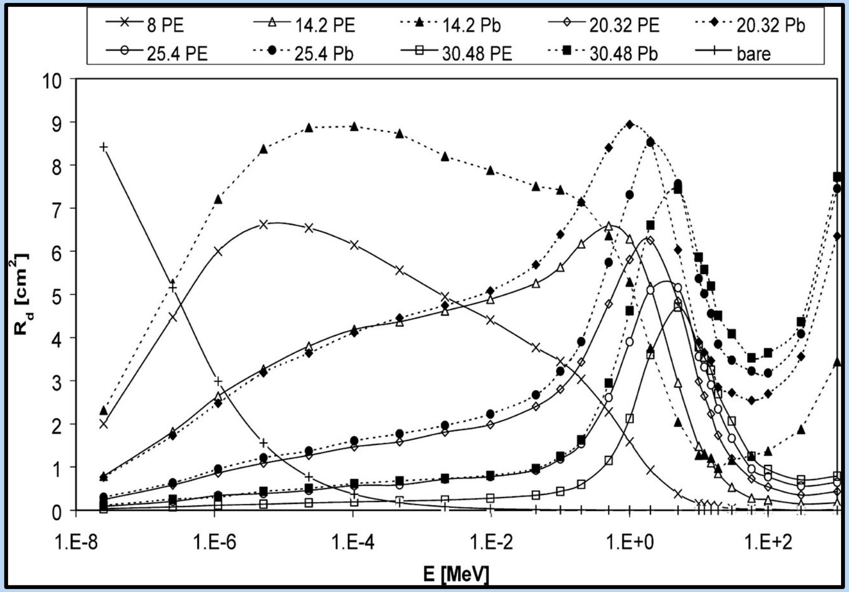

HENSA project

- Rectangular geometry.
- Higher efficiency (larger ^{3}He detectors).
- Scalability: Simplified setup
- Wider Energy Range: up to the GeV.

High Efficiency Neutron Spectrometry Array

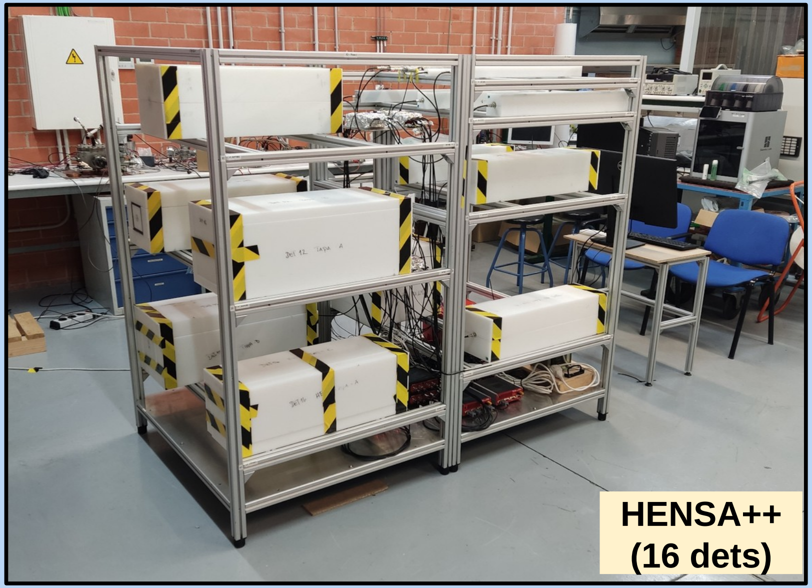

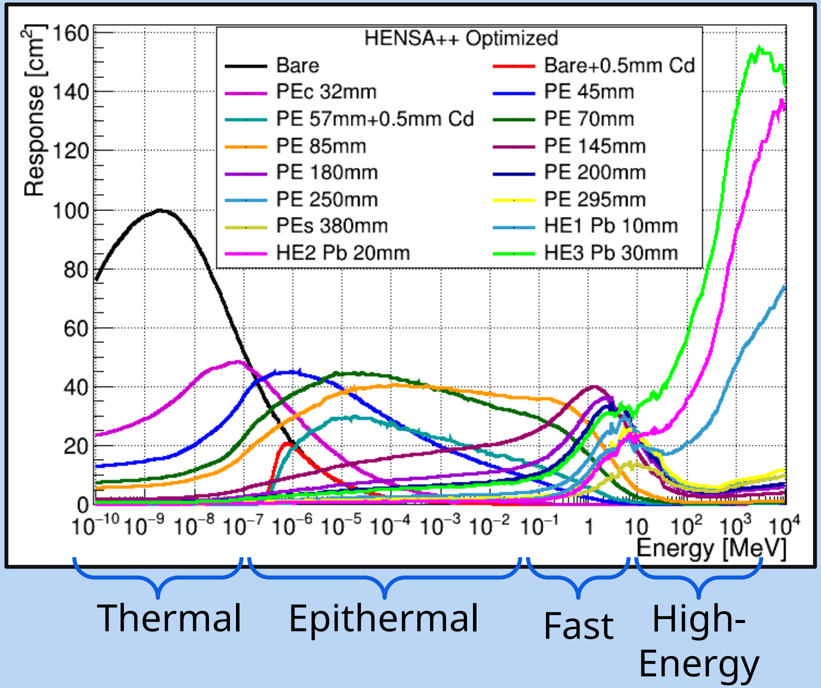

HENSA uses

- Underground labs' background characterization (LSC, LNGS, Felsenkeller)
- Cosmic-ray neutron spectrum + space weather (OAJ, DESY)

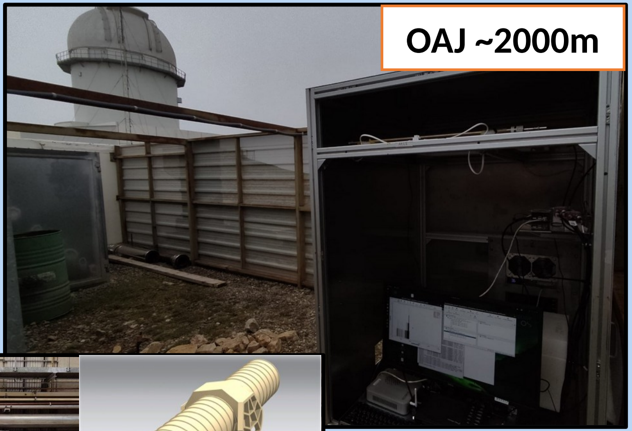

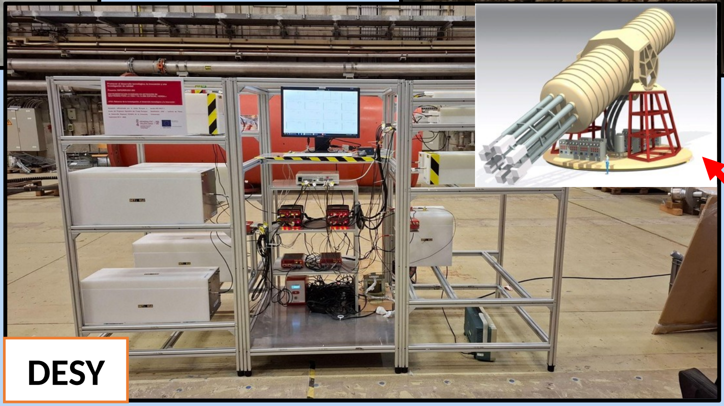

Dark matter experiments (WIMP)

Dark matter experiments (Axions)

Unfolding

Unfolding consists on extracting the **flux magnitude and energy distribution** from the measured **rates** and the **response**.

$$C_i = \sum_{j=1}^{m} R_{ij}\phi_j \qquad i = 1, 2, ..., n$$

Linear inverse problem (n < m)!!!

Detector **counting rate** (measurement)

Detector **response** (calculated)

Neutron **flux** (magnitude we want to determine)

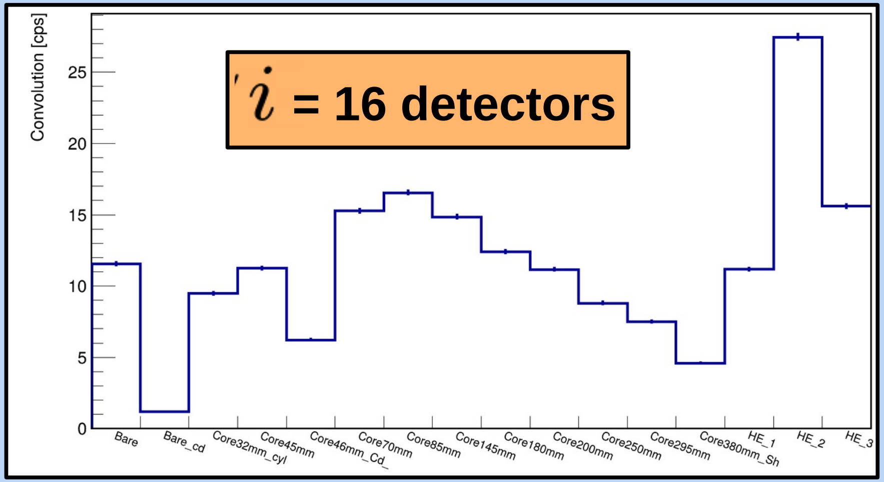

The unfolding methods are based on the **use of a priori information.**

POU

- Many different unfolding algorithms exist (MITOM, FRUIT, MAXED, GRAVEL, …), but none have a standardized uncertainty evaluation.

- Our code is called POU (Prior Optimizer for Unfolding).
  - Use of a parametric space for the prior.
  - The output solution is a combination of accepted solutions. ------> Systematic assessment of the errors.

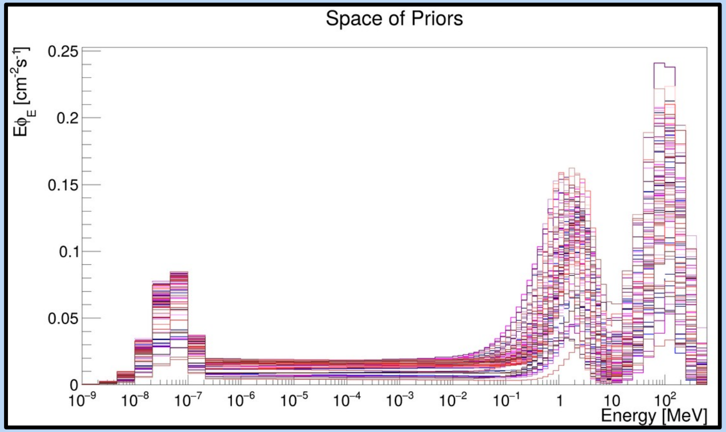

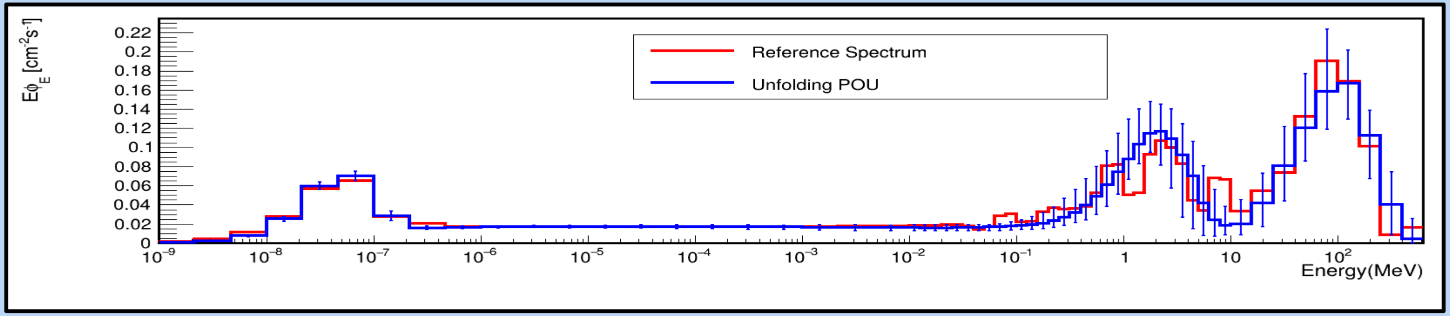

A. Quero et al,
POU: A novel parametric-iterative unfolding algorithm for Bonner Sphere Spectrometry.
Accepted RPC

Extra: Future BRIKEN?

Low-resolution neutron spectrometer for beta-delayed neutron experiments

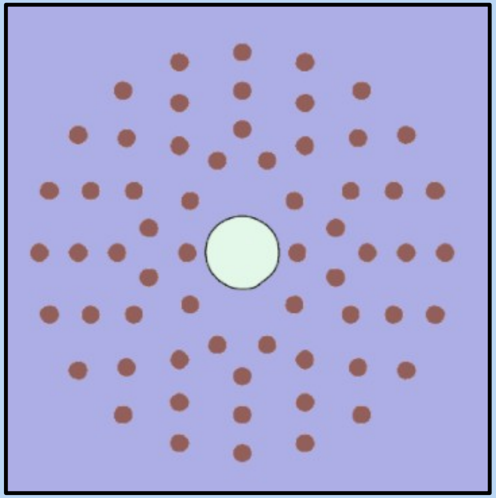

Different spatial positions → Different energy response

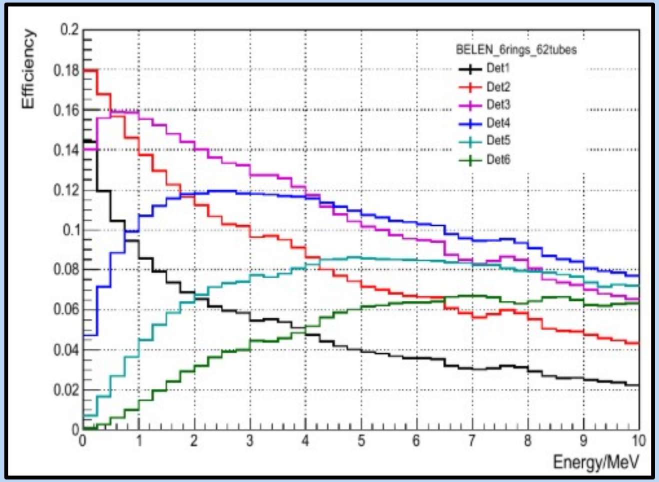

Conceptual test with 252Cf

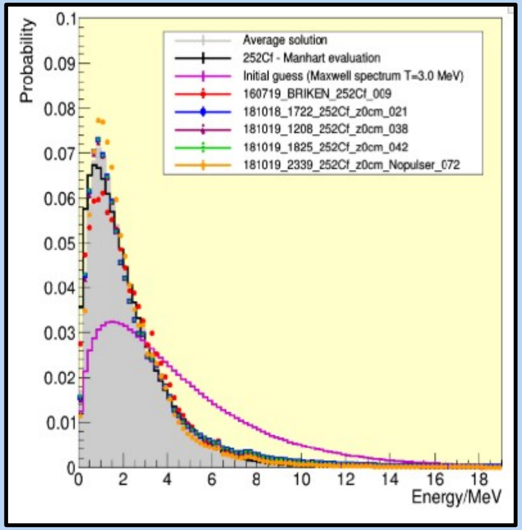

Neutron dosimetry and very high flux enviroments

WPE (Essen)

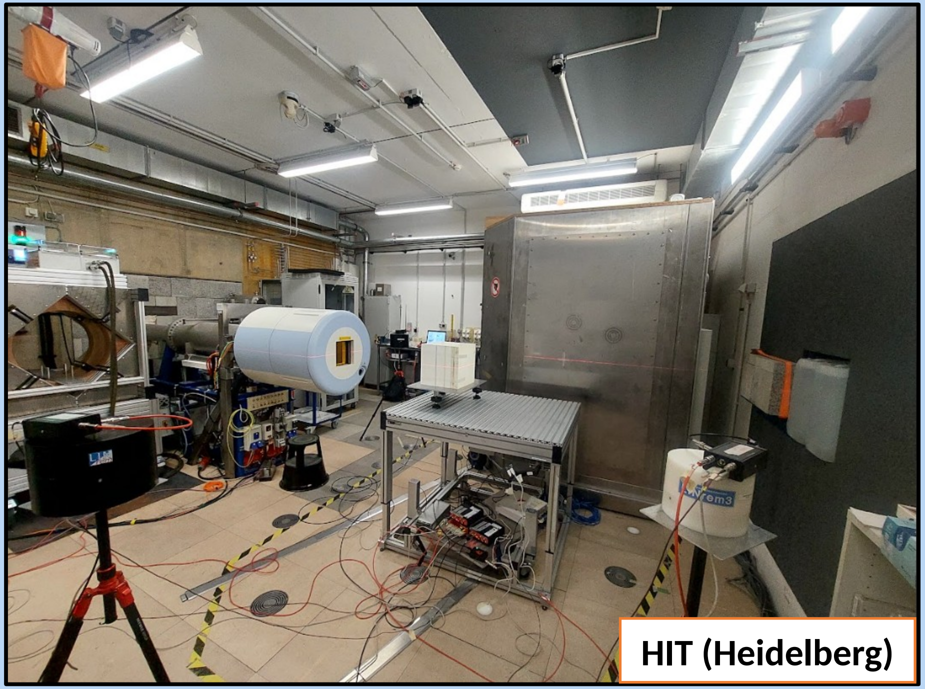
HIT (Heidelberg)

Hadrontherapy and neutrons

Stray or secondary neutrons produced during hadrontherapy pose a potential risk for long-term cancer, especially in **pediatric patients**, and evaluation of effect in **pregnant women**.

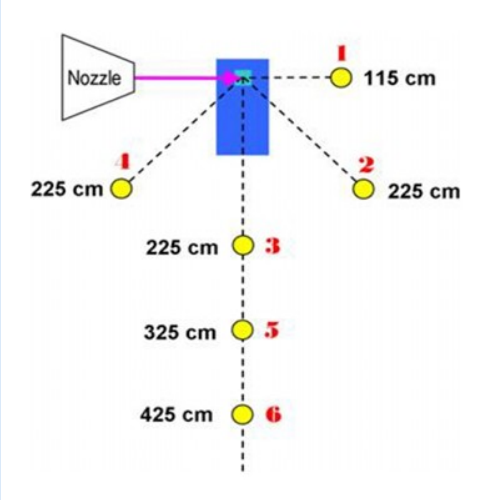

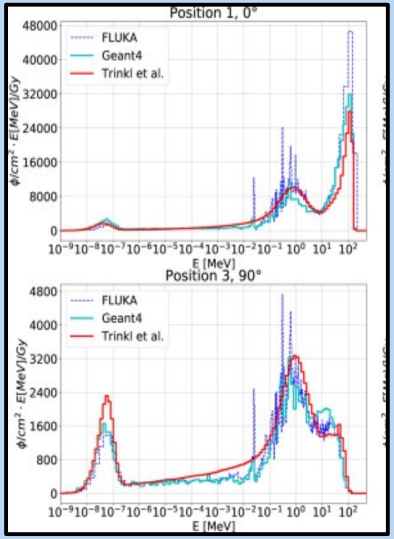

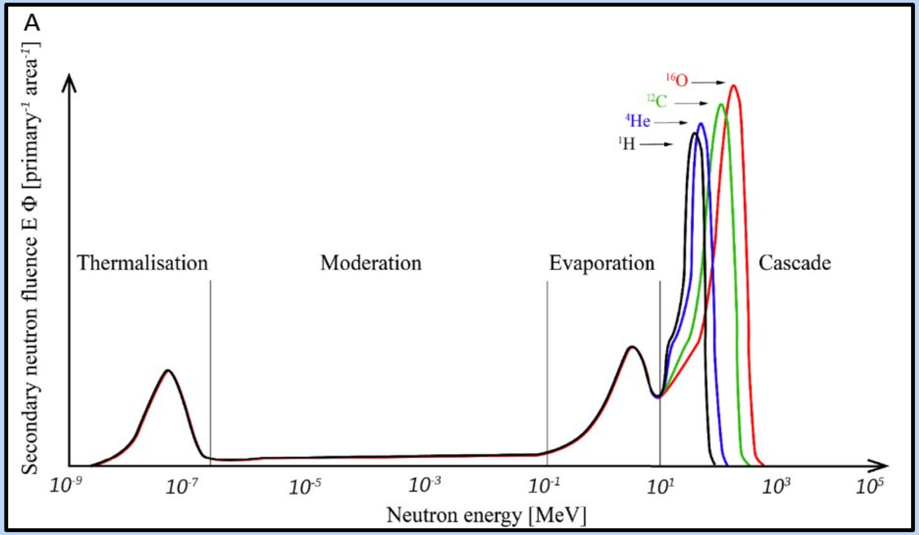

Some challenges:

- **Angular** dependence
- **Wide energies range**
- **Projectile** dependence
- Dependent on the **technology**
- **Very high flux**

Data stream in hadrontherapy

- Pulsed fields
- Very high instantaneus rate
- Very high gamma and neutron secondary production
- Possible charged particles reach your detector

Pileup and dead time

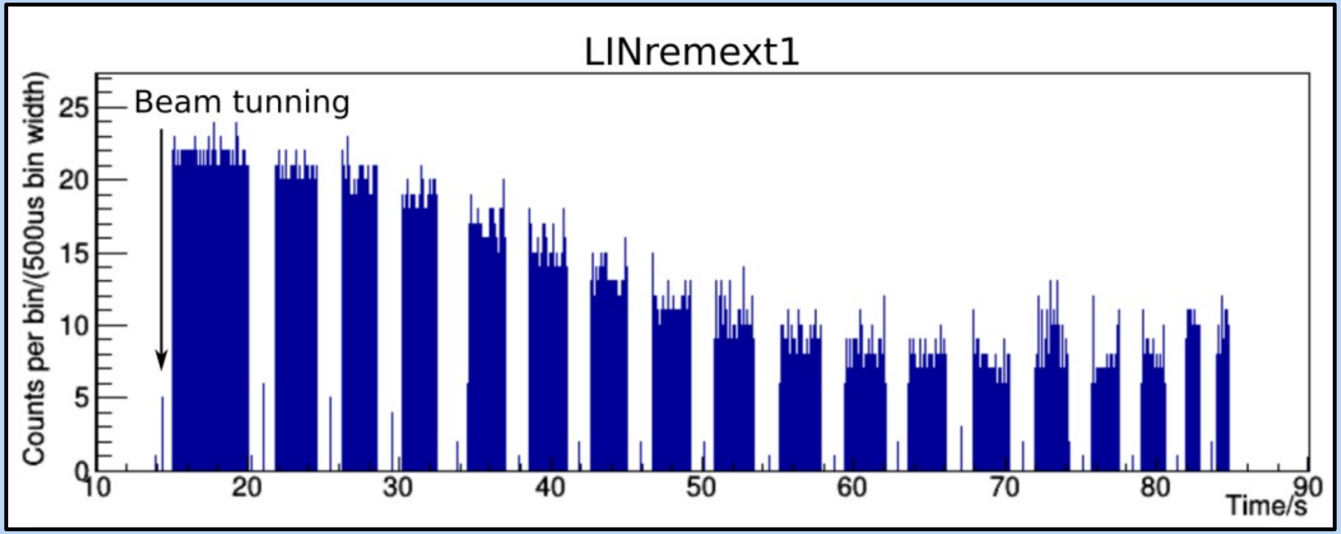

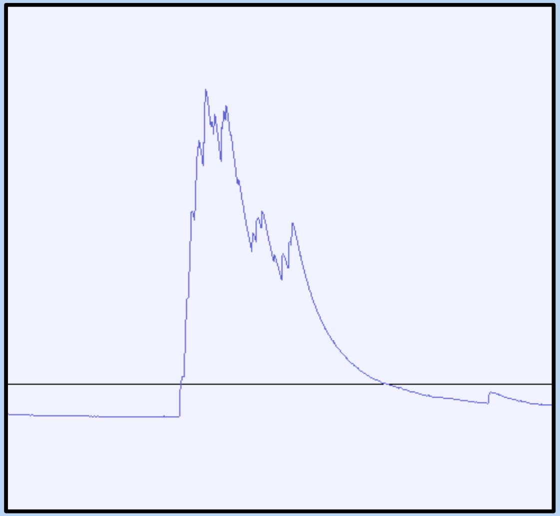

Comercial dosimeter

Most of the commercial dosimeter are not suited for pulsed neutron fields (pile-up effect). **They present underestimation of the dose beyond 10 nSv/burst.**

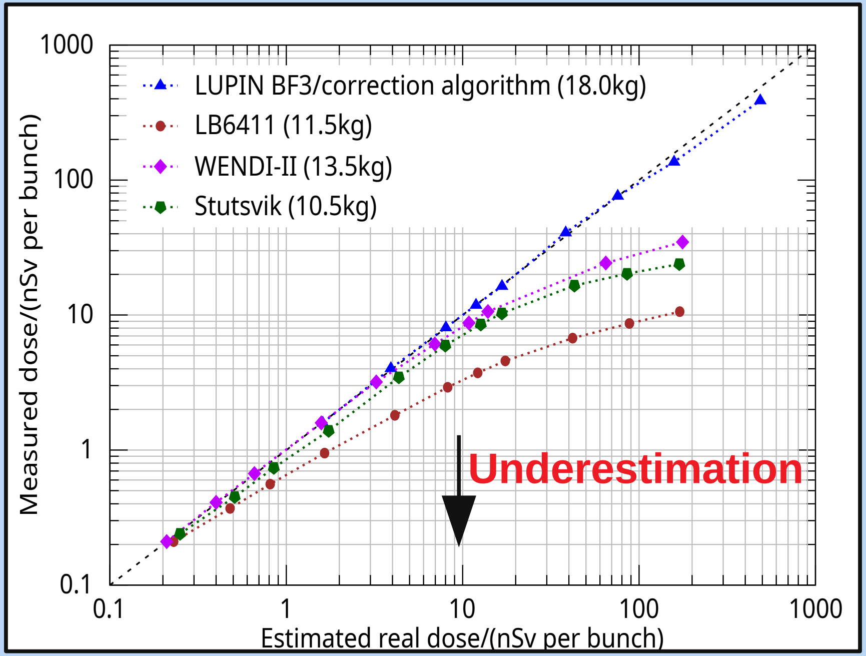

Caresana+ NIMA 737 (2014)

GSI

LINrem: Ambient neutron dosimeter

- Precise response with “light” weigth.
- DAQ suited for complex radiation fields.
- Digital acquisition and readout.
- Compatible with ICRU95 (new standard)
- Very low gamma efficiency

& passive

Patents granted in the US, EU, JP

TRL6 → Proved that work in a relevant enviroment

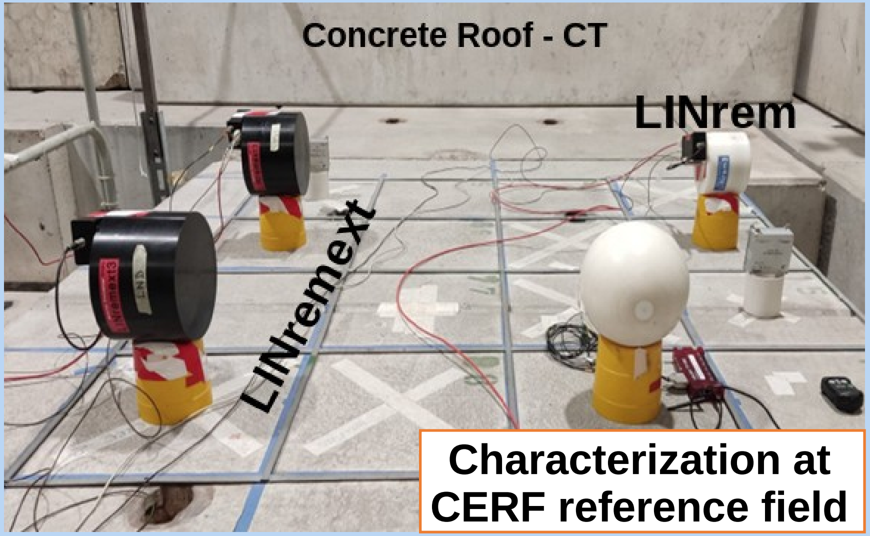

Characterization at CERF reference field

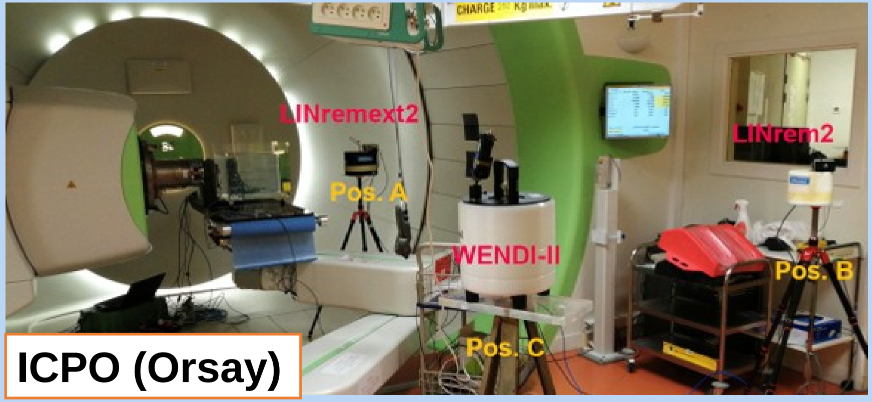

ICPO (Orsay)

LINrem software solution

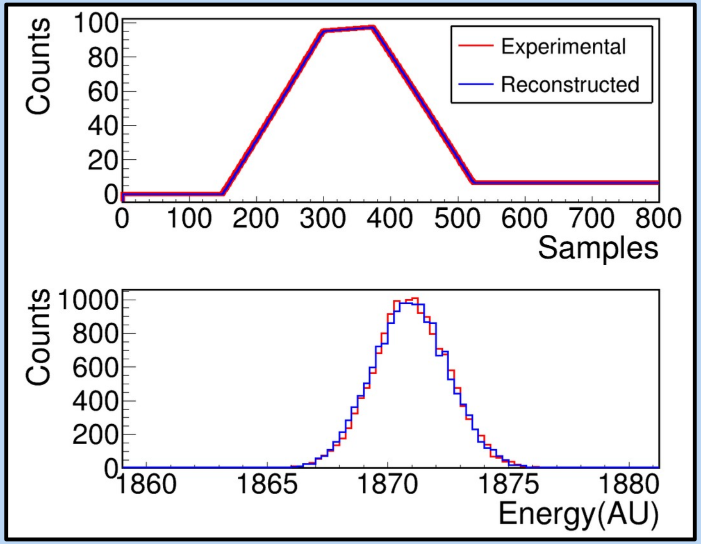

+

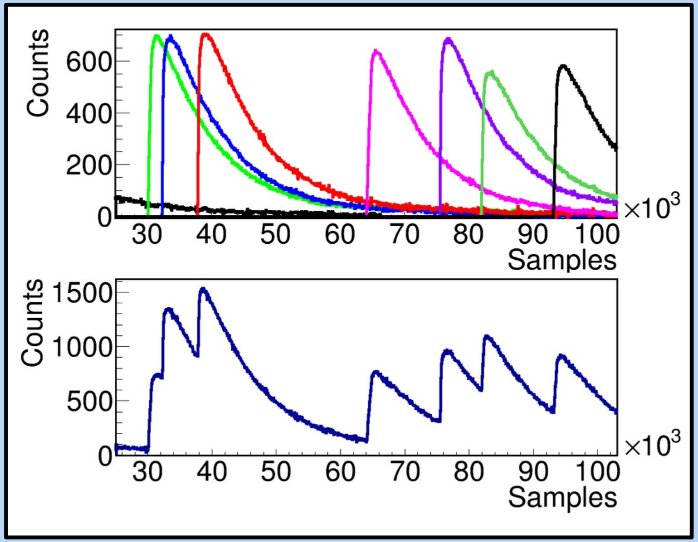

DAQ firmware emulation

Data stream simulation

LINrem solution

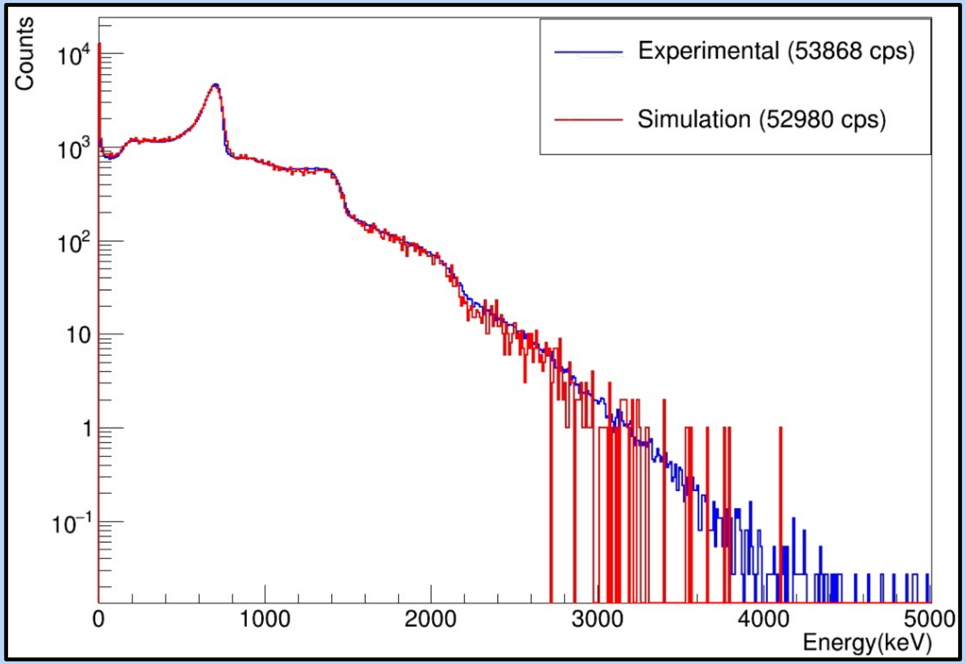

Accurate energy simulation

Recover linearity

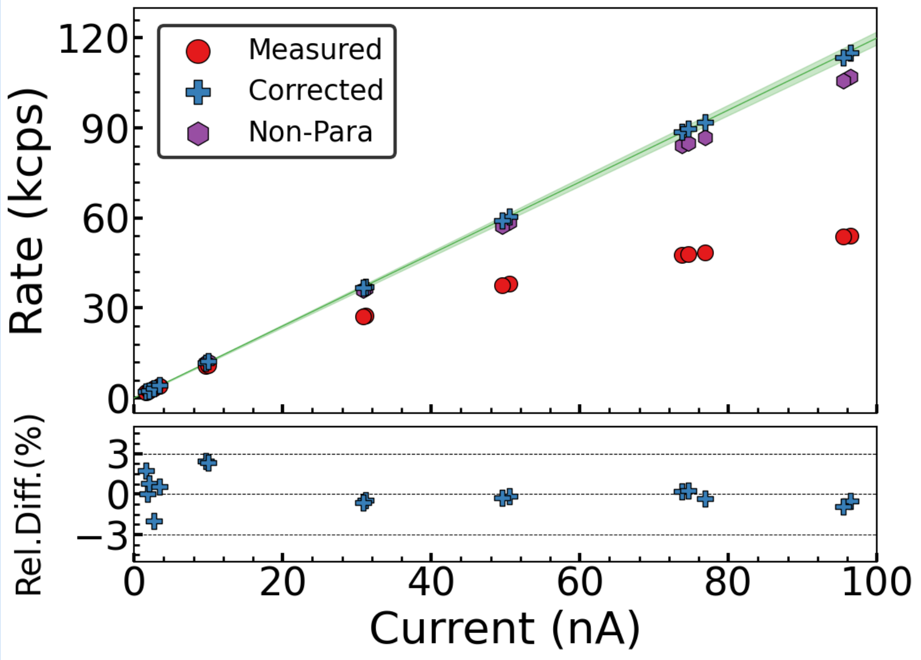

FEBEX?

STRUCK SIS3316
16 ch
14 bit
250MHz

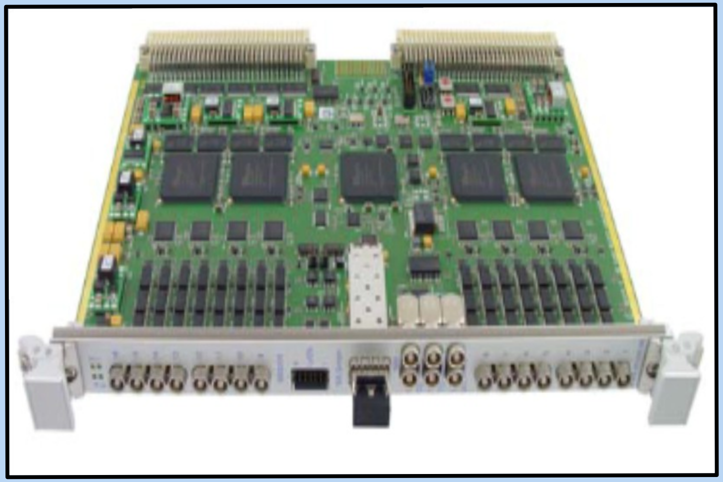

Same structure as FEBEX

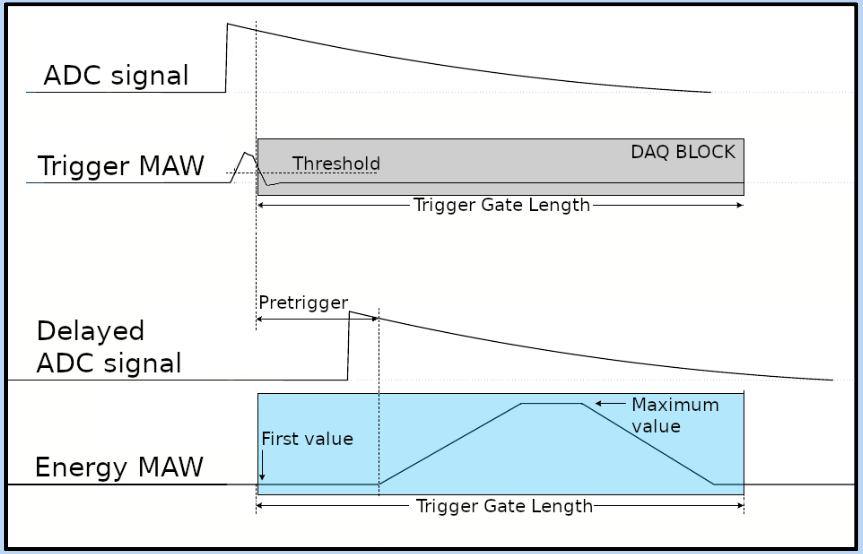

Thank you!

How were the elements from the universe made?

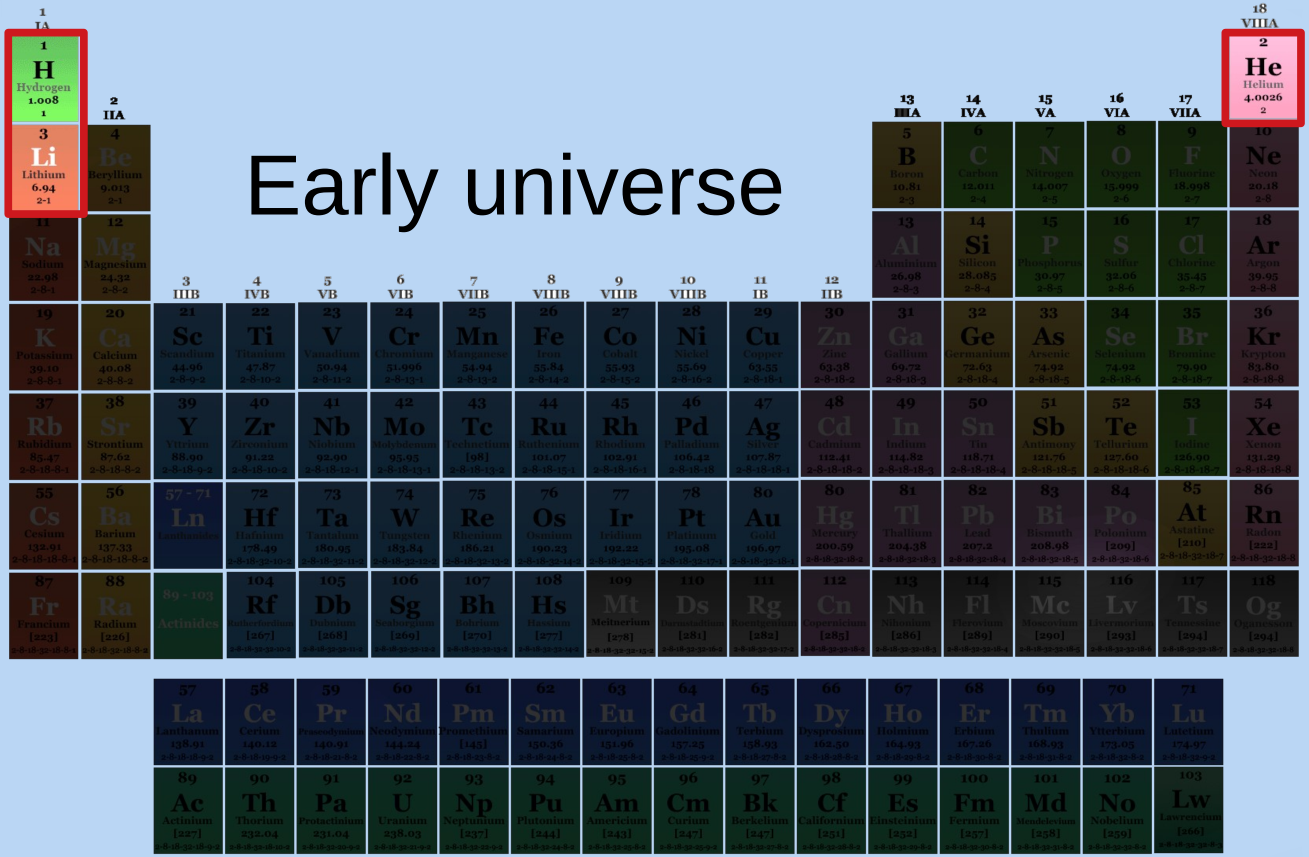

Stellar nuclesynthesis

In the core of stars, **nuclear fusion** takes place.

1. H burning (PP-Chain / CNO-cycle)
2. He burning (Triple-α)
3. .....

Stops at Fe (Z=26)!

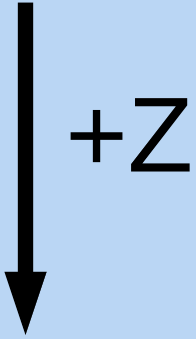

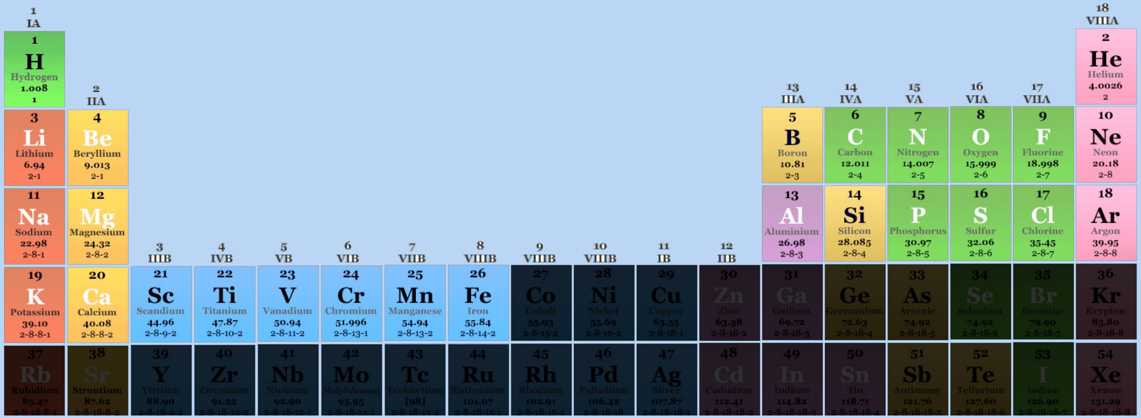

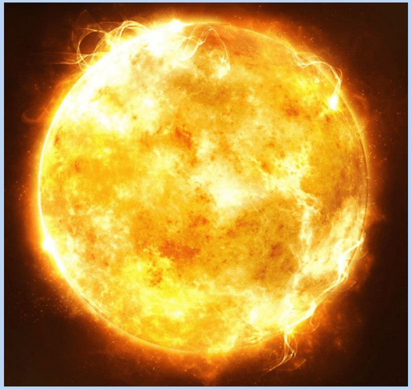

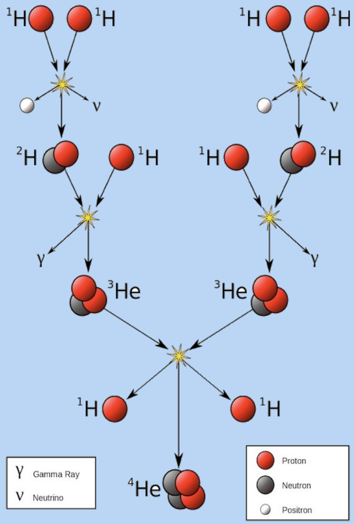

Science Learning Hub (Adapted)

And heavy nuclei?

In 1957, the B²FH and Cameron papers proposed a solution for the formation of heavy elements:

Neutron capture (n,γ)

↓ Tends to instability

β⁻-decay

↓ Tends to estability

Z increase

$$\overbrace{{}^{A}_{Z}X + n \rightarrow}^{\text{Neutron capture}} \underbrace{{}^{A+1}_{Z}X \rightarrow {}^{A+1}_{Z+1}Y + e^{-} + \bar{\nu}}_{\beta^{-}\text{- decay}}$$

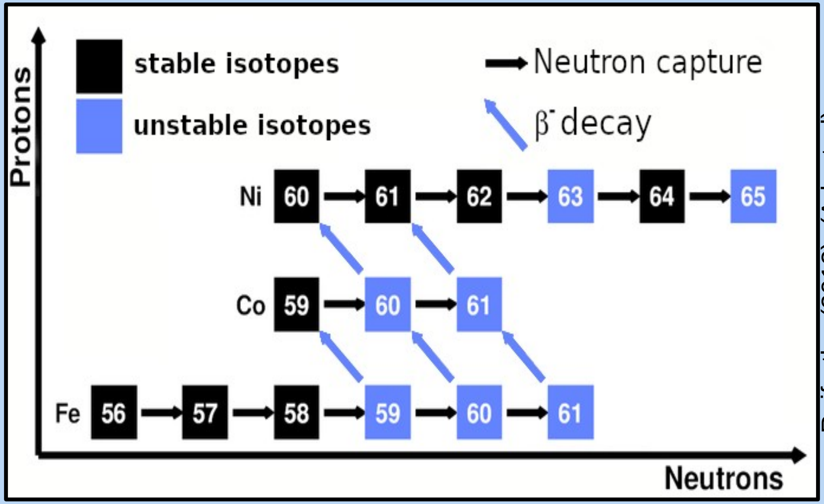

Reifarth+ (2013). (Adapted)

BigRIPS

Production

^{238}U beam + Be target

In-flight fission

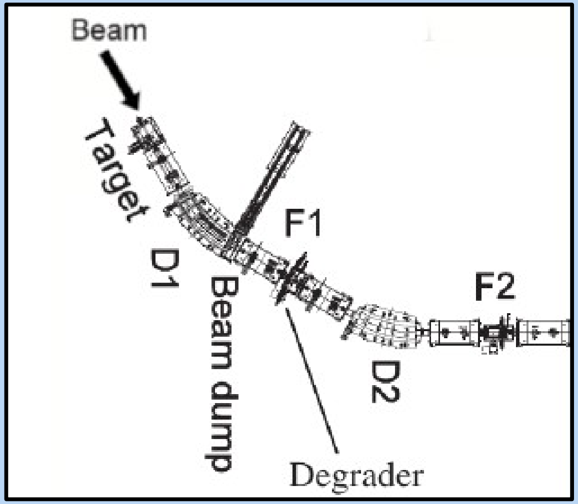

Identification

ToF−Bρ−ΔE method

Isotope identification

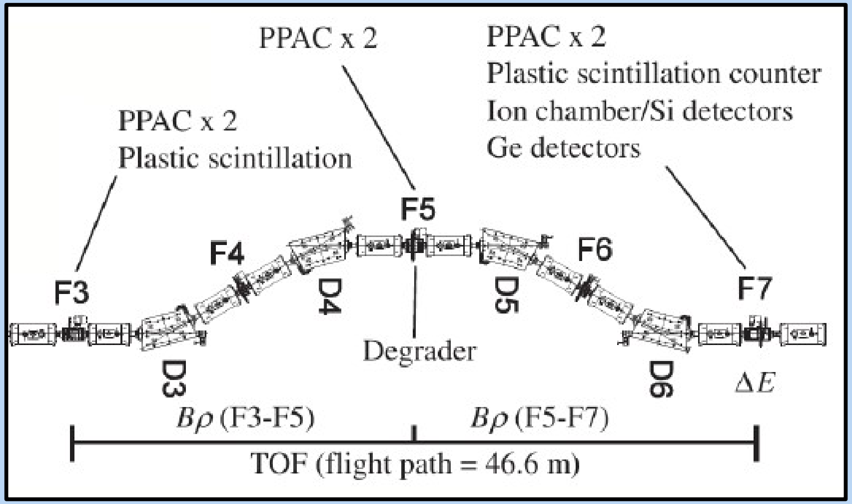

Kubo+ PTEP (2012)

Fukuda+ NIMB 317(2013)

Advanced implantation array: AIDA

- Detect **implanted ions** and **β-decays**.
- Stack of 6 Doubled-sided Silicon Strip Detectors (DSSDs).
- Each side contains 128 strips ---> **Position reconstruction.**
- Allows the detection of Implanted ions (**GeV**) and β-decay (tenths **MeV**).

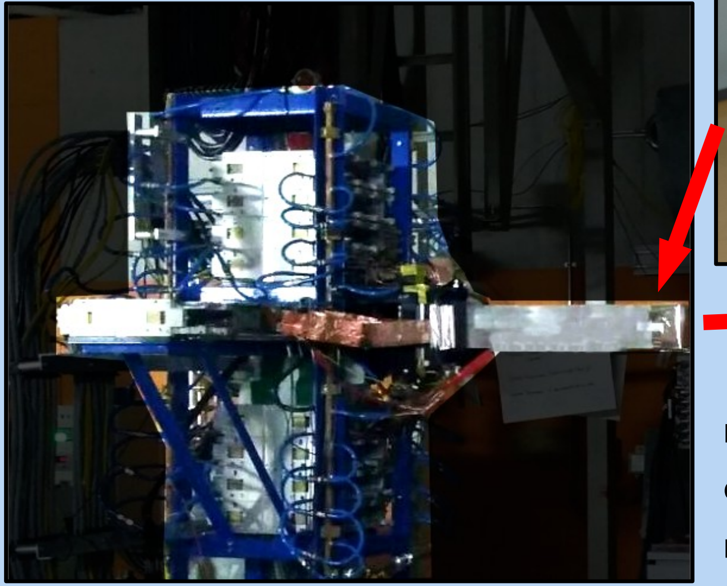

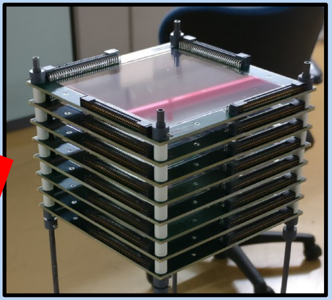

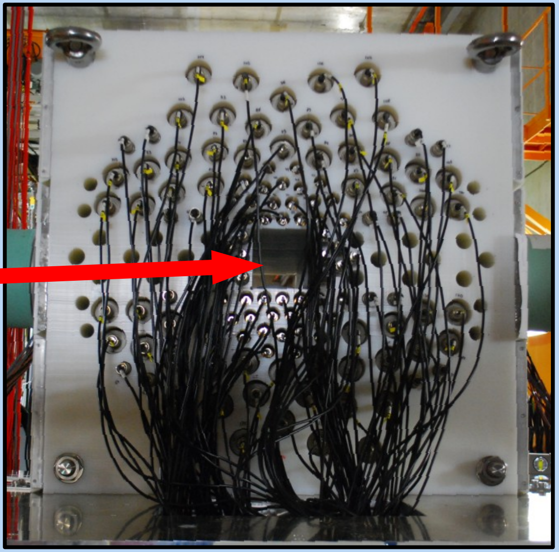

Hall+ NIMA 1050 (2023)

Griffin PhD Thesis (2019)

Hall PhD Thesis (2020)

BRIKEN characterization

- We conducted several **calibration measurements** using a **^{252}Cf source.**
- **Two** different detector **configurations** (with and w/o HPGe clovers)
- **Innovative digital** implementation of the **Neutron Multiplicity Counting** methodology to determine the detector's efficiency.

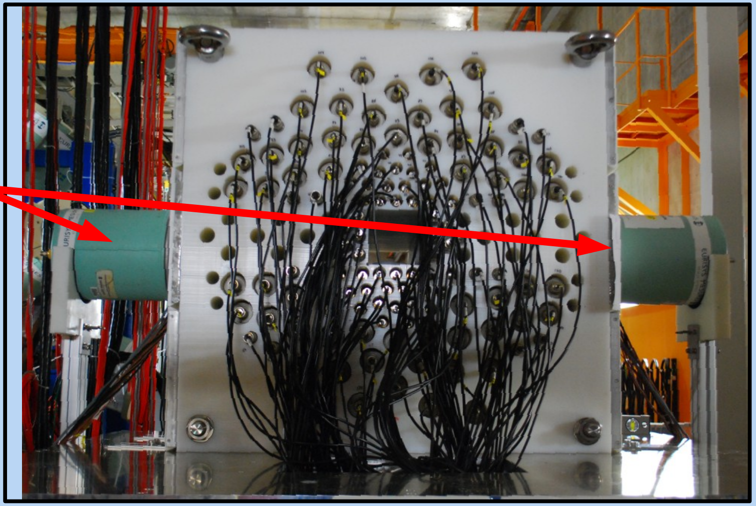

$$\varepsilon = \frac{2\nu_{s1}}{\nu_{s2}}\frac{D}{S}$$

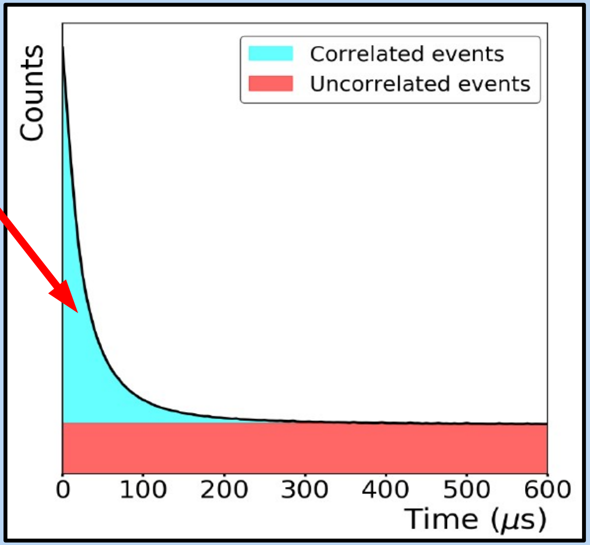

^{252}Cf calibration measurements

- We employed **two equivalent methods** to evaluate the background that yielded compatible results.
- **Sizable effect** of the **clover** presence on the neutron **efficiency**

Setup	ε_{Neu} (%)	σ_{Total}(%)
No Clover	60.19	+0.13 -0.08
Clover	62.03	+0.12 -0.06

Non-Clover

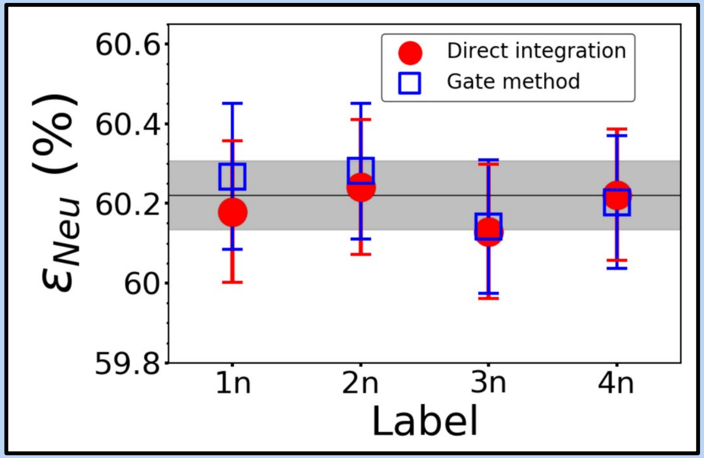

Clover

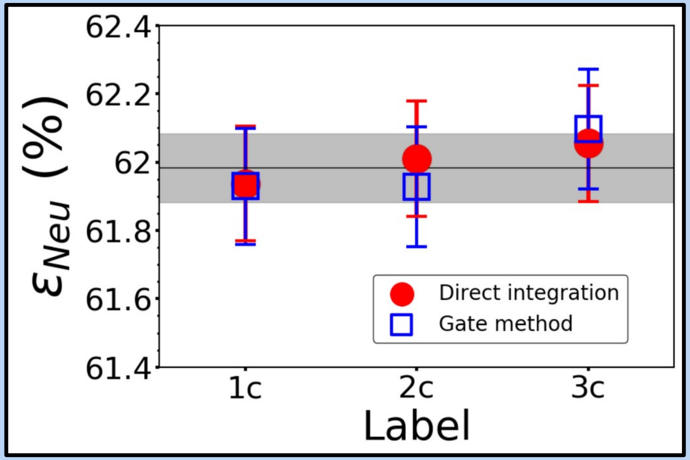

Neutron transport

The crystal clovers act as a **neutron scatterer**, shadowing the detectors behind them and increasing the efficiency of the inner tubes.

Setup	ε_{Neu} (%)	σ_{Total}(%)
No Clover	60.19	+0.13 -0.08
Clover	62.03	+0.12 -0.06

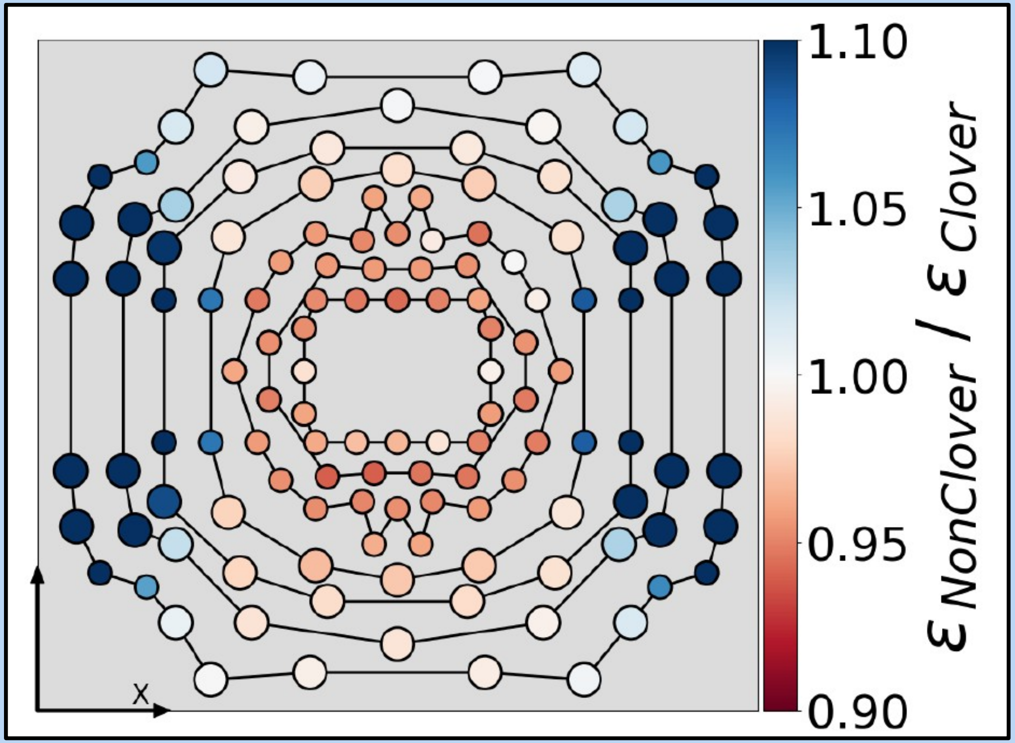

Non clover simulation

	Efficiency (%)	Error(%)
Simulation	62.28	0.03
Experimental	60.21	+0.13 -0.08

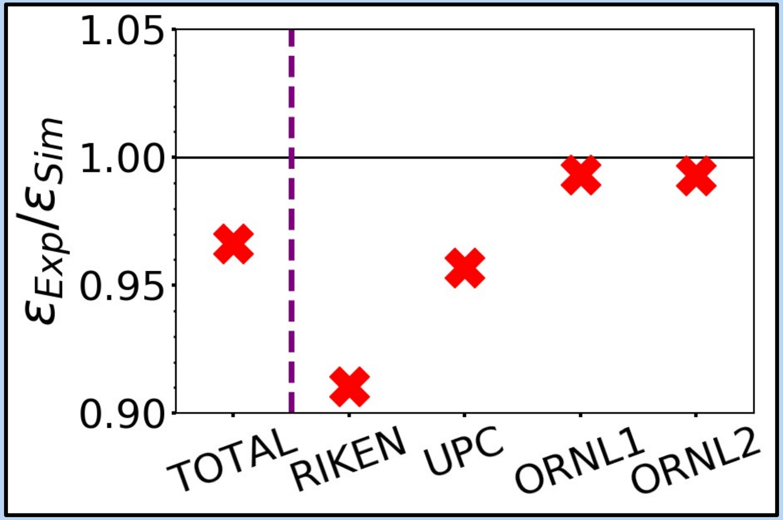

- Simulation **overestimation** of ~3.3%.
- The discrepancies are produced mainly by the **RIKEN's** and **UPC's** tubes.
- Partially attributed to the **gain reduction** at the edges of the active area of ^{3}He tubes.

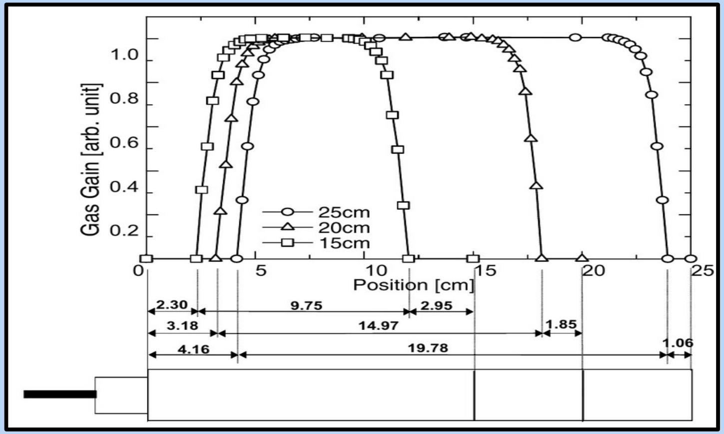

Kudo+ NIMB (2004)

Peplowski+ NIMA (2020)

Non clover simulation

	Efficiency (%)	Error(%)
Simulation	60.38	0.03
Experimental	60.21	+0.13 -0.08

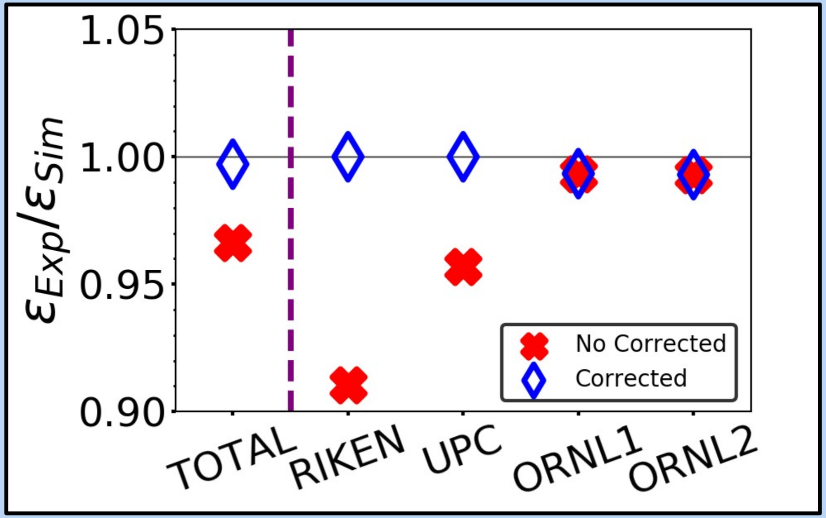

- Simulation **overestimation** of ∼3.3%.
- The discrepancies are produced mainly by the **RIKEN's** and **UPC's** tubes.
- Partially attributed to the **gain reduction** at the edges of the active area of ^{3}He tubes.
- Common aproach of applying correction factors to **reacalibrate** the simulation:
  - 0.91 for the RIKEN tubes.
  - 0.96 for the UPC tubes.

Merger and coincidence curves

- implant-β coincidence ---> **Decay curve (iβ)**

The analysis is based on the **statistical coincidence** of multiple events.

Tolosa+ NIMA (2019)

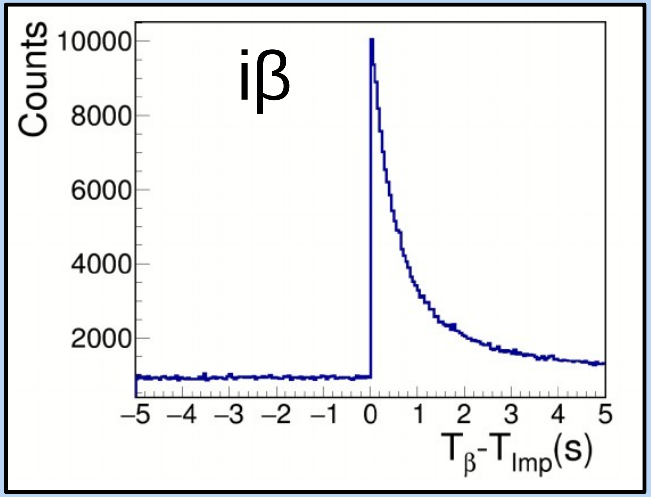

Spacial constrains are set to reduce the accidental background.

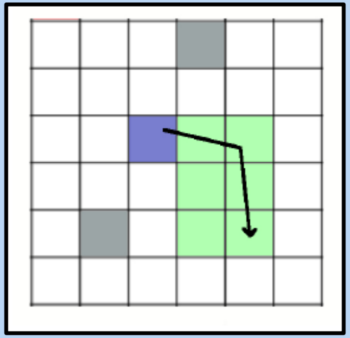

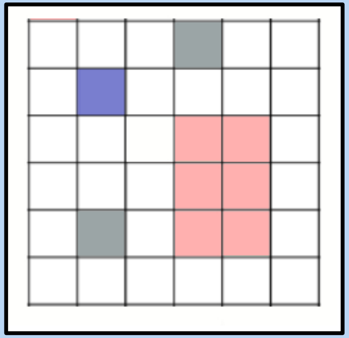

Merger and coincidence curves

- implant-β coincidence ---> **Decay curve (iβ)**
- β-neutron coincidence ---> **Moderation curve (βn)**

The analysis is based on the **statistical coincidence** of multiple events.

Tolosa+ NIMA (2019)

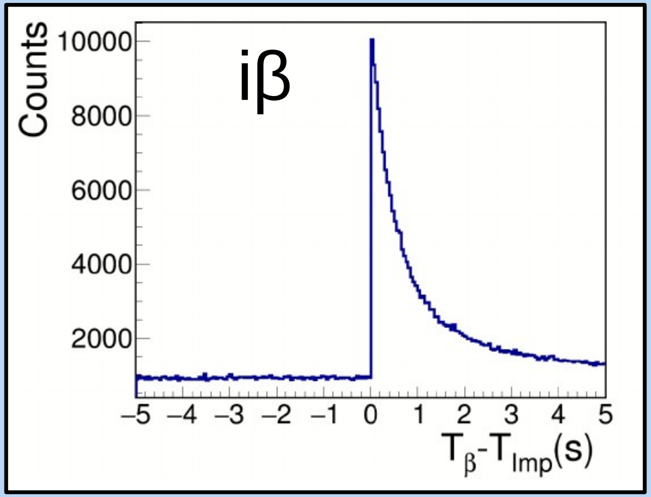

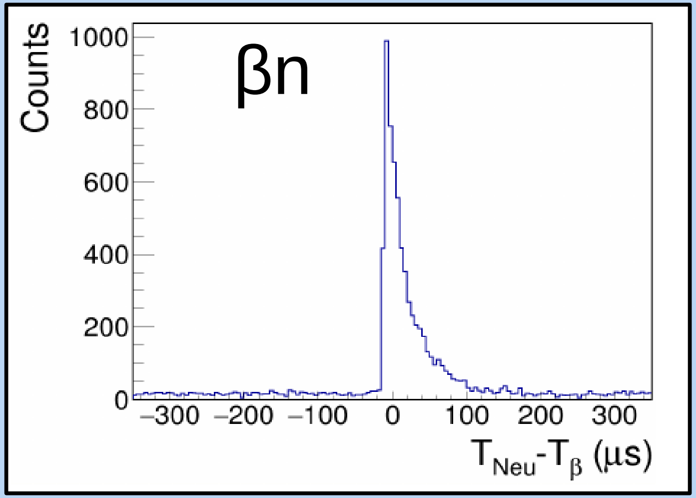

Improve signal to noise ratio

Methods of **reducing** the background:

– β energy threshold.

Threshold only on rear strips

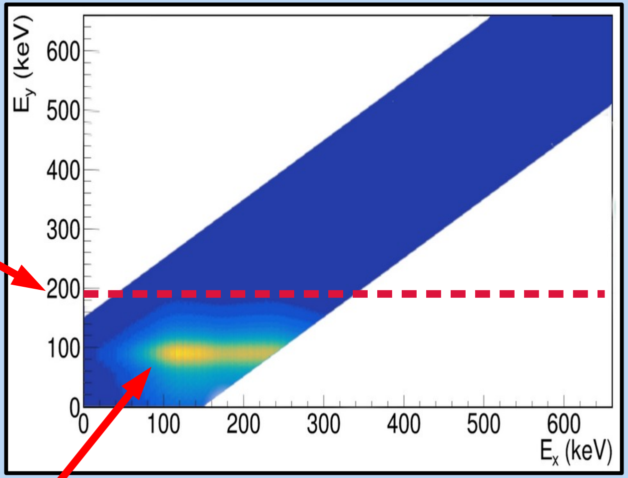

Electronic noise

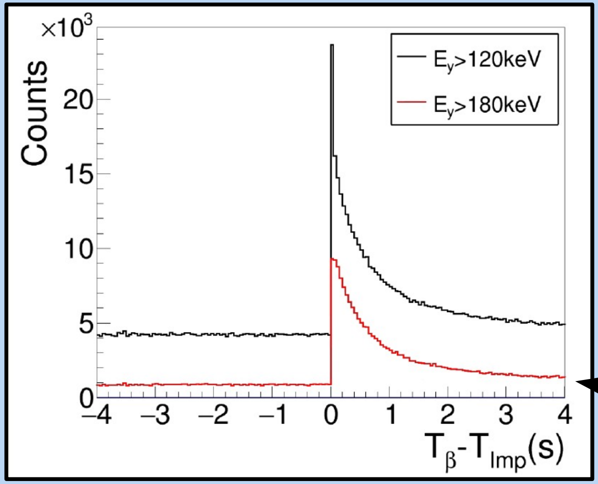

Background reduction of a factor 4

Improve signal to noise ratio

Methods of **reducing** the background:

- β energy threshold.
- Build **vetoes for β and neutron** events using ancillary detectors.

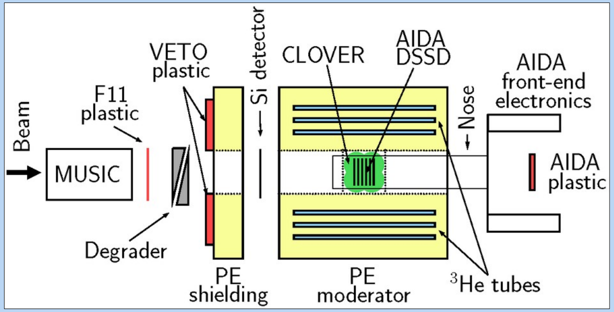

Tolosa+ NIMA (2019)

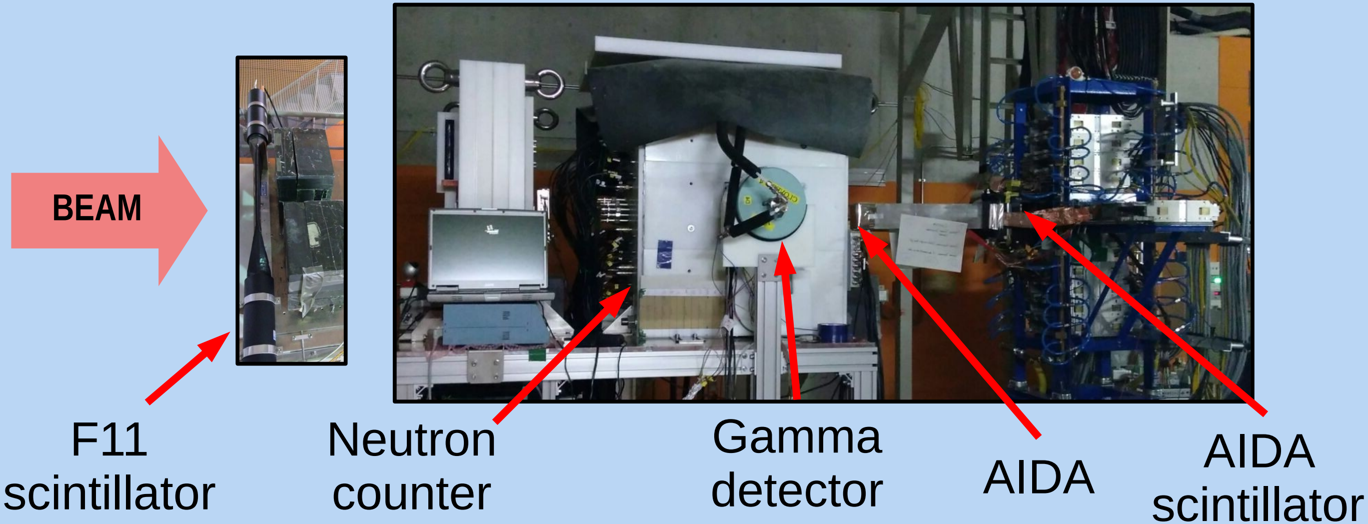

β-anc coincidence

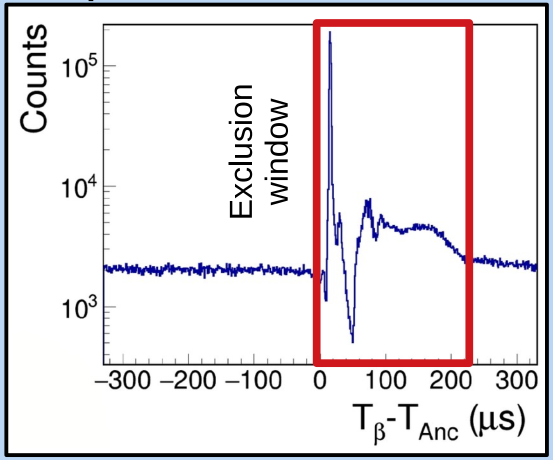

Inconsistent residuum case: ^{156}Pr

- High statistics ($3 \cdot 10^6$ implants)
- Large Q_β (8.8 MeV) and $Q_{\beta n}$ (2.8 MeV)
- Well-measured decay chain

^{156}Pr	Value	σ_{Total}	IAEA
$T_{1/2}$(ms)	511.6	8.1	444 (6)
P_{1n}(%)	1.84	0.12	-

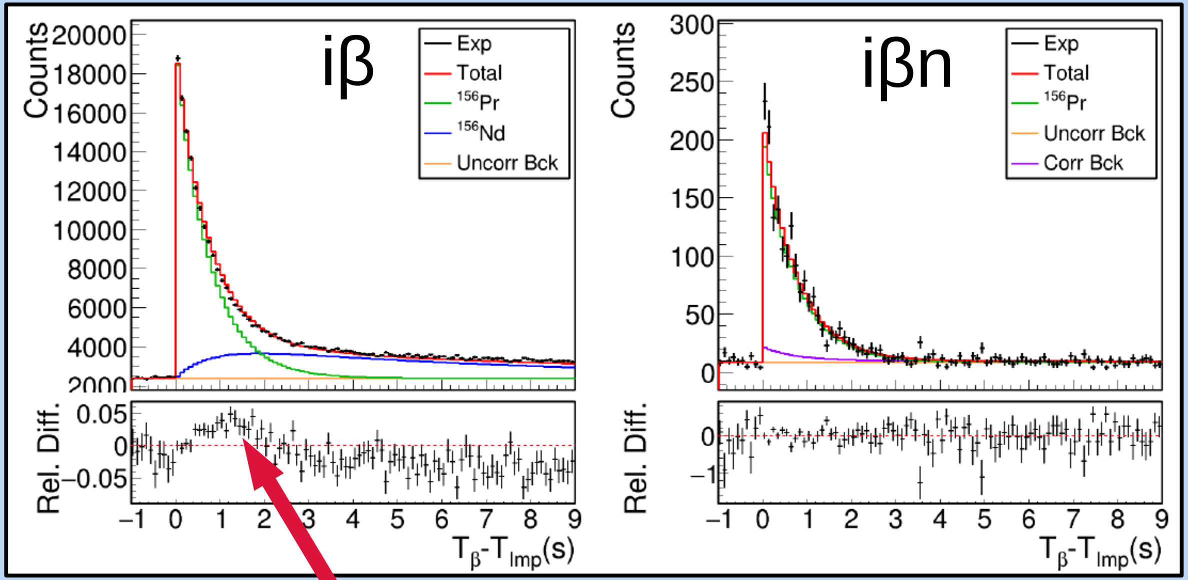

- Large discrepancy with previous measurements.
- Possible existence of an isomeric state.
- Clear **systematic deviation** on the residual!

Low statistic case: ^{162}Nd

- Very low statistics (3000 implants)
- Qβ (7 MeV) and Qβn (3 MeV)
- Well-measured decay chain

^{162}Nd	Value	σ_{Total}	IAEA
$T_{1/2}$(ms)	308.1	63.9	310 (200)
P_{1n}(%)	3.73	1.46	-

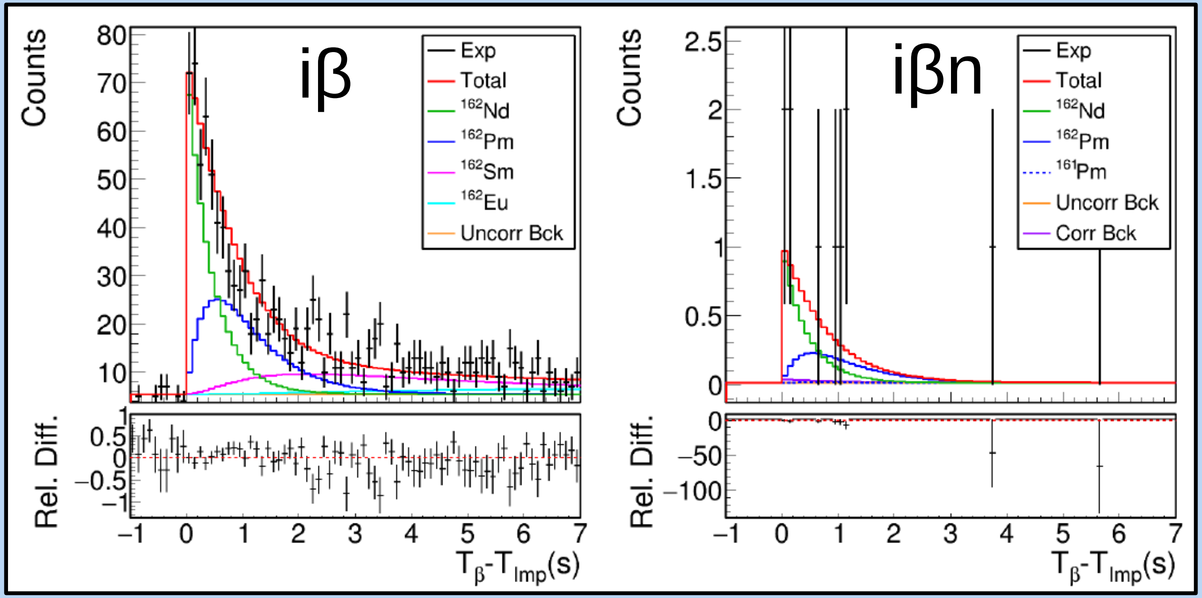

- Result with a large uncertainty but compatible with previous measurements.
- Unreliable 1-neutron gated fit. P_{1n} determined using an alternative method used only for ^{153}Ba and ^{162}Nd.

Small P_{1n} case: ^{154}Ce

- High statistics ($2.4\cdot10^5$ implants)
- Small Q_β (5.64 MeV) and $Q_{\beta n}$ (1.28 MeV)
- Decay chain measured with high precision.

^{154}Ce	Value	σ_{Total}	IAEA
$T_{1/2}$(ms)	691.3	8.4	722 (14)
P_{1n}(%)	0.31	0.07	-

Very small P_{1n} but high accuracy

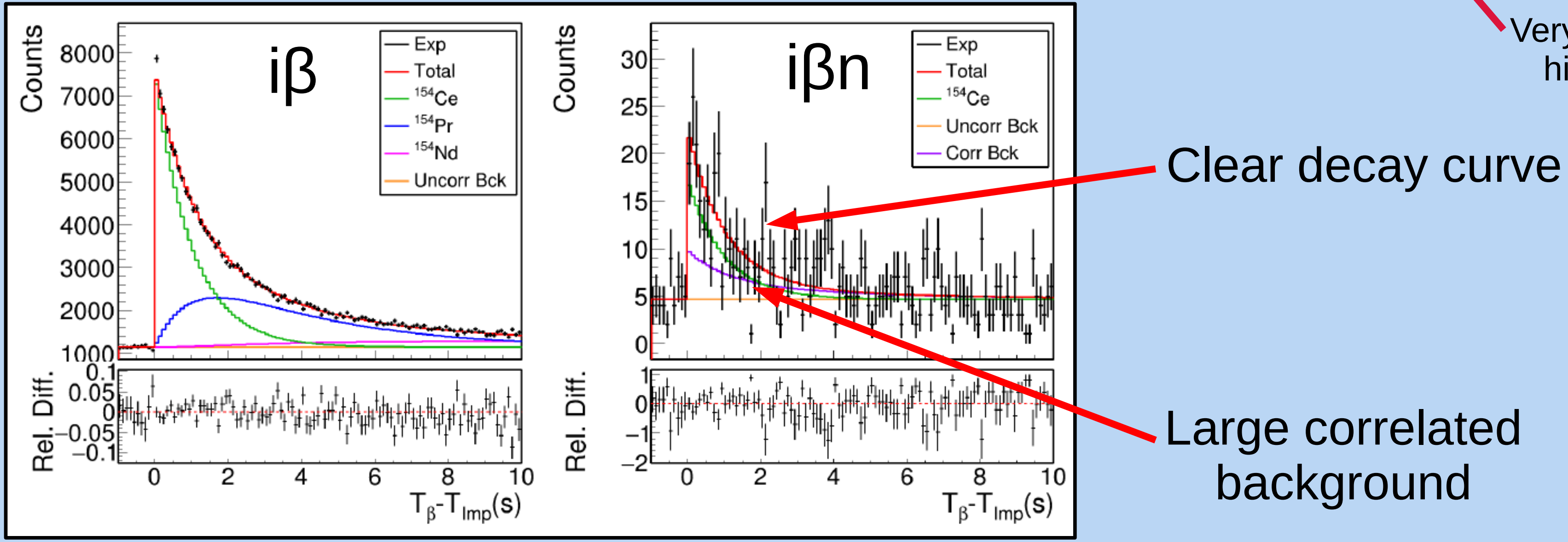

Neutron efficiency

Neutron detection efficiency depends on the **neutron energy spectra**, which is **unknown for all the cases** studied in this thesis.

Assumption that:

$$\langle \varepsilon_n(E) \rangle \approx \varepsilon_n(\langle E \rangle)$$

This thesis nuclei **<E> ≤ 1 MeV**

↓

Neutron efficiency --> **isotope-independent.**

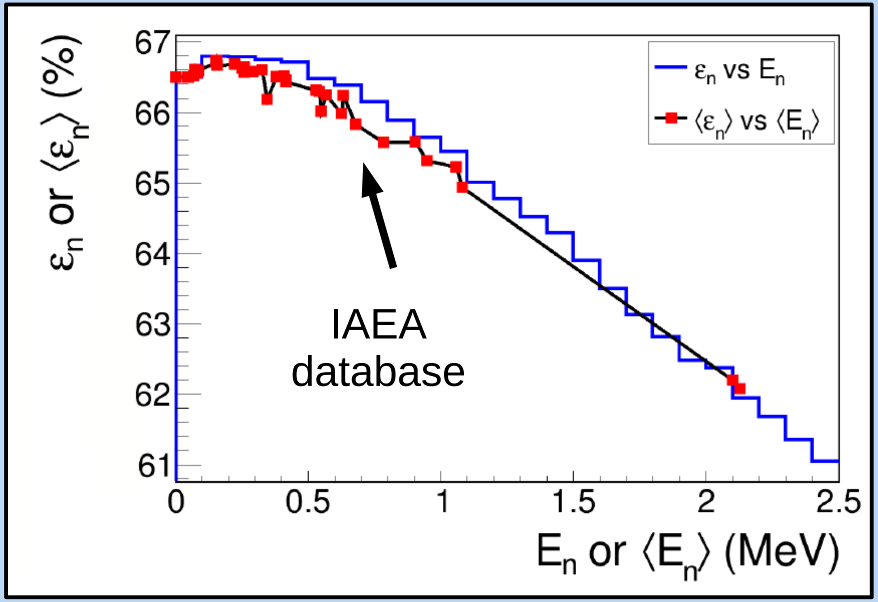

Nominal eff: 66.5(6) %
Corrections:
β-neutron coincidence: 98.5%
Veto induced dead time: 95.6%

Final effective neutron efficiency:
ε_n = 62.5(6) %

Nuclear structure calculations

- **Revision** of the Marketin et al. Model (QRPA).
- The calculation includes **GT and FF** transitions.

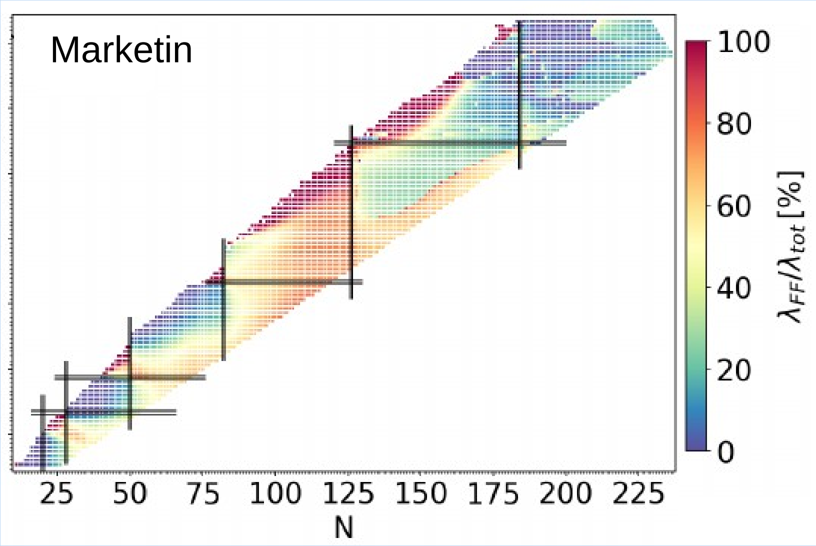

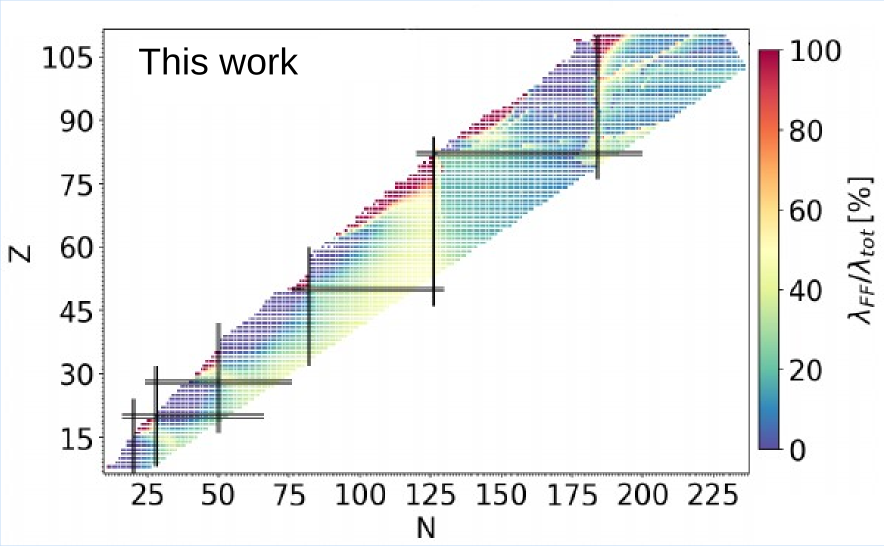

Smearing function

- The QRPA calculation only computes **some** of the excited levels.
- To account for **higher-order terms**, we add a **smearing function** to obtain a smoother distribution.
- The **σ** is a **free parameter** that can be adjusted to reproduce the experimental data. We selected a value of **1.6 MeV**.

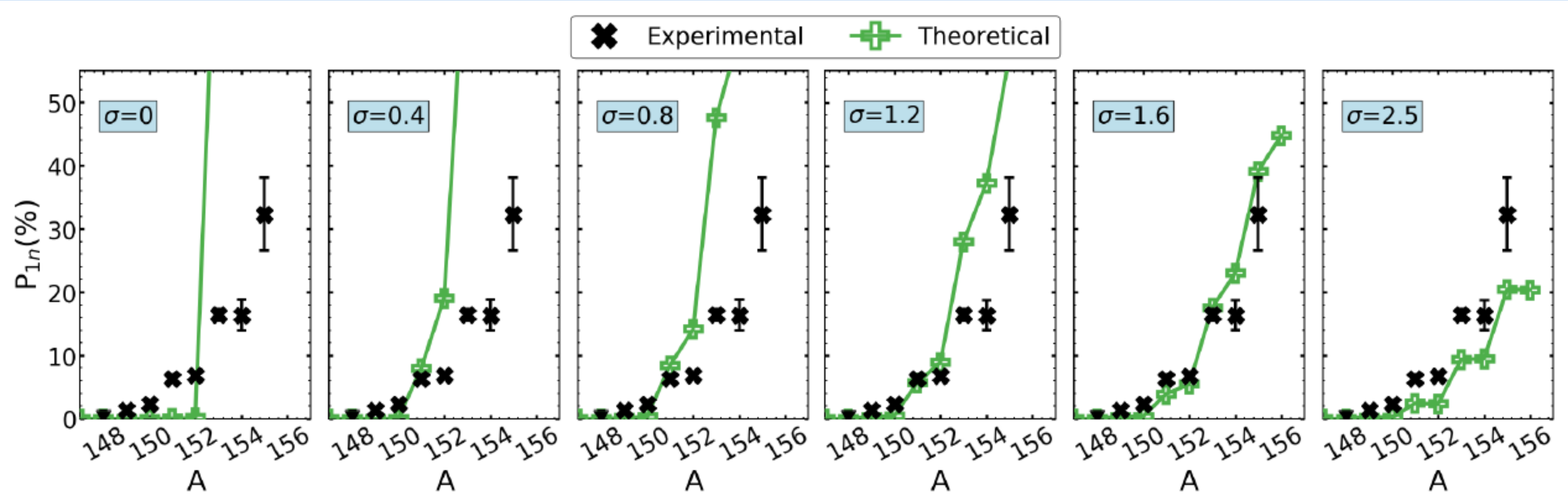

Slow neutron-capture process

- $T_{n\gamma} >> T_\beta$
- Low neutron density.
- Operates along the valley of stability, nuclei nucleai are stable or very long-lived.
- Starts around the iron group.
- This process is extremely slow, operating over hundreds to thousands of years.

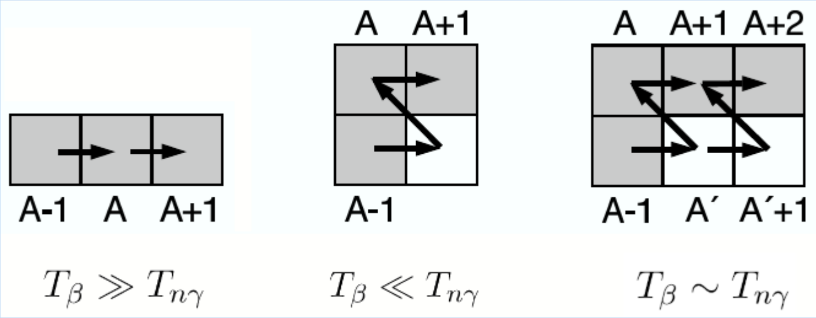

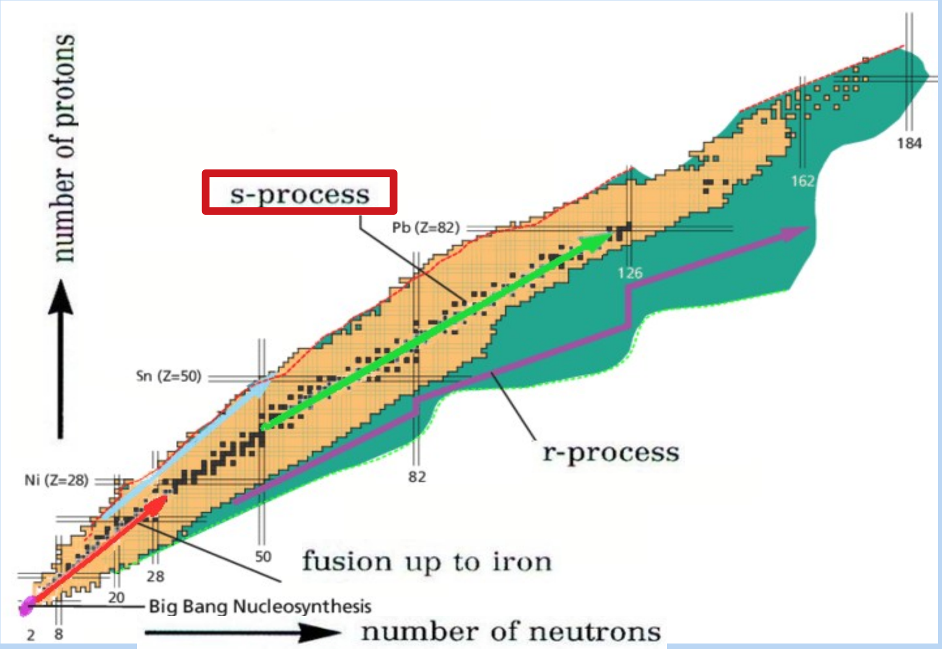

T. Rodríguez, Journal of Physics: Conference Series 503 (2014)

Rapid neutron-capture process

- Extremely high neutron density environment.
- Operates far from the valley of stability, creating very neutron-rich, unstable isotopes.
- This process is fast, operating over μs to ms.

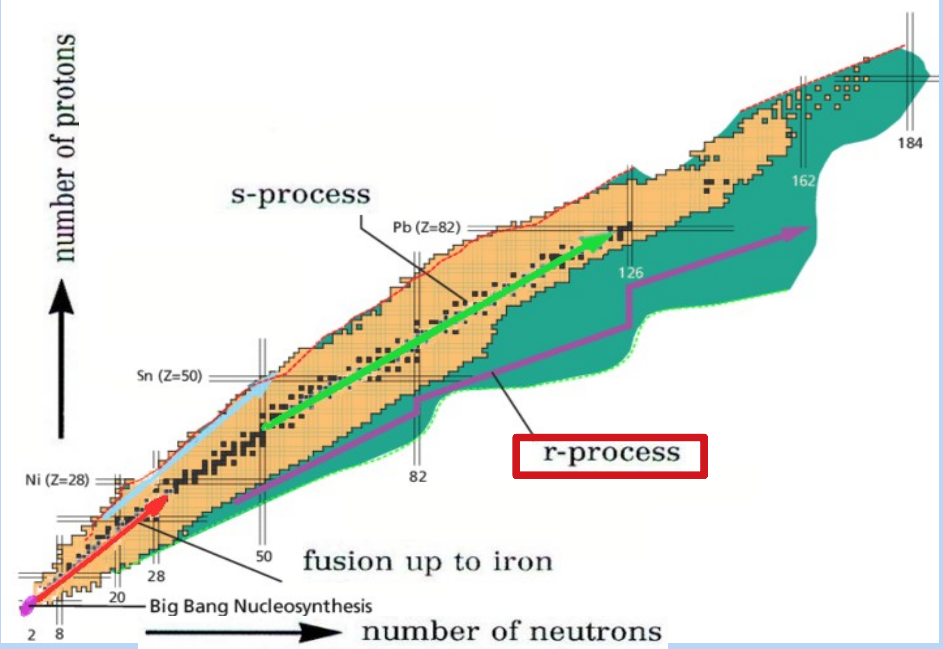

T. Rodríguez, Journal of Physics: Conference Series 503 (2014)

Rapid neutron-capture process

- Extremely high neutron density environment.
- Operates far from the valley of stability, creating very neutron-rich, unstable isotopes.
- This process is fast, operating over μs to ms.
- Three reaction channels compete:
  - Neutron capture (n,γ)
  - Photodissociation (γ,n)
  - Beta-decay

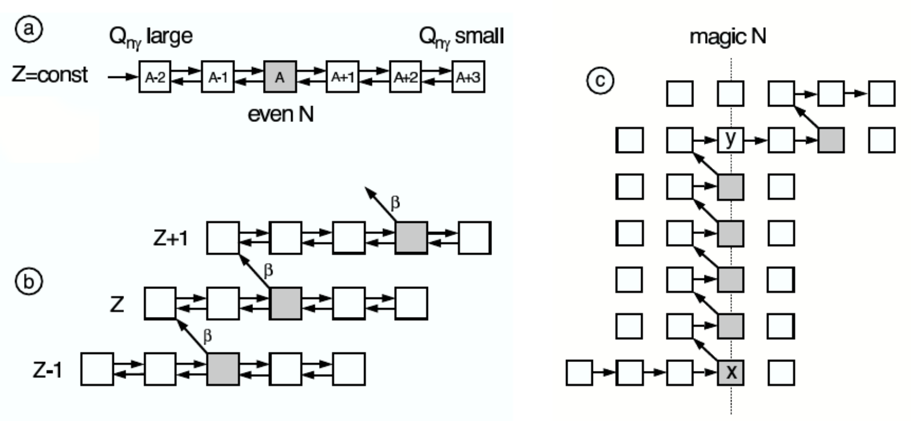

REP importance

On the r-process we can distinguish between two astrophysical environments.

Hot r-process:

High temperatures (T∼1 GK).

Tnγ = Tγn << Tβ.

(n,γ) ↔ (γ,n) equilibrium.

Cold r-process:

Lower temperatures (<0.5 GK).

Tnγ = Tβ << Tγn.

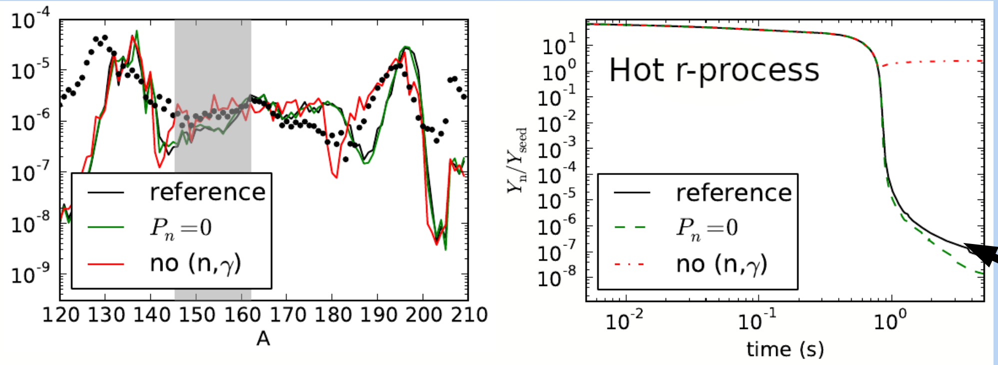

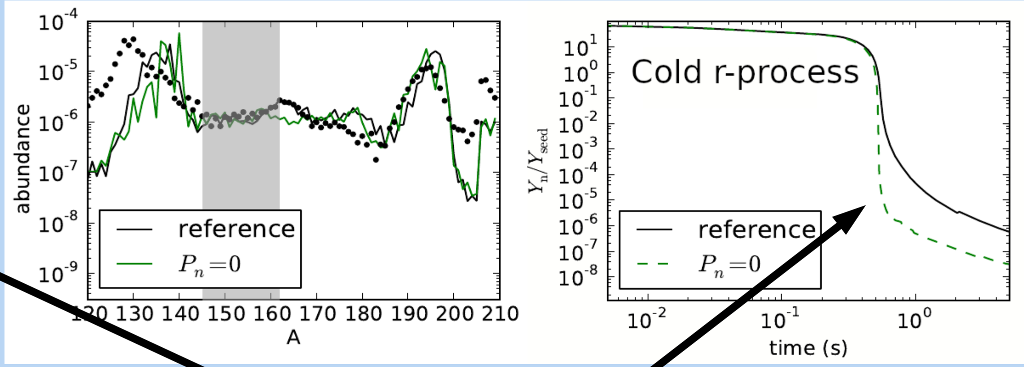

The REP is the only r-proces peak formed after the freeze-out phase.

RIKEN Nishina Center

Rare Isotope Beam Factory (RIBF)

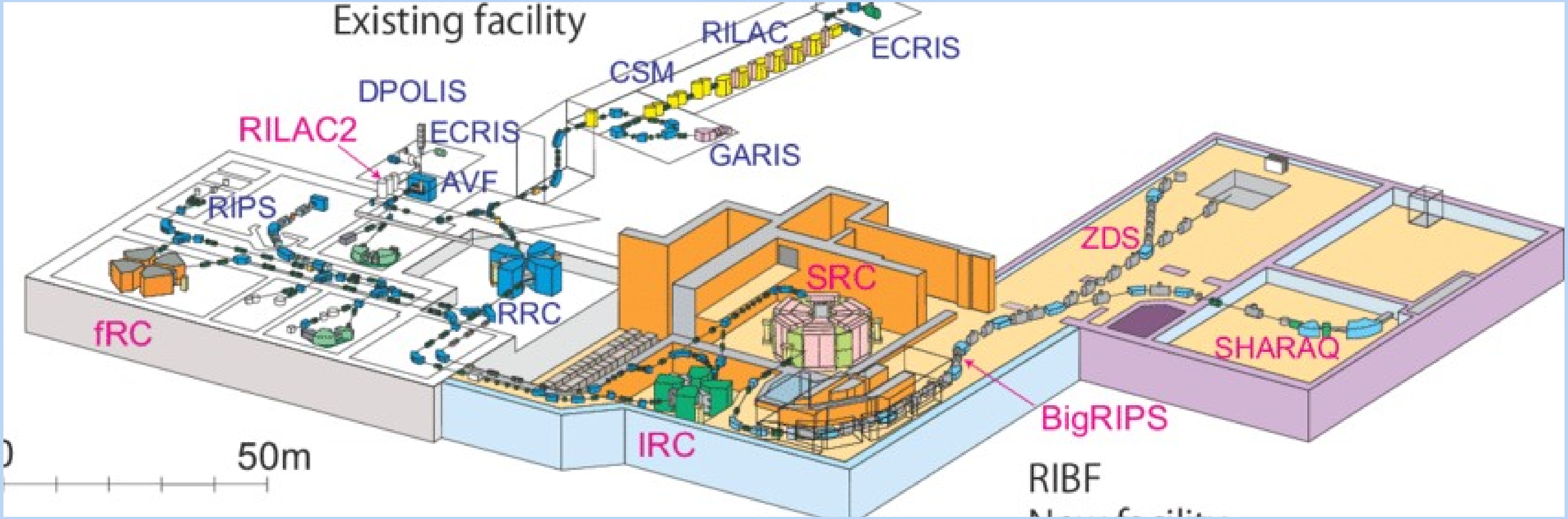

BigRIPS

Superconducting Radioactive Isotope Beam Separator

Goal:

- Production
- Separation
- Identification

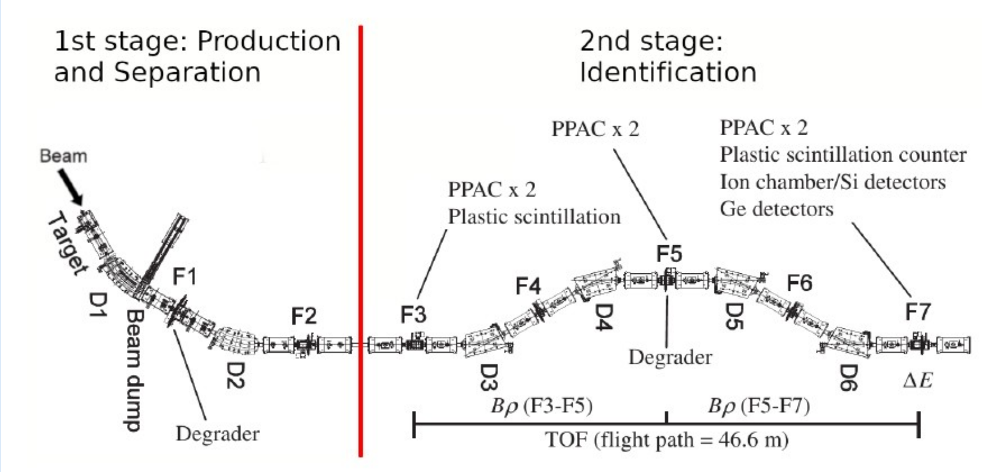

Setup:

- 14 Superconducting Tripled Quadrupoles
- 6 dipoles magnets
  - Forming 7 focal points
- Position-Sensitive Plate Avalanche Counters (PPACs)
- MUlti-Sampling Ionization Chamber (MUSIC)

BigRIPS

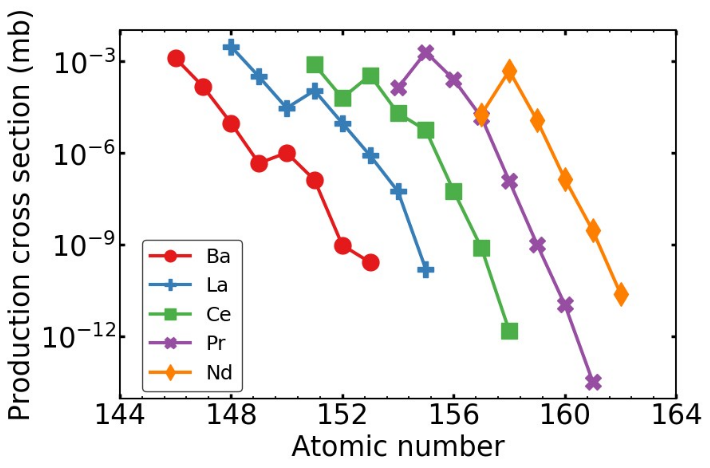

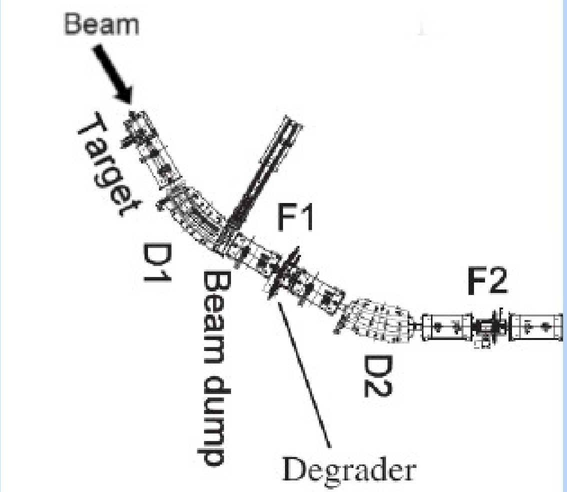

The production and separation take place in the first part of BigRIPS (F1 to F3).

Production:

Primary 238U beam: 350MeV/a and 40pnA.

Beryllium target to produce in-flight fission.

Energy-based separation:

Employs the magnetic rigidity of D1 and D2.

The A/Q produces a substantial background removal.

Identification

<u>ToF−Bρ−ΔE</u> method to measure A/Q and Z:

- Plastic scintillators at F3 and F7 --> ToF/velocity
- Magnetic dipoles --> Bρ
- MUSIC at F7 --> ΔE

$$\frac{A}{Q} = \frac{B\rho}{\beta\gamma}\frac{c}{m_{\mathrm{u}}}.$$

$$-\frac{dE}{dx} = \frac{4\pi e^4 Z^2}{m_e \beta^2 c^2} nz \left[\ln\left(\frac{2 m_e \beta^2 c^2}{I}\right) - \ln(1-\beta) - \beta^2\right]$$

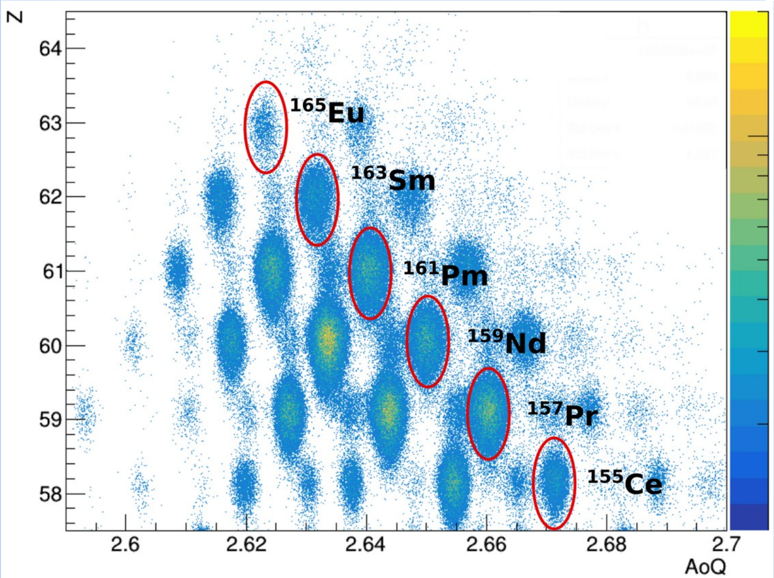

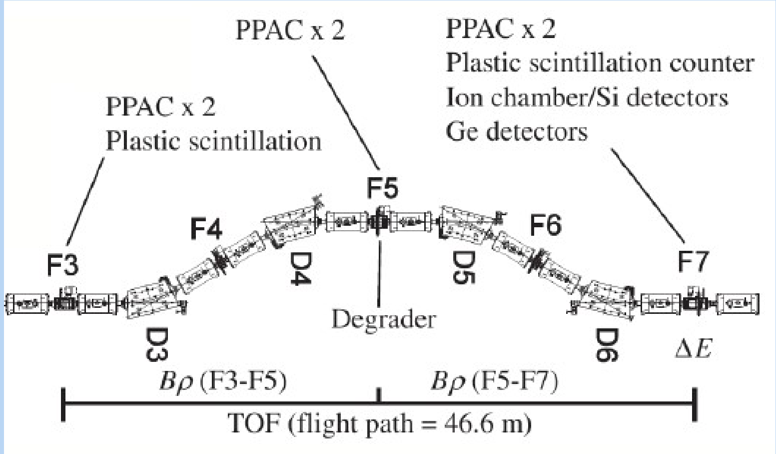

Neutron detection: BRIKEN

- 140 ^{3}He detectors distributed in 7 rings.
- HDPE moderator 90x90x75 cm.
- 2 Clover type HPGe gamma detectors.
- Ancillary (F11, Si…).

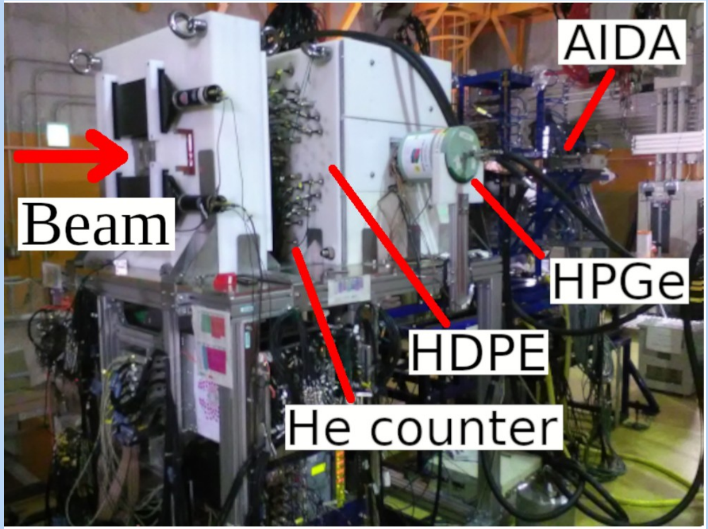

- Acquisition is done using STRUCK modules SIS3316 and SIS3302.
- The modules are controlled by a software called GASIFIC 7.0.

DAQ syncroniszation

3 DAQ runs in parallel:

- BigRIPS uses LUPO.
- BRIKEN uses SIS3316 / SIS3302.
- AIDA uses FEE64.
- Global clock that synchronise the 3 DAQs

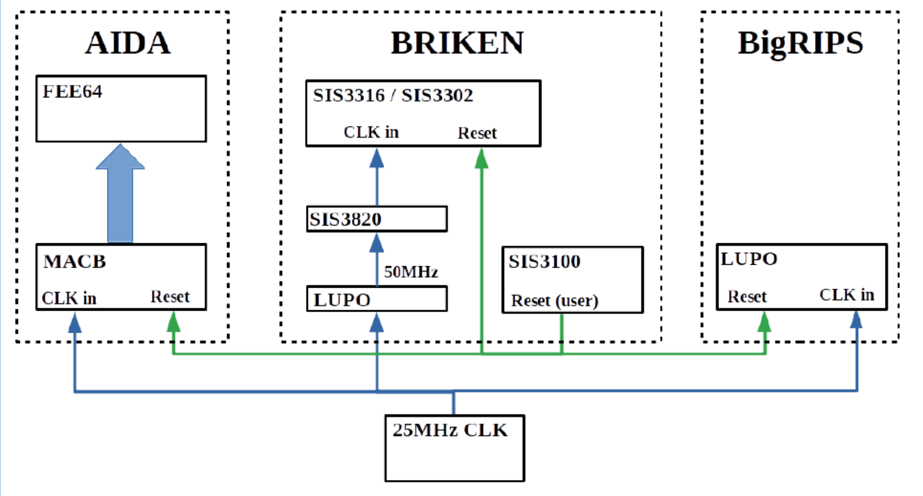

Experimental runs

The RIBF-148 experimental measurements spanned 100 hours.

We employed three configurations with three different degrader widths.

Degrader width (mm)	2.8		3		3.3	
Measurement time (h)	64		14		4	
	Implants	r_1	Implants	r_1	Implants	r_1
151Ba	$5.7 \cdot 10^3$	0.0006	$1.8 \cdot 10^3$	-	$2.1 \cdot 10^2$	-
153La	$4.3 \cdot 10^4$	0.0008	$1.3 \cdot 10^4$	0.0007	$1.8 \cdot 10^3$	0.0009
154La	$5.8 \cdot 10^3$	0.0008	$1.7 \cdot 10^3$	0.0008	$2.4 \cdot 10^2$	0.0022
155Ce	$8.3 \cdot 10^4$	0.0008	$2.3 \cdot 10^4$	0.0007	$3.6 \cdot 10^3$	0.0013
156Ce	$2.4 \cdot 10^4$	0.0008	$6.5 \cdot 10^3$	0.0007	$9.6 \cdot 10^2$	0.0011
157Pr	$2.9 \cdot 10^5$	0.0008	$7.8 \cdot 10^4$	0.0007	$1.3 \cdot 10^4$	0.0010
158Pr	$3.3 \cdot 10^4$	0.0007	$9.0 \cdot 10^3$	0.0009	$1.5 \cdot 10^3$	0.0003
159Nd	$2.0 \cdot 10^5$	0.0008	$5.3 \cdot 10^4$	0.0008	$8.8 \cdot 10^3$	0.0011
160Nd	$6.5 \cdot 10^4$	0.0009	$1.7 \cdot 10^4$	0.0008	$2.9 \cdot 10^3$	0.0010

Neutron Multiplicity Counting

- From 2016 to 2018, we conducted several calibration measurements to evaluate the neutron detection.
  - Several angles
  - Several orientation
  - 2 different detectors configuration
- We only had an uncalibrated source.
- We employed the Neutron Multiplicity Counting to determine the detector efficiency.

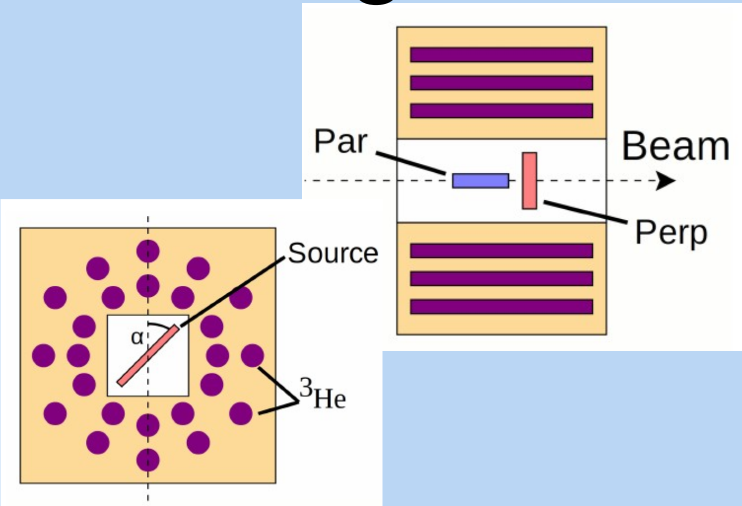

$$\varepsilon = \frac{2\nu_{s1}}{\nu_{s2}} \frac{D}{S}$$

^{252}Cf neutron source

The facility can not facilitate a calibrated source

Impossibility of using an external source

Impossibility of moving the setup to a calibration facility

We used an uncalibrated source

The information given by the manufacturer:

- Nominal activity: 3.7 Mbq (with large undetermined uncertainty)
- Impurities: ^{249}Cf=0.0631%,^{250}Cf=7.69% and ^{251}Cf=0.037%

Neutron Multiplicity Counting

This method advantages:

- Does not require of a calibrated source.
- Offers uncertainties around 1% for the neutrons' yield determination.
- Comparable to metrological standard techniques.
- Digital electronics
- 252Cf fission properties are well characterized.
- BRIKEN detector has high efficiency.

252Cf undergoes spontaneous fission, emitting multiple neutrons time-correlated neutrons.

Neutron Multiplicity Counting

From this individual fission events one can detect groups of correlted neutrons:

- Singles (S)
- Double (D)
- ...

double neutron events

$$\varepsilon = \frac{2\nu_{s1}}{\nu_{s2}} \frac{D}{S}$$

reduced moments

individual neutron events

Rossi-alpha distribtion

Sort the time differences between each detected neutron and all subsequent neutrons within a defined time window.

Non-correlated neutron coincidence --> Flat background.

Correlated neutron coincidence --> More likely to be detected within short time intervals.

From this plot, we compute D with two equivalent methodologies

- Direct Integration
- Gate method

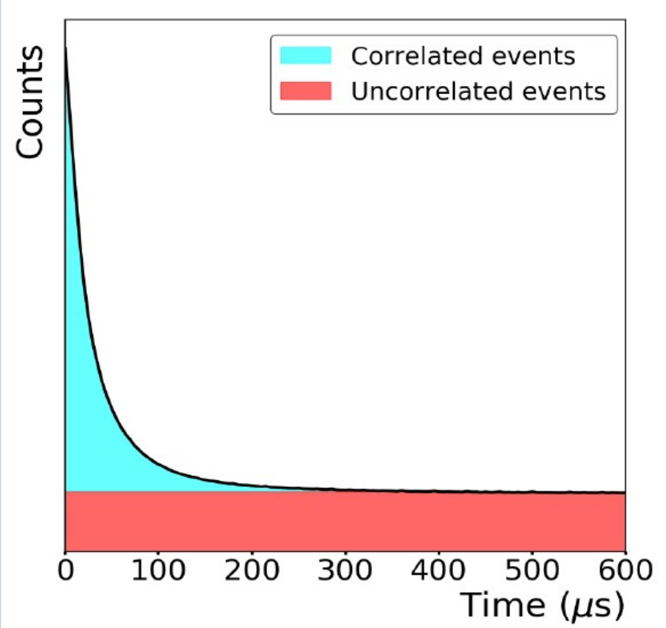

Results error

Systematic errors:

- Source contamination: Contribution of 250Cf included as +0.1 of error.
- Source anisotropy: negligible due to the 4pi detector setup.
- Dead time: negligible due to very low detection rate (<200 cps).

Setup	ε_{Neu} (%)	σ_{Total}(%)	σ_{Stat}(%)	σ_{Syst}(%)
No Clover	60.19	+0.13 -0.08	$\pm$0.08	+0.1
Clover	62.03	+0.12 -0.06	$\pm$0.06	+0.1

Isotopes contamination

- The main contaminants are ^{250}Cf and ^{248}Cm.
- In the period considered only ^{250}Cf has a measurable effect.
- The correction can be rounded to +0.1%

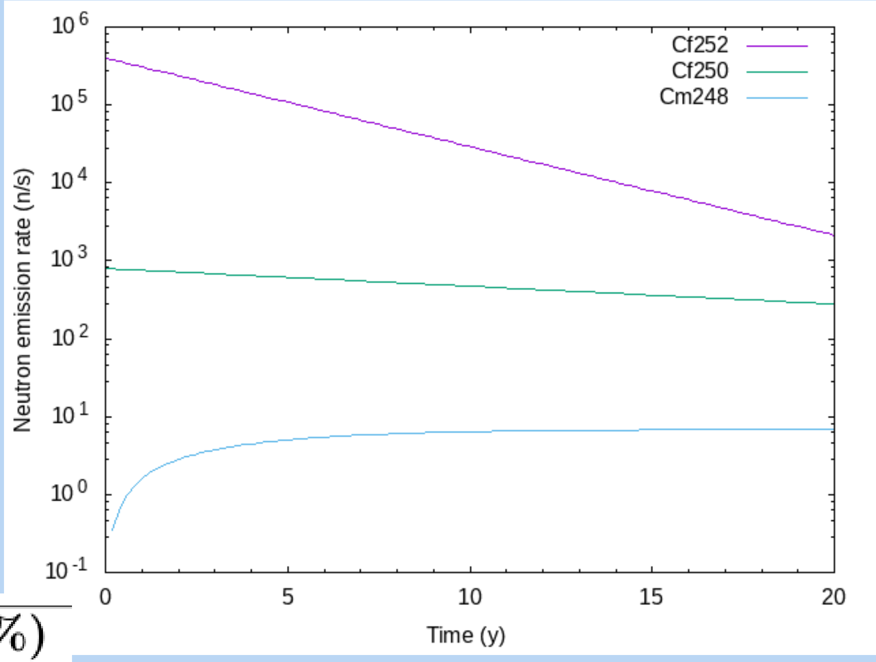

Month/Year	Absolute efficiency correction (%)
07/2016	+0.07
06/2017	+0.09
11/2018	+0.11

Simulations

MC simulations to characterize our detectors' efficiency.

- Used ParticleCounter 4.7.
- Compiled with Geant4 10.1.3.
- G4DL4.5 data library.

We simulated both geometries (non-clover/clover) with a detailed description of the 3He detectors and a simplified version of the HPGe germanium crystals.

252Cf spectrum recommendation from Manhart

- Benchmark with the experimental calibrations

BRIKEN energy response

- No effect on Z (missplacement of AIDA).

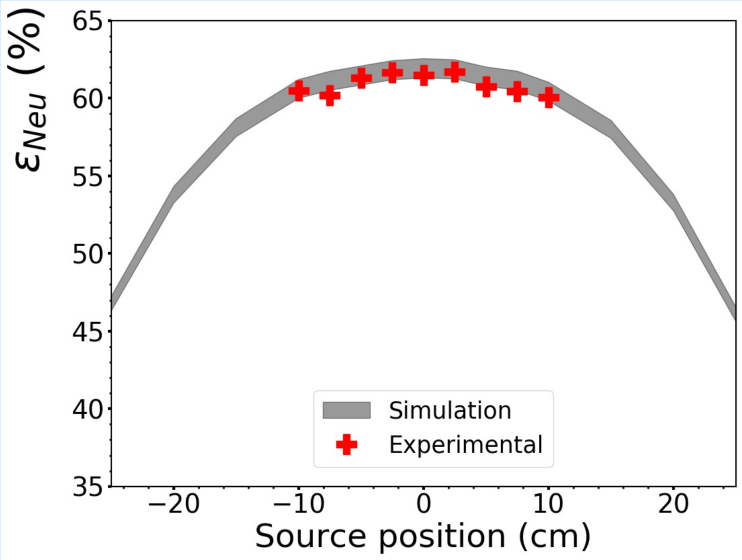

AIDA sorting

AIDA consist of: 6 **DSSDs**

↓

Each with two sides of **128 strips**

↓

Each is registered by a **self-trigger channel**

↓

No interchannel event correlation. Only a list of time-ordered items.

→ Correlation is build via software: **AIDAsort**

AIDA sorting: cluster information

Event type:

>=1 high-energy item: Implantation event

No high-energy item: Low-energy event

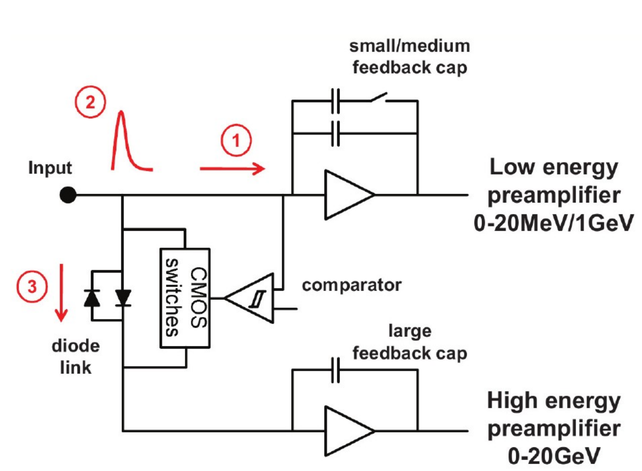

Stopping layer:

Defined as the last stack that has triggered the high-energy branch.

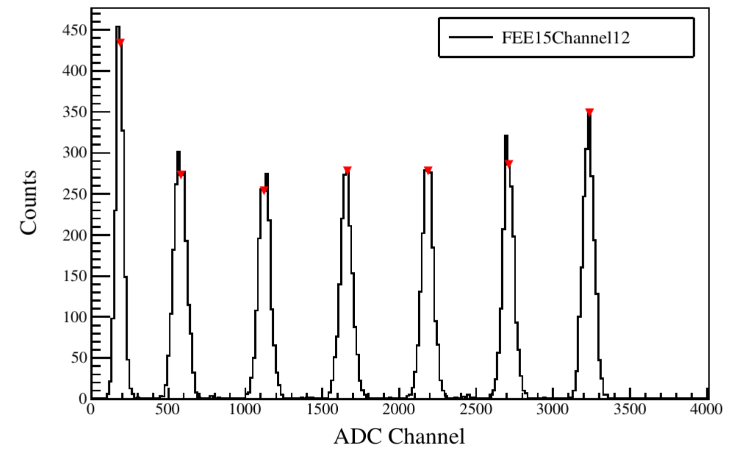

AIDA sorting: cluster information

Event type:

>=1 high-energy item: Implantation event

No high-energy item: Low-energy event

Stopping layer:

Defined as the last stack that has triggered the high-energy branch.

Position:

Using the double side detectors clusters have a trigger in x and y, therefore one can define a “pixel”.

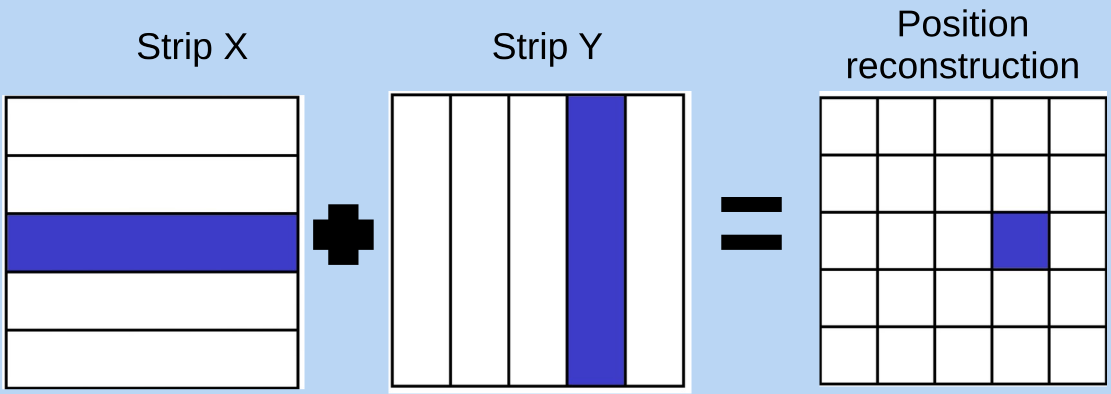

AIDA sorting: cluster information

Event type:

>=1 high-energy item: Implantation event

No high-energy item: Low-energy event

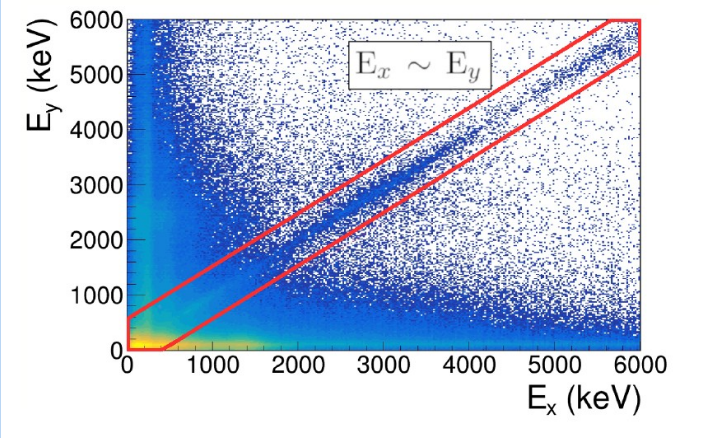

Position:

Using the double side detectors clusters have a trigger in x and y, therefore one can define a “pixel”.

Energy:

Addition of all the items’ energy included in the cluster.

A consistency condition is imposed Ex~Ey

Improve signal to noise ratio

Methods of **reducing** the background:

– β energy threshold.

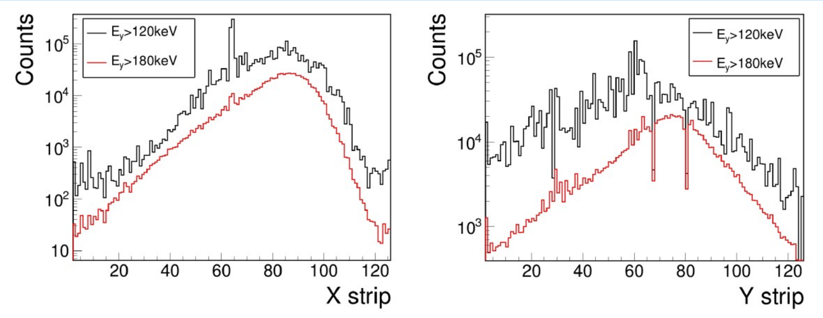

Threshold only on rear strips

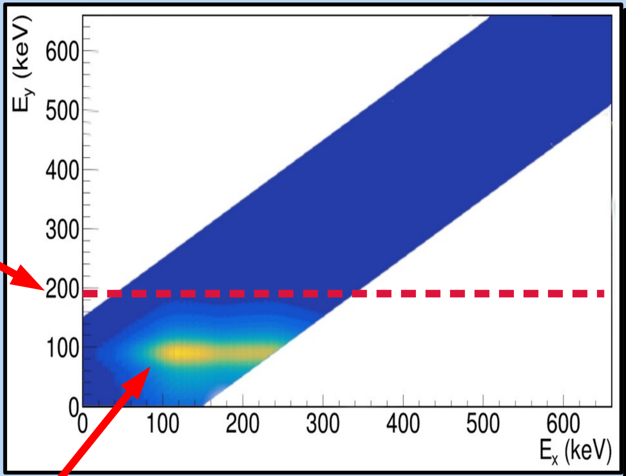

Electronic noise

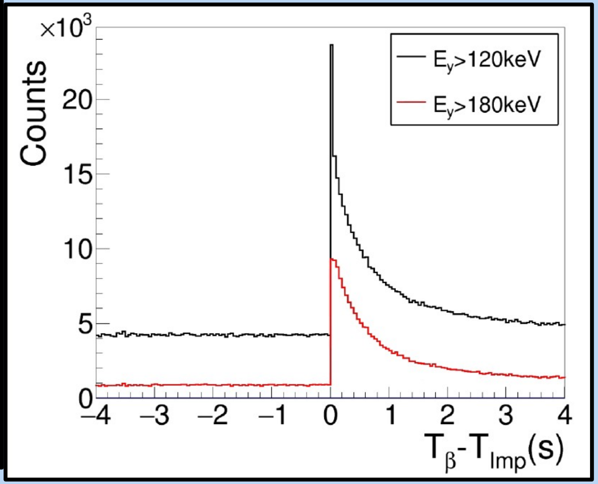

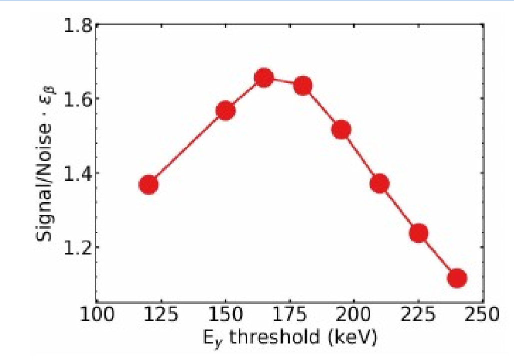

Improve signal to noise ratio

Methods of **reducing** the background:

- β energy threshold.
- Build **vetoes for β and neutron** events using ancillary detectors.

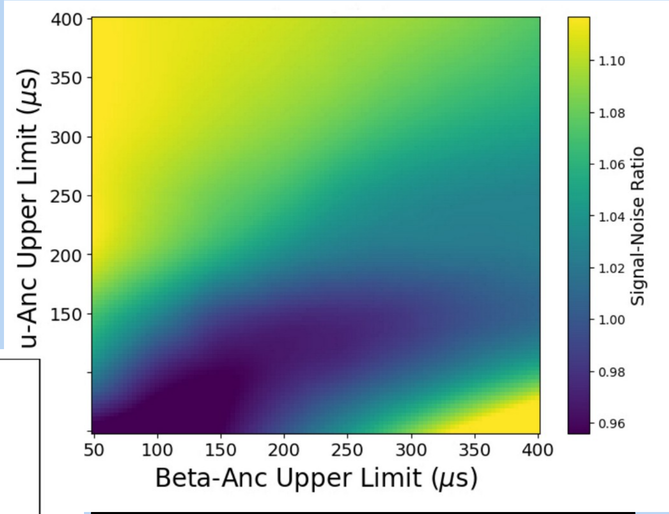

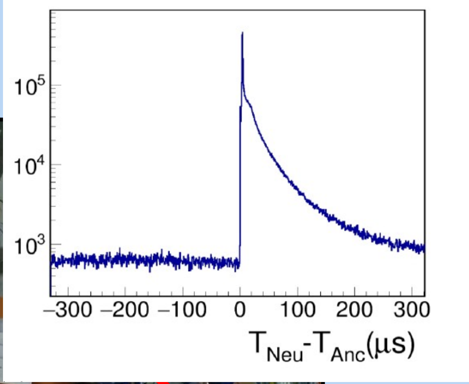

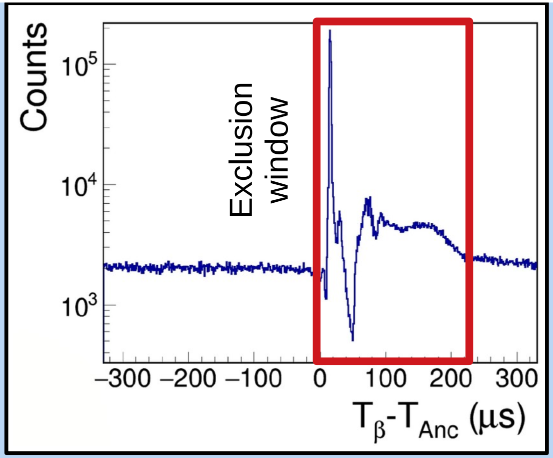

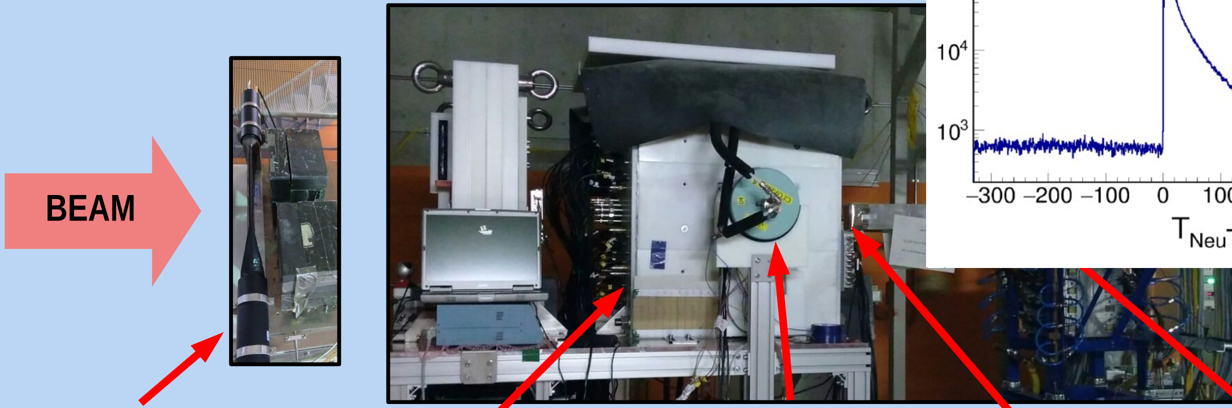

Merger and correlation curves

- Transfering the identification in BigRIPS to AIDA.
- We can asume instantaenusi transmission from F11 to AIDA.
- Some ions do not reach AIDA due to the beam dispersion.

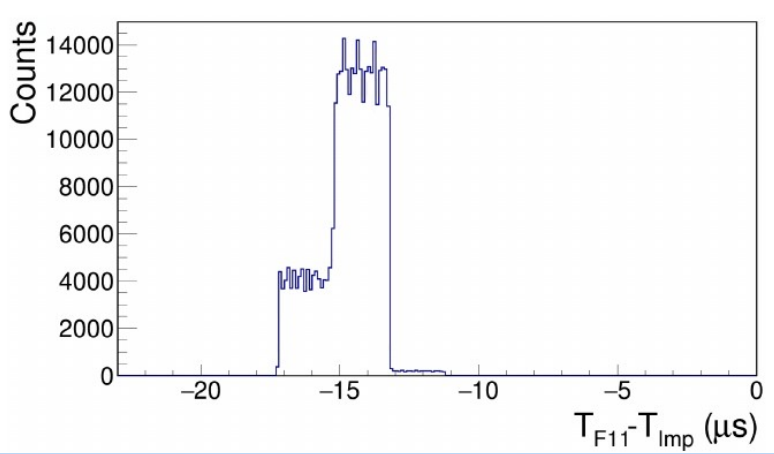

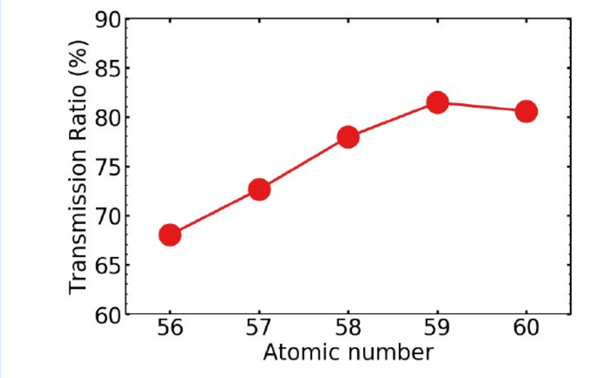

Other P_{1n} results from BRIKEN

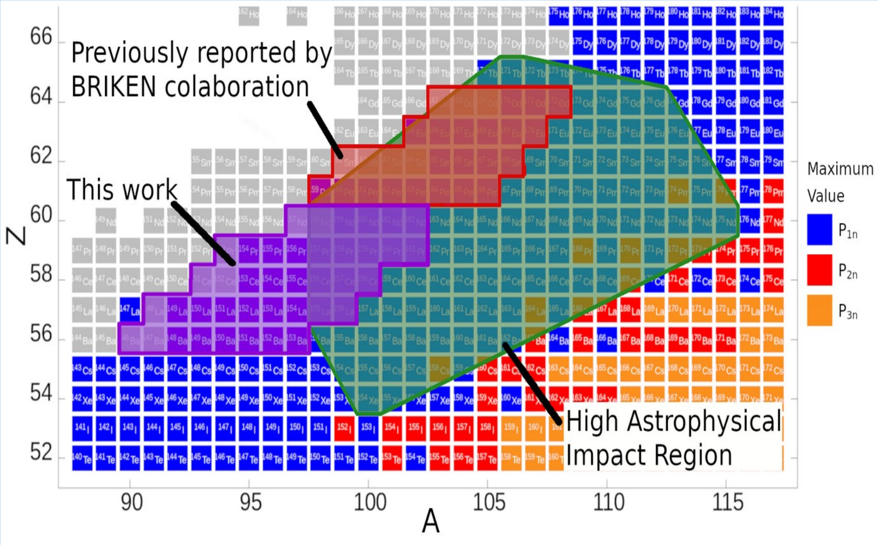

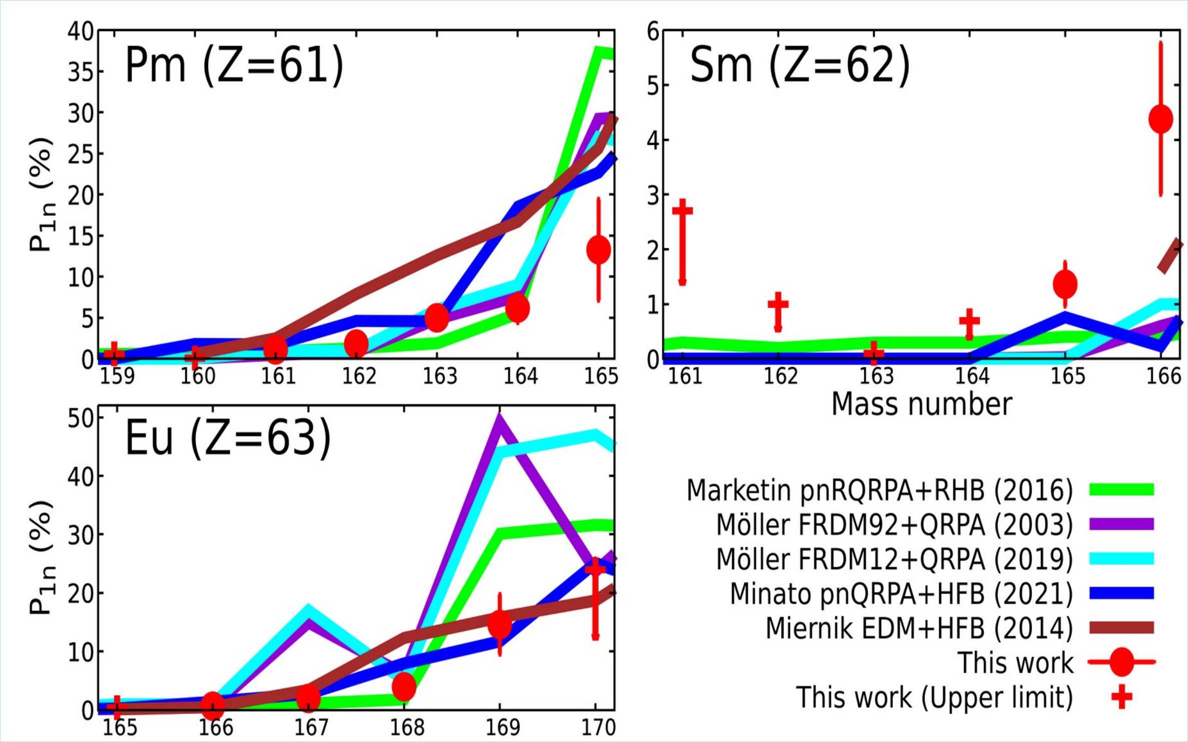

G. G. Kiss, et al., ApJ936 (2022)

^{86}Ga decay chain

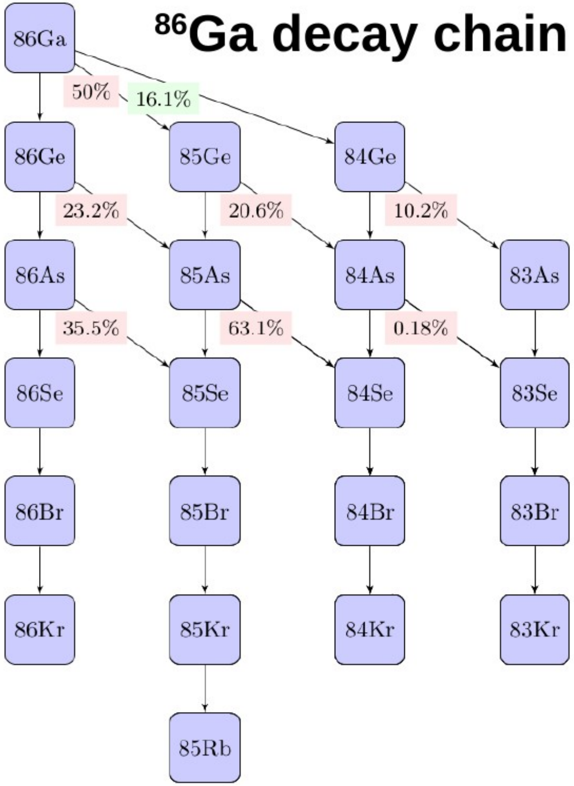

Fit function: Example from A. Tolosa

$$f_{\beta}(t) = \sum_{i \in \beta} \bar{\varepsilon}_{\beta}^{i} \lambda_i N_i(t) + \mathrm{bck}_{\beta}(t)$$

$$f_{\beta 1n}(t) = \sum_{j \in \beta 1n} \bar{\varepsilon}_{\beta}^{j} \bar{\varepsilon}_{n}^{j} P_{1n}^{j} \lambda_j N_j(t) + \mathrm{bck}_{1n}(t)$$

$$f_{\beta 2n}(t) = \sum \bar{\varepsilon}_{\beta}^{k} \left(\bar{\varepsilon}_{n}^{k}\right)^2 P_{2n}^{k} \lambda_k N_k(t) + \mathrm{bck}_{2n}(t)$$

$$N_k(t) = N_1 \prod_{i=1}^{k-1} \left(b_{i,i+1} \lambda_i\right) \times \sum_{i=1}^{k} \frac{e^{-\lambda_i t}}{\prod_{j=1 \neq i}^{k} \left(\lambda_j - \lambda_i\right)}$$

$$b_{i,i+1} = P_{1n}^{i}, P_{2n}^{i} \; or \; 1 - P_{1n}^{i} - P_{2n}^{i}$$

- ε are averaged efficiencies (weighted by β-intensity distribution)
- Only number of decays & parent P_{xn} (& $T_{1/2}$*) are set free during the fit.
- The rest of parameters ($T_{1/2}$ & P_{xn} of other isotopes, efficiencies, background) are fixed.

Theoretical models

RHB Relativistic Hartree Bogoliubov

FRDM: Finite Range Droplet Model for mass model

QRPA: Quasi random particle approximation

HFB: Hartree-Fock-Bogoliubov

HF: Hauser-Feshbach

pnFAM: proton-neutron Finite Amplitude Method

pnRQRPA: proton-neutron Relativistic Quasiparticle Random-Phase Approximation

EDM: Effective density model.

Nuclear structure calculations

- Revision of the Marketin et al. model:
  - Self-consistent Covariant Density-Functional Theory (CDFT)
  - Ground-states: RHB model with the D3C* parametrization.
  - Excited states: pn-RQRPA

$$k = \left[\zeta_0^2 + \tfrac{1}{9}w^2\right]_{(0)} + \left[\zeta_1^2 + \tfrac{1}{9}(x+u)^2 - \tfrac{4}{9}\mu_1\gamma_1 u(x+u) + \tfrac{1}{18}W_0^2(2x+u)^2 - \tfrac{1}{18}\lambda_2(2x-u)^2\right]_{(1)} + \left[\tfrac{1}{12}z^2\left(W_0^2 - \lambda_2\right)\right]_{(2)}, \quad (11a)$$

$$ka = \left[-\tfrac{4}{3}uY - \tfrac{1}{9}W_0(4x^2 + 5u^2)\right]_{(1)} - \left[\tfrac{1}{6}W_0 z^2\right]_{(2)}, \quad (11b)$$

$$kb = \tfrac{2}{3}\mu_1\gamma_1\{-[\zeta_0 w]_{(0)} + [\zeta_1(x+u)]_{(1)}\}, \quad (11c)$$

$$kc = \tfrac{1}{18}[8u^2 + (2x+u)^2 + \lambda_2(2x-u)^2]_{(1)} + \tfrac{1}{12}[(1+\lambda_2)z^2]_{(2)}, \quad (11d)$$

In the Condon-Shortley phase convention [48] the matrix elements for β^- transitions are

$$w = -g_A\sqrt{3}\frac{\langle f \| \sum_k r_k\left[\boldsymbol{C}_1^k \otimes \boldsymbol{\sigma}^k\right]^0 \boldsymbol{t}_-^k \| i\rangle}{\sqrt{2J_i+1}}, \quad (13a)$$

$$x = -\frac{\langle f \| \sum_k r_k \boldsymbol{C}_1^k \boldsymbol{t}_-^k \| i\rangle}{\sqrt{2J_i+1}}, \quad (13b)$$

$$u = -g_A\sqrt{2}\frac{\langle f \| \sum_k r_k\left[\boldsymbol{C}_1^k \otimes \boldsymbol{\sigma}^k\right]^1 \boldsymbol{t}_-^k \| i\rangle}{\sqrt{2J_i+1}}, \quad (13c)$$

$$z = 2g_A\frac{\langle f \| \sum_k r_k\left[\boldsymbol{C}_1^k \otimes \boldsymbol{\sigma}^k\right]^2 \boldsymbol{t}_-^k \| i\rangle}{\sqrt{2J_i+1}}, \quad (13d)$$

$$w' = -g_A\frac{2}{\sqrt{3}}\frac{\langle f \| \sum_k r_k \boldsymbol{I}(1,1,1,1,r_k)\left[\boldsymbol{C}_1^k \otimes \boldsymbol{\sigma}^k\right]^0 \boldsymbol{t}_-^k \| i\rangle}{\sqrt{2J_i+1}}, \quad (13e)$$

$$x' = -\frac{2}{3}\frac{\langle f \| \sum_k r_k \boldsymbol{I}(1,1,1,1,r_k)\boldsymbol{C}_1^k \boldsymbol{t}_-^k \| i\rangle}{\sqrt{2J_i+1}}, \quad (13f)$$

$$u' = -g_A\frac{2\sqrt{2}}{3}\frac{\langle f \| \sum_k r_k \boldsymbol{I}(1,1,1,1,r_k)\left[\boldsymbol{C}_1^k \otimes \boldsymbol{\sigma}^k\right]^1 \boldsymbol{t}_-^k \| i\rangle}{\sqrt{2J_i+1}}. \quad (13g)$$

Nuclear structure calculations

$$E^b_{g.s.}(Z+1, N-1) \approx E^b_{g.s.}(Z,N) + \left.\frac{dE}{dZ}\right|_{(Z,N)} + \left.\frac{dE}{dN}\right|_{(Z,N)} + E^{\text{lowest}}_{2qp}$$

Ground-State binding energy

Lowest two-quasiparticles energies

By definition

Chemical potential

$$\lambda_p = \left.\frac{dE}{dZ}\right|_{(Z,N)} \qquad \lambda_n = \left.\frac{dE}{dN}\right|_{(Z,N)} \tag{6.6}$$

Therefore

$$\Delta B = E^b_{g.s.}(Z,N) - E^b_{g.s.}(Z+1, N-1) \approx \lambda_n - \lambda_p - E^{\text{lowest}}_{2qp} \tag{6.7}$$

Where λ_p and λ_n represent the proton and neutron Fermi energies, respectively. The correction term E^{lowest}_{2qp} accounts for odd-even effects and is determined as follows based on the parent nucleus composition:

$$E^{\text{lowest}}_{2qp} = \begin{cases} E^{\text{lowest}}_{\pi} + E^{\text{lowest}}_{\nu} & \text{(even-even parent)} \\ E^{\text{lowest}}_{\nu} & \text{(even-odd parent)} \\ E^{\text{lowest}}_{\pi} & \text{(odd-even parent)} \\ 0 & \text{(odd-odd parent)} \end{cases} \tag{6.8}$$

Here, E^{lowest}_{π} (E^{lowest}_{ν}) denotes the unperturbed proton (neutron) quasiparticle energies.

Combining equations 6.4 and 6.7, we can compute the energy conversion from the QRPA frame to the daughter reference as follows:

$$E^*_m \approx E^{\text{QRPA}}_m + \Delta B - (\lambda_n - \lambda_p) = E^{\text{QRPA}}_m + Q_\beta - \Delta M_{nH} - (\lambda_n - \lambda_p) \tag{6.9}$$

Nuclear structure calculations

- Revision of the Marketin et al. model:
  - Correction on the phase integral limits (missing m_e)
  - Proper implementation of the residual interactions.
  - Correction of some phases on the matrix eleemnts.

$$B^{\pm}_{\lambda J} = \left| \sum_{pn} < p||T^J||n > (X^{\lambda J}_{pn} u_p v_n + (-1)^J Y^{\lambda J}_{pn} v_p u_n) \right|^2 .$$

$$\begin{pmatrix} A^J & B^J \\ B^{*J} & A^{*J} \end{pmatrix} \begin{pmatrix} X^{\lambda J} \\ Y^{\lambda J} \end{pmatrix} = E_\lambda \begin{pmatrix} 1 & 0 \\ 0 & -1 \end{pmatrix} \begin{pmatrix} X^{\lambda J} \\ Y^{\lambda J} \end{pmatrix} . \qquad (3.28)$$

The matrices A and B are defined in the canonical basis [9]

$$\begin{aligned} A^J_{pn,p'n'} &= H^{11}_{pp'}\delta_{nn'} + H^{11}_{nn'}\delta_{pp'} \\ &+ (u_p v_n u_{p'} v_{n'} + v_p u_n v_{p'} u_{n'}) V^{phJ}_{pn'np'} + (u_p u_n u_{p'} u_{n'} + v_p v_n v_{p'} v_{n'}) V^{ppJ}_{pnp'n'} \\ B^J_{pn,p'n'} &= (-1)^{j_{p'} - j_{n'} + J} (u_p v_n v_{p'} u_{n'} + v_p u_n u_{p'} v_{n'}) V^{phJ}_{pp'nn'} \\ &- (u_p u_n v_{p'} v_{n'} + v_p v_n u_{p'} u_{n'}) V^{ppJ}_{pnp'n'} . \end{aligned}$$

$$V^{T=0}_\tau = \mathbf{1}_1 \mathbf{1}_2$$

However, the isovector part

$$V^{T=1}_\tau = \vec{\tau}_1 \vec{\tau}_2 = 4\tau_{1z}\tau_{2z} + 2\tau_{1+}\tau_{2-} + 2\tau_{1-}\tau_{2+}$$

Talys Spin-Parity

We do not have a detailed description of these excited states but we can assume that all are populated by GT.

The other required information is the initial state from which the parent nucleus decayed. We can assume it was the ground state.

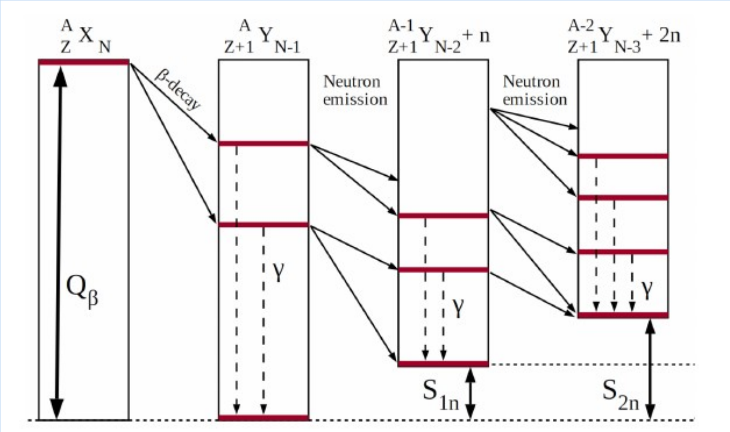

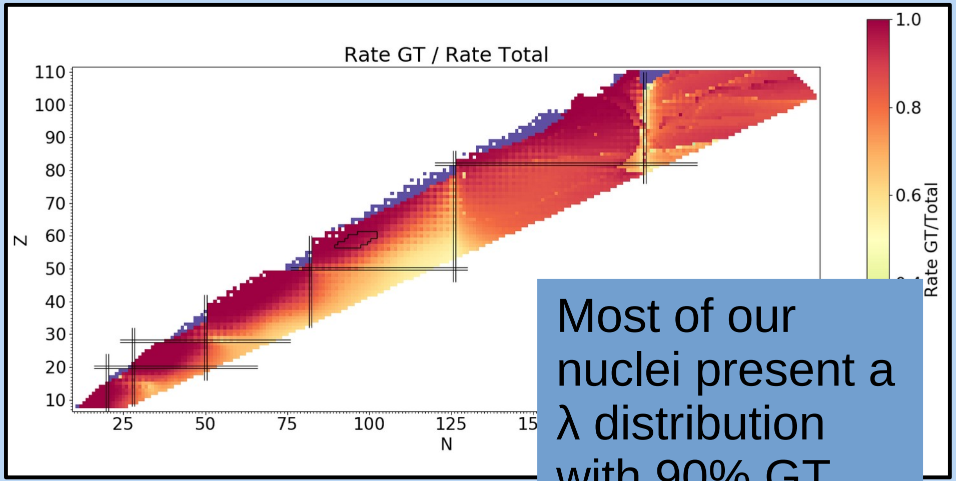

Most of our nuclei present a λ distribution with 90% GT

Hauser-Feshbach

This method describe the statistical decay of a compound nucleus.

It is the combination of the incident particle and the taget creating a short-lived nucleus.

$$P_{xn} = \int_0^{Q_\beta} \lambda(E_x) \cdot p_{xn}(E_x) \; dE_x$$

$$p_{xn}(E_x) = \frac{\Gamma_{xn}(E_x)}{\Gamma_n(E_x) + \Gamma_\gamma(E_x)}$$

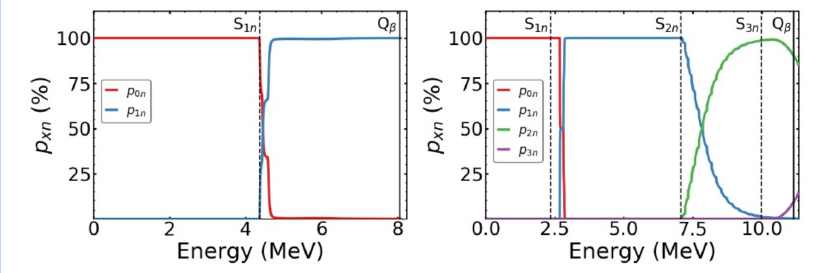

(a) ^{157}Pr (b) ^{165}Pr

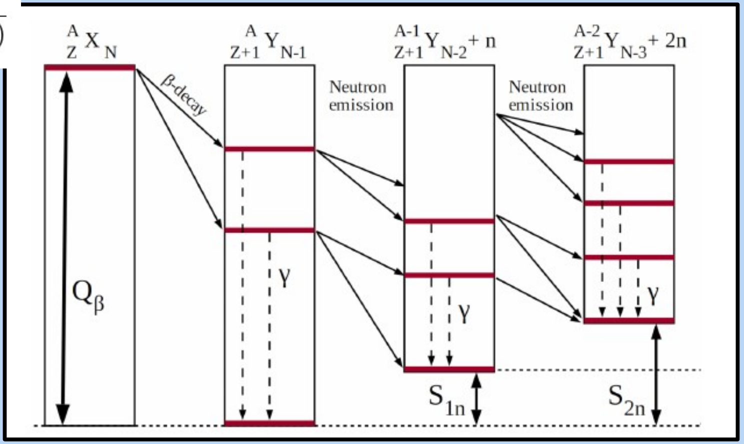

Inputs:

Level Densities
γ-Strength function
Optical model

Transimission coeficient

Mass models

- Skyrme-Hartree-Fock-Bogoliubov (HFB) [109]
- Gogny-Hartree-Fock-Bogoliubov (HFB1D) [110]
- Finite-Range Droplet Macroscopic (FRDM) [33]

$$Q_{\beta^-} = M(Z,N) - M(Z+1,N-1)$$
$$S_{xn} = -M(Z+1,N-1) + M(Z+1,N-x-1) + xM_n$$

Model	Q_β	S_{1n}	Both
FRDM	0.039	0.055	0.034
HFB	0.042	0.058	0.041
HFBD1M	0.043	0.069	0.041

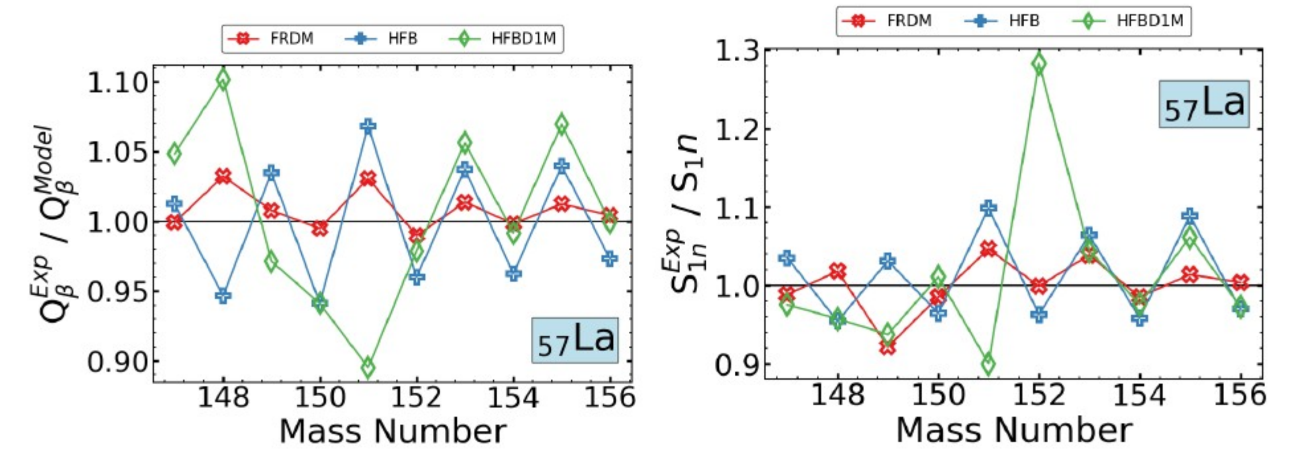

(a) Q_β (b) S_{1n}

Sigma ajustment

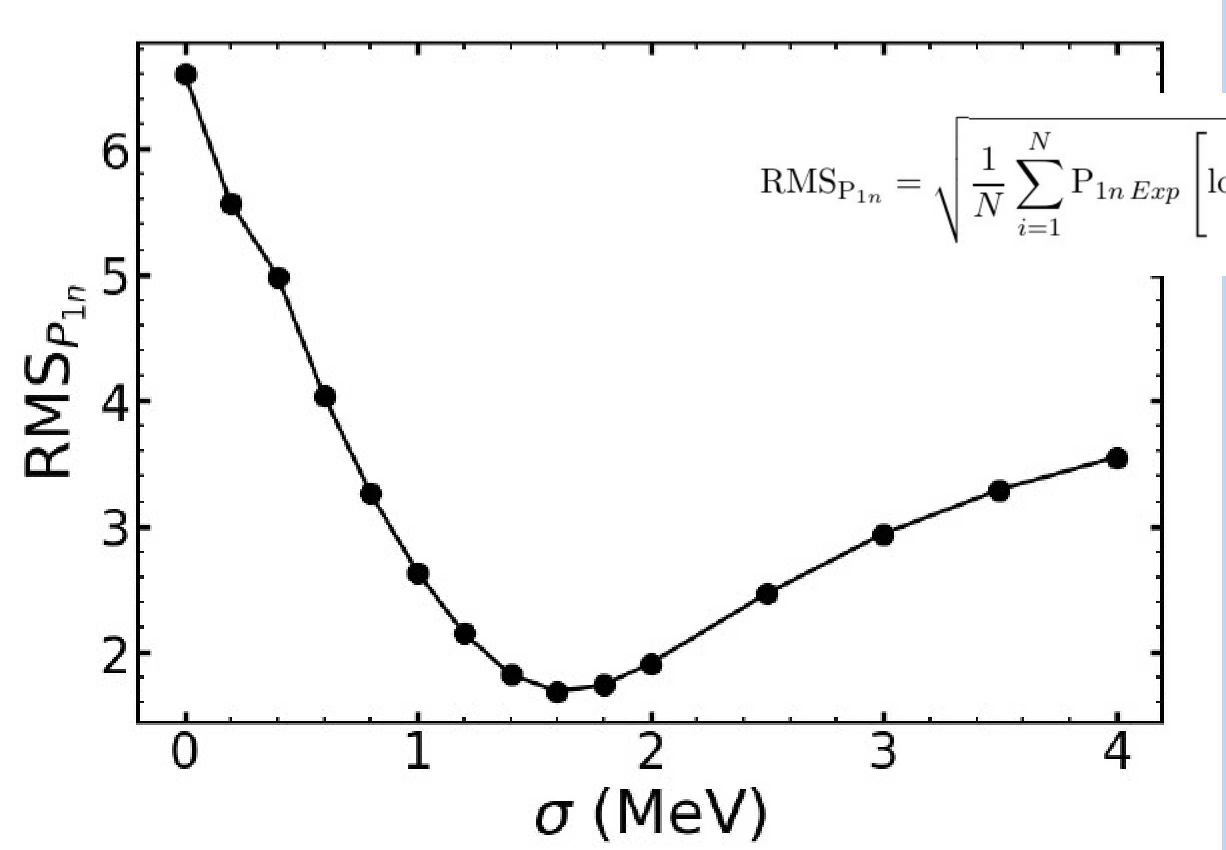

$$\mathrm{RMS}_{\mathrm{P}_{1n}} = \sqrt{\frac{1}{N}\sum_{i=1}^{N} \mathrm{P}_{1n\,Exp}\left[\log_{10}\left(\frac{\mathrm{P}_{1n\,\mathrm{Theory}}}{\mathrm{P}_{1n\,\mathrm{Exp}}}\right)^{2}\right]}$$